Casa abierta al tiempo
UNIVERSIDAD AUTÓNOMA METROPOLITANA
Unidad Iztapalapa

Laboratorio de Biopolímeros

Division of Biological and Health Sciences

Postgraduate Program in Biotechnology

"Production and purification of chitosanase and Hydrophobins of *Lecanicillium lecanii*: design of drug nanocarrier delivery system"

THESIS

To obtain the degree of

Doctor in biotechnology

PRESENTS

M. in B. Jennyfer Hernández Alcántara

Matriculation number: 2192802272

ORCID: 0009-0000-2000-4808

heralca13@gmail.com

Director
Dra. Keiko Shirai Matsumoto
Codirector
Dr. Makoto Anraku
Asesor
Dr. Jesús Rojas Osnaya

JURY
Chair: Dr. Zaizy Rocha Pino
Secretary: Dr. Carmen Guadalupe Hernández Valencia
Member: Dr. Hector Bernardo Escalona Buendia
Member: Dr. Jesús Rojas Osnaya

Iztapalapa, Mexico City, February 11, 2026.

The Doctorate in Biotechnology at the Autonomous Metropolitan University is included in CONACYT's National Program for Quality Postgraduate Studies (PNCP).

This thesis was carried out at the Biopolymers Laboratory and Pilot Plant for Bioprocessing of Agro-industrial and Food By-products (Pilot Plant 10) of the Biotechnology Department of the Biological and Health Sciences Division, Autonomous Metropolitan University, Iztapalapa Campus, under the supervision of Dr. Concepción Keiko Shirai Matsumoto.

The formulation of the nanocarrier and *in vivo* and *in vitro* tests were carried out at the Faculty of Pharmaceutical Sciences, Sojo University, Japan, under the supervision of Dr. Makoto Anraku and the guidance of Dr. Hideaki Nakamura, thanks to the UAM international mobility grant for the research stay.

Mexico City, February 11, 2026.

The Academic Committee of the Postgraduate Program in Biotechnology by the Division of Biological and Health Sciences of the Universidad Autónoma Metropolitana, Iztapalapa Campus, approved the thesis:

"**Production and purification of chitosanase and Hydrophobins of *Lecanicillium lecanii*: design of drug nanocarrier delivery system**"

Presented by:

M. in Biotech, B. Eng. Jennyfer Hernández-Alcántara

Tutorial committee:

Director: Dra. Keiko Shirai Matsumoto.

Universidad Autónoma Metropolitana-Iztapalapa, Biotechnology Department, Laboratory of Biopolymers and Pilot Plant of Bioprocessing of Agro-Industrial and Food By-Products

Codirector:

Dr. Makoto Anraku

Department of Biopharmaceutics, Graduate School of Pharmaceutical Sciences, Kumamoto University, Kumamoto, Japan.

Assessor:

Dr. Jesus Rojas Osnaya

Universidad Autónoma Metropolitana-Cuajimalpa, Natural Sciences Department.

H. Jury:

Chair: Dr. Zaizy Rocha Pino. (UAM-I)

Secretary: Dr. Carmen Guadalupe Hernández Valencia (UAM-I)

Member: Dr. Hideaki Nakamura (Sojo University, Japan)

Member: Dr. Jesús Rojas Osnaya (UAM-C)

Acknowledgements

I would like to thank Dr. Keiko Shirai sensei for the many moments we have shared over the years, her valuable advice and insightful comments on my academic development, her thoughtful corrections, and the trust she has placed in me at every stage. Thank you for showing me that success is built on hard work and commitment.

To Dr. Makoto Anraku sensei, thank you for welcoming me with open arms during my stay in Japan, for all the knowledge you shared, and for the kindness and patience with which you always treated me.

To Dr. Hideaki Nakamura sensei, for always teaching me with dedication, patience, and trust.

To Dr. Jesus Rojas, for his support and guidance during the experimental work.

To my friends Marina san, Anthony, Nowshin, and Inna, for the long conversations, the laughter, the moments we shared, and for being my friends on the other side of the world.

To my friends Jessi, Andy, and Cris, for the long conversations that made the long hours in the lab more bearable.

To my incredible friend, Dr. Manuel, thank you for all your support, affection, and good experiences over the years.

To my lab mates, Erwin and Ricardo, for your kind words and kindness.

Especially to my colleague, best friend, and sister M. in Bio. Jossephlynt, thank you for being my person, for the shoulder to cry on, and for every push you always give me. I love you with all my heart.

To my father, thank you for always being by my side, for your love, your effort, and for teaching me, with your words and your example, to move forward.

To my mother, for being the purest reflection of passion, loyalty, and love; for being my guide and showing me that extraordinary women do exist. Thank you so much for always believing in me, Mom.

To Dr. Yahir, for being my friend, colleague, and family. This journey has been better with you. Thank you for all your support, for pushing me to continue even when I felt I couldn't go on, for your love, and for every moment we shared. Together we have completed this stage and together we are starting a new one.

Index

Table Index

Figure Index

Summary

This doctoral research focused on the production, purification, characterization and biotechnological applications of enzymatic and protein systems derived from *Lecanicillium lecanii*, highlighting their potential in sustainable industrial and biomedical processes. The study was divided into three sections, encompassing the development of chitosanases for chitosan derivatives, the functional production of hydrophobins and their use as biolubricants, and the design of hydrophobin-based nanoparticles for targeted drug delivery.

In the first stage, chitosanases were produced through submerged fermentation using chitosan with a degree of acetylation of 18.6% as both the inducer and the sole carbon source. The enzymatic process was optimized in 3 L and subsequently scaled up to a 50 L bioreactor, maintaining operational parameters such as pH, temperature, and oxygen transfer. Purified enzymes displayed molecular weights of 31 and 44 kDa, with optimal activity at 50 °C and pH 6. These chitosanases efficiently hydrolyzed substrates, including acetylated and desacetylated substrates, producing chitooligosaccharides (COS) with a degree of polymerization between 2-6 and low molecular weight chitosan ranging from 8 to 102 kDa. Control of hydrolysis conditions enabled the generation of partially acetylated derivatives at pilot scale, revealing their potential for pharmaceutical, agricultural, and food applications.

The second stage focused on the extraction, purification, and functional evaluation of hydrophobins class I and II (8.7 and 5.8 kDa) obtained from *L. lecanii* cultures grown on chitosan-based media. Both hydrophobins reduced the contact angle on hydrophobic and hidrofilic surfaces.

HFBII were used to explore the biomedical potential of hydrophobins class II from *L. lecanii* as nanocarriers for the anticancer agent pirarubicin (THP). Hydrophobins Class II were structurally characterized by circular dichroism, dynamic light scattering, and electrophoretic analyses to determine their suitability as nanoscale delivery systems. Two nanoparticle formulations were developed: THP-hydrophobin nanoparticles and glucosamine-modified THP–hydrophobin nanoparticles. These nanostructures exhibited mean diameters of 87.43 ± 2.05 nm and 188.30 ± 8.85 nm, respectively, with excellent stability under physiological

conditions. In vitro assays using C26 carcinoma cells demonstrated efficient internalization, strong cytotoxicity, and a redox- and pH-responsive release mechanism consistent with the tumor microenvironment. In vivo tests on tumor-bearing mice confirmed selective tumor accumulation, enhanced antitumor efficacy, and reduced systemic toxicity, particularly for the glucosamine-functionalized formulation

The third section focuses on emulsions formulated with jatropha oil and hydrophobins I and II, which demonstrated physicochemical stability and tribological properties comparable to the commercial lubricant CIMSTAR-60. Furthermore, microbiological tests revealed a significant decrease in the proliferation of fungal growth (*Fusarium, Aspergillus, Cladosporium, and Cephalosporium*), supporting their application as eco-friendly, antimicrobial biolubricants for machining processes.

Overall, this research demonstrates the remarkable versatility of *Lecanicillium lecanii* as a biotechnological platform for producing enzymes and surface-active proteins with applications that span from sustainable materials processing to targeted cancer therapy. The chitosanases and hydrophobins characterized herein contribute to advancing environmentally responsible bioprocesses and innovative biomedical solutions.

Introduction

Microorganisms are biological resources used in a variety of applications such as biological control and the production of enzymes, lipids, peptides, and proteins, among others (Bulathsinhalage *et al*., 2019).

Entomopathogenic fungi are a group of microorganisms used in pest control because they cause pathogenesis in insects, such as *Beauveria bassiana, Lecanicillium lecanii*, and *Metarhizium anisopliae* (Almeida *et al*., 2022; Mantzoukas, S, *et al*., 2023). These types of microorganisms develop in hydrophobic environments, such as the cuticle of insects, and are reported to produce a large number of enzymes such as peptidases, proteases, chitinases, and lipases, because pathogenesis is mediated by mechanical forces and enzymatic processes (Sharma, R., & Sharma, P., 2021)

Lecanicillium lecanii has the ability to hydrolyze chitin, which forms part of the exoskeleton of arthropods and the cell wall of fungi, due to the production of proteins and enzymes, including hydrophobins, proteases, and chitinases, as part of the effector mechanism of antagonism (Rocha-Pino *et al*., 2018; Rojas-Osnaya *et al*., 2020). Among the enzymes that can be produced are chitosanolytic enzymes or chitinases (EC 3.2.1.132). Chitosanases in contrast, belong to the glycosyl hydrolase family, characterized by their ability to hydrolyze the β-(1,4) glycosidic bonds present in chitosan chains, releasing glucosamine monomers and oligomers. Chitosanolytic enzymes are functionally classified into endo-, exo-, and hexo-enzymes according to their active-site architecture, substrate recognition mode, and hydrolytic pattern. Endo-chitosanases possess groove-shaped active sites that facilitate the random hydrolysis of internal β-(1,4) linkages via acid‑base catalysis, resulting in the formation of chitosan oligosaccharides of variable length and a rapid decrease in polymer molecular weight. In contrast, exo-chitosanases exhibit pocket-shaped active sites that restrict access to internal bonds and promote sequential hydrolysis from the non-reducing ends. In contrast, hexo-chitosanolytic enzymes act on short oligosaccharides with high structural specificity, recognizing both the degree of polymerization and the acetylation pattern, thereby enabling fine and controlled depolymerization of chitosan (Shinya *et al*., 2017). These hydrolysis products have been of great interest in various applications, such as

prebiotics in food, in the pharmaceutical industry due to their antioxidant activity, as well as being used as a functional food ingredient and even in agriculture due to their antimicrobial properties. (Vela Gurovic *et al*., 2015; Cao *et al*., 2018)

The production of extracellular chitinases has been carried out using submerged fermentation (SmF) and solid-state fermentation (SSF) systems. (Rocha-Pino *et al*., 2011; Rojas-Osnaya *et al.,* 2020) The use of colloidal chitosan, chitosan powder, shrimp shells, and squid as inducing substrates for the induction of these enzymes has been reported. It has been reported that chitinases can be produced by bacteria (Cahyaningtyas *et al*., 2021) and fungi (Kumar *et al*., 2020; Aktuganov *et al*., 2019). Among the most common genera for bacteria *are Bacillus, Pseudomonas,* and *Streptomyces*, while for fungi there are few reports belonging to the genera *Aspergillus, Gongronella*, and *Trichoderma.* In plants, there are reports of its production in leek roots and *Capcicum annum* leaves, etc. (Wang *et al*., 2008; Thadathil *et al*., 2014; Zhou *et al*., 2022; Xu, Y. *et al*., 2022).

On the other hand, for the development of fungi and their infectious processes, it is necessary to produce molecules that allow adhesion to the cuticle of the hosts, growth of aerial hyphae in the development of the fungus, etc. These molecules must have surfactant characteristics because they need to reduce the surface tension in aqueous environments, as surfactants do. such as hydrophobins.

Hydrophobins (HFB) are a group of small (5-20 kDa) globular proteins that are highly surface-active and capable of self-assembling to form amphipathic membranes. This allows them to reduce surface tension and interact between surfaces with different hydrophobicity (Singh *et al*., 2018; Kulkarni, S. *et al*., 2022). Their most relevant characteristic is their ability to spontaneously adhere to all types of surfaces due to their capacity to self-assemble into an amphipathic membrane (Rocha-Pino *et al*., 2018).

In this context, this doctoral thesis is based on the comprehensive use of biomolecules produced by *Lecanicillium lecanii* under sustainable bioprocesses and a circular economy approach. Chapter 1 addresses the production of chitosanase from *L. lecanii* on a laboratory scale (3 L) to a pilot plant scale (50 L) using aeration parameters for scaling. The chitosans were identified and characterized for use in the production of low molecular weight chitosans

(LMWC) and chitooligosaccharides . This work addresses the first report of chitinases from *L. lecanii*.

Chapter 2 explores the biomedical application of hydrophobins class II as nanocarriers for pirarubicin. It addresses the production, characterization, and evaluation in vitro in C26 cells as well as in vivo in mice carrying colon adenocarcinoma tumors of the formulated nanoparticle systems.

In Chapter 3, residual biomass from submerged crops is used to obtain and purify hydrophobins class I and II, which are used as biolubricants in turning processes. The physicochemical, tribological, and microbiological properties of the formulated emulsions are evaluated, thus proposing a viable and environmentally friendly alternative to conventional petroleum-based lubricants.

This work presents an integrative strategy for the valorization of *Lecanicillium lecanii* as a versatile biotechnological resource. By linking enzyme production, functional protein applications, and nanomedicine within a single microbial platform, this work contributes original knowledge and practical solutions aligned with the principles of sustainability, innovation, and translational impact. In this way, large-scale production and multifunctional use of chitinases and hydrophobins not only contribute to the development of sustainable bioprocesses but also promote the efficient use of biological resources through the recovery of multiple biomolecules from the same crop, integrating applications in the industrial and biomedical sectors with significant impact.

Justification

Currently, the use of proteins and enzymes has become highly relevant due to the wide range of biotechnological and industrial applications they offer. Among these, chitinases stand out for their ability to hydrolyze chitin or chitosan, generating chitins of different molecular weights and chitooligosaccharides (COS), which have antioxidant, antibacterial, and antitumor properties (Wu *et al*., 2013; Zou *et al*., 2018; Zhai *et al*., 2021; Liu *et al*., 2022). Currently, commercially available chitinases are mainly produced by bacteria of the genus *Bacillus* and *Streptomyces* (Sigma-Aldrich, 2023; Creative Enzyme, 2023). However, most

of the reported studies are limited to the laboratory scale. In this context, increasing interest in chitosan-derived materials and chitooligosaccharides due to their recognized bioactivity, biodegradability, and wide applicability in pharmaceutical, agricultural, and food industries. Despite this interest, the controlled enzymatic production of chitosan derivatives at pilot and industrial scales remains limited by enzyme availability, process scalability, and reproducibility.

In this context, hydrophobins, amphiphilic proteins with the ability to self-assemble on surfaces, improving adhesion to hydrophobic surfaces and stabilizing oil/water emulsions, are produced in the same culture like chitosanases, they have been studied in a variety of applications due to these characteristics, such as oil recovery, as an excipient for oral drugs, and pesticide detection (Rocha-Pino *et al*., 2018; Rojas-Osnaya *et al*., 2024).

On the other hand, replacing hydrocarbon derivatives in industrial applications is an urgent necessity due to their environmental impact. In this regard, biolubricants made from natural sources represent a sustainable alternative to conventional lubricants, as they are biodegradable, renewable, and less toxic (Narayana *et al*., 2022). However, biolubricants have limitations related to their stability, tribological behavior, and compatibility with different surfaces.

Furthermore, due to their biocompatible nature and their ability to evade and minimize interactions with biological fluid components, thereby avoiding detection by the mononuclear phagocytic system responsible for eliminating harmful or foreign particles in the body, HFBs have also been proposed as nanocarriers in drug delivery systems (Fang *et al*., 2014). The International Agency for Research on Cancer (IARC) estimates that by 2040 the number of people with cancer will increase to 26 million, making it extremely important to develop new coatings that improve the bioavailability, stability, and specificity of drugs (Ferlay *et al*., 2020). Generally, the use of free chemotherapeutic agents has a significant disadvantage due to their low specificity and the significant toxic effects they generate (Ding *et al*., 2017). Such is the case with pirarubicin (THP), an antibiotic of the anthracycline family, which has been widely used as a first-line treatment in various types of cancer, such as hematological neoplasms, acute leukemias, malignant lymphomas, breast cancer, and

colon cancer (Greish *et al.,* 2005). Its unrestricted use has severe adverse effects, such as hepatotoxicity, cardiotoxicity, and nephrotoxicity.

Hypothesis

Chitosanase type I obtained from *L. lecanii* cultures will enable the hydrolysis of chitosans with a specific degree of polymerization which, in conjunction with HFBs I and II, will produce a nanocarrier for pirarubicin that will improve the low water solubility and cytotoxicity of the free drug.

Objectives

General objective:

- Produce and purify chitosanolytic enzymes and hydrophobins from *Lecanicillium lecanii* in submerged cultures for use in the development of a drug nanocarrier and as a biolubricant.

Specific objectives:

- Produce chitosanolytic enzymes and hydrophobins in submerged cultures of *L. lecanii*.
- Design a comprehensive treatment process for the purification of chitinases and hydrophobins.
- Characterize the chitosanases and hydrophobins obtained.
- Produce and characterize hydrophobin-jatropha oil-based emulsions as biolubricants.
- Evaluate the viability of the biolubricant in real lathe machining processes, as well as its microbiological implications.
- Produce and characterize a hydrophobicin-chitosan-based nanocarrier for the encapsulation of pirarubicin.
- Study the effects of the nanocarrier on the release of pirarubicin, its cytotoxic effects in vitro and in vivo, as well as its antitumor activity in murine systems.

Chapter 1: Low molecular weight chitosan and chitooligosaccharides produced by chitosanases from *Lecanicillium lecanii* in pilot-scale submerged cultures.

1.1. Introduction

Chitosanases (EC 3.2.1.132) are enzymes of the glycosyl hydrolase family with the ability to rupture β-(1,4)-glycosidic bonds present in chitosan chains, releasing profusely *D*-glucosamine (GlcN), *N*-acetyl-*D*-glucosamine (GlcNAc), and oligosaccharides. Based on substrate specificity, the classification of these enzymes is into three subclasses: subclass I: those that can cleave GlcNAc-GlcN and GlcN-GlcN bonds; subclass II enzymes that can only cleave GlcN-GlcN bonds; and subclass III can cleave GlcN-GlcNAc and GlcN-GlcN bonds (Thadathil and Velappan, 2014). All subclasses cannot cleave GlcNAc-GlcNAc bonds. The ability of chitosanases to break down partially deacetylated chitosan depends on the type of glycosidic bonds present in the chain and the degree of acetylation (DA) of the chitosan. The identity of the reducing and non-reducing ends in the chain determines the enzyme specificity, controllability, and avoidance of undesirable side products, and enhances bioactivities (Xu *et al*. 2022).

The products of enzymatic chitosan hydrolysis are low molecular weight chitosan (LMWC) and chitooligosaccharides (COS). LMWC has been studied in drug delivery systems due to its advantage of more efficient renal clearance compared to high or medium molecular weight chitosans (Kean and Thanou, 2010). Additionally, it has been explored as a dietary supplement, as it mitigates the toxic effects of heat-processed toxins, such as acrylamide, by reducing oxidative stress, preserving mitochondrial function, and supporting developmental processes (Kumar and Mohideen, 2025). The chemical breakdown of chitosan produces a heterogeneous mixture of COS, which hampers the identification of its structure and bioactivity. In this regard, COS are used as prebiotics in food (Xu *et a*l. 2022). However, for more specific applications, such as in the pharmaceutical 64 industry, the degree of polymerization and DA are crucial for their mucosal adhesion and antioxidant activity (Thomas *et al.* 2023), and also in agriculture because they exhibit antimicrobial properties (Wang *et al*. 2021). This diversity of applications underscores the potential of chitosanases in various industries, encouraging their large-scale production. On the one hand, there are several efforts on the use of *Escherichia coli* and *Pichia pastoris* as hosts for heterologous

expression (Liu *et al.* 2009; Luo *et al.* 2020). Promising studies are using recombinant chitosanases, such as enzymes from *Bacillus* expressed in *E. coli*, in a soluble and active form; however, their production needs further research and development, as it requires lysis to release the recombinant chitosanase (Liu *et al*. 2009). The cost of downstream processing hinders large-scale production. Additionally, *E. coli* produces inclusion bodies and demands an expensive transcriptional inducer for the cloned gene (Brzezinski, 2011). Luo *et al*. (2020) claimed that *P. pastoris* was efficient in the production of extracellular chitosanase of *Bacillus amyloliquefaciens*, achieving protein folding with high cell density in fermentation and offering genetic stability (Pan *et al*. 2022). Nevertheless, the AOX1 promoter of *P. pastoris* is induced by methanol, which is toxic, flammable, and explosive. Another drawback is that cultures with added methanol require more oxygen, thus making aeration a hurdle in industrial-scale fermentation (Pan *et al*. 2022).

On the other hand, bacteria and fungi are capable of producing chitosanases (Kumar *et al*. 2020; Thadathil and Velappan, 2014). Bacteria as chitosanase-producing microorganisms have the constraint that chitosan exerts inhibitory action, slowing down the bacterial growth (Brzezinski, 2011). Fungi from the genera *Aspergillus*, *Gongronella*, *Trichoderma*, and *Fusarium* have also been reported as chitosanase producers, 87 presenting suitable excretion protein systems (Wang *et al*. 2008; Thadathil and Velappan, 2014; Xu *et al.* 2022; Abedin *et al.* 2023). Other advantages are that fungi are capable of growing in low water activity substrates, limiting bacterial contamination, and also are tolerant to acidic pH (Matsumoto *et al*. 2004), offering the possibility of better chitosan availability, since chitosan dissolves at pH<6. In this regard, *Lecanicillium lecanii* is an entomopathogenic fungus that produces chitinases, proteases, and lipases that can be produced in solid and submerged cultures (Matsumoto *et al.* 2004; Fenice *et al*. 2012; Rocha-Pino *et al.* 2013; Rojas-Osnaya *et al*., 2020). In spite of this, chitosanases have also been identified through *L. lecanii* genome analysis in the Kyoto Encyclopedia of Genes and Genomes database (KEGG) and BLASTP (Radwan *et al*. 2019). So far, there are no reports of chitosanases produced by the genus *Lecanicillium*. Moreover, this study presents an approach to pilot-scale submerged culture (50 L), purification, and characterization of chitosanases for the production of COS and LMWC.

1.2. Materials and methods

1.2.1. Materials

Chitosan was obtained by heterogeneous deacetylation of biologically extracted chitin. Chitin was extracted from *Litopenaeus vannamei* cephalothoraces, employing successive solid-state fermentations of *Lactobacillus brevis* and *Rhizopus oligosporus* (Aranday-García *et al.* 2017). Chitosan characterization involved the determination of ash, moisture, fat, and residual protein contents, as well as the molecular weight by intrinsic viscosity and the DA by proton nuclear magnetic resonance (^{1}H NMR) (AOAC, 1977; Aranday-García *et al*. 2017). Glycol chitosan, chitinase from *Streptomyces griseus*, and cellulase from *Trichoderma longibranchiatum* were purchased from Sigma-Aldrich (St. Louis, US). COS were purchased from Kitto Life (Pyeongtaek-si, South Korea). All other chemicals and reagents used in this study were of analytical grade.

1.2.2. Starter Culture

The inoculum consisted of a spore suspension in Tween 80 (0.01% w v^{-1}) with a final concentration of $1x10^7$ spores mL^{-1} obtained from potato dextrose agar culture of *Lecanicillium lecanii* (ATCC 26854) strain at 28°C.

1.2.3. Chitosanases production in submerged cultures

Submerged cultures in a 3 L bioreactor (Applikon BV, Delft, Netherlands) with Czapeck medium supplemented with 5, 10, or 15 g L^{-1} of chitosan (DA 18.6%). The chitosan suspension as sole carbon source was prepared by dissolution of chitosan (30 g L^{-1}) in acetic acid solution (0.1 M) under constant stirring. The concentrated chitosan solution was sterilized and added to the medium according to the final concentration (5, 10, or 15 g L^{-1}). The composition of the Czapeck medium (g L^{-1}) was $NaNO_3$ (3.73), Na_2HPO_4 (3.0), $MgSO_4$ (0.5), KCl (0.5), and $FeSO_4$ (0.096). The culture medium was inoculated with *L. lecanii* spore suspension up to $1x10^7$ spores mL^{-1} at pH 6 and 28°C for 144 h (Matsumoto *et al*. 2004). The rotation speed of 100, 125 or 150 rpm were tested. Further, chitosan concentration and rotation speed was selected based on the highest chitosanase activity, and growth. The submerged cultures using Czapeck medium supplemented with chitosan were scaled up in a stirred tank bioreactor of stainless steel with a reactor and impeller diameter ratio, Da/Di, 3.63 and liquid height to impeller diameter ratio, HL/Di, 1.88 and nominal capacity of 70 L,

under culture conditions of 1 volume of air volume of liquid^{-1} min^{-1} (vvm) at 26°C and pH 6 for 144 h.

1.2.3.1. Determination of the volumetric oxygen mass transfer coefficient (k_La), oxygen transfer rate (OTR), and viscosity of culture media.

The volumetric oxygen mass transfer coefficient (k_La) was determined using the gassing-out method, employing nitrogen to displace the oxygen present in the culture (Van Riet, 1979). The oxygen was measured using an AppliSens low drift DO_2 sensor (Applikon BV, Delft, Netherlands). Oxygen transfer rate (OTR) was estimated using the k_La obtained under abiotic conditions and the saturation concentration of oxygen (C*) and oxygen concentration in the media (C) (Michelin *et al.* 2013). The oxygen transfer rate (OTR) was determined using equation 1.

$$OTR = k_L a\left(C^* - C\right) \quad (1)$$

Viscosity was determined experimentally at the initial and final time of culture using a viscometer (Brookfield, Middleborough, US) with an RV-2 cone spindle (Brookfield, Middleborough, US) at several shear rates for 10 min. All viscosity measurements were repeated four times, performed at a constant temperature of 25°C.

1.2.4. Sample analyses

1.2.4.1. Determination of chitosanase activity

Chitosanase activity was determined by quantifying the reducing sugars produced by the hydrolysis of chitosan using the 3, 5-dinitrosalicylic acid (DNS) technique described by Miller *et al.* (1959). In a typical procedure, 150 µL of the EC, pellet (concentrated chitosanase), and supernatants of the salting-out procedure, fractions from chromatographic procedures, or purified chitosanase were mixed with 150 µL of a chitosan solution (1% w/v-1) in acetate buffer (0.1 M) at pH 6. The chitosanase enzyme 153 unit (U) was defined as the amount of enzyme capable of releasing 1 µmol of reducing sugars, equivalent to GlcN min-1 (Kumar *et al.* 2020).

1.2.4.2. Protein content

The concentration of soluble protein in the broth, EC, pellet, supernatants of the salting-out procedure or fractions from chromatographic procedures was determined using the Lowry method, modified by Peterson, with bovine serum albumin as the protein standard (Peterson, 1977). For non-soluble protein, 0.2 g of biomass was treated with 5 ml of boiling H_3PO_4 (0.1 M) for 7 min. It was then subjected to centrifugation at 14,534 x *g* for 15 min at 4 °C, and the protein in the supernatant was determined using the Lowry method, as modified by Peterson (1977).

The experimental data of total protein, soluble protein and non-soluble protein, as an indirect determination of fungal growth were fitted to the logistic model by non-linear regression analysis using STATISTICA 7 (Statsoft, Inc., Tulsa, USA). The logistic model (equation 2) provides suitable prediction of entire growth curve of *L. lecanii*, since lag phase upto stationary phase (Mulchandani *et al*. 1988) (equation 2).

$$P = \frac{P_{\max}}{\left(1+\left(\frac{P_{\max}-P_0}{P_0}\right)\right)e^{(-kt)}} \quad (2)$$

where $P_{\max}$ was the maximum protein concentration in the culture (mg mL^{-1}) at the time, P_0 was the initial product concentration, and k (h^{-1}) is the growth rate constant.

1.2.5. Purification of chitosanases

1.2.5.1. Chromatographic methods

The broth was centrifuged at 14,534 x *g* for 15 min at 4°C (Thermo Scientific, Osterode, Germany), the pellet consisted of biomass while the supernatant was considered the crude enzyme (EC). EC was subjected to precipitation with $(NH_4)_2SO_4$ at 4°C. After centrifugation at 14,534 x *g* for 60 min at 4°C, the pellet and supernatant were separated. Then, the chitosanase activities and soluble protein content were measured in both fractions, as described in sections 2.6.1 and 2.6.2, respectively. Subsequently, the pellet was solubilized in Tris-HCl buffer (0.05 M) and loaded into a HiPrepTM 26/60 Sephacryl™ S-100 (Sigma-Aldrich, St. Louis, US) molecular exclusion column (SEC) in a Fast Protein Liquid Chromatograph (ÄKTA FPLC GE, Uppsala, Sweden). The elution was carried out at an

isocratic flow rate of 1.0 mL min^{-1} using Tris-HCl (0.05 M) at pH 7.8, supplemented with NaCl (0.15 M) (Rojas-Osnaya *et al.* 2020). The fractions with chitosanase activity were concentrated using ultrafiltration units with a 10 kDa molecular weight cutoff membrane (Merck, Darmstadt, Germany). Afterward, the retentate was solubilized in Tris-HCl (30 mM) buffer, pH 7.8, and injected into a DEAE Sepharose anionic exchange column (AEC) (Bio-Rad, Hercules, US). Elution was performed using Tris-HCl (30 mM), pH 7.8, spiked with NaCl (1 M), with a gradient from 0% to 100% at a flow rate of 1 mL min^{-1}. The fractions obtained with chitosanase activity were filtered using ultrafiltration units with a 10 kDa cutoff, as described above.

1.2.5.2. Electrophoretic analysis

The EC and the fractions obtained were analyzed by electrophoresis using one-dimensional acrylamide gels under denaturing conditions (SDS-PAGE), as proposed by Laemmli (1970), with Precision Plus Protein Standard Unstained (Bio-Rad, Hercules, US) as a reference. The gels were stained with Coomassie blue R-250 (Bio-Rad, Hercules, CA, USA) and analyzed using ImageJ 1.41 (National Institutes of Health, USA) (Schneider *et al.* 2012).

Zymograms were conducted on acrylamide gels under semi-denaturing conditions using 4-methylumbelliferyl-*N*-acetyl-β-*D*-glucosamine and chitosan glycol as substrates to confirm the presence of enzyme activity during each purification step. Renaturation was promoted by incubating the gel for 6 h at 20 °C in acetate buffer (50 mM) with 1% (v v^{-1}) Triton X-100. The enzymatic reaction was promoted by placing the gel in agitation in acetate buffer (pH 6) at 50 °C for 1 h. In gel disclosure zymogram with 4-methylumbelliferyl-*N*-acetyl-β-*D*-glucosamine, the enzyme activity was visualized as fluorescent zones under ultraviolet illumination employing a UV Transilluminator 2000 (Bio-Rad, Hercules, US) (Rojas-Osnaya *et al.* 2020).

On the other hand, gels with glycol chitosan were stained with Congo red at 0.1% (w v^{-1}) for 15 min and subsequently washed out with a NaCl (1 M) solution until discolored bands appeared (Lee *et al.* 2014).

1.2.6. Establishment of conditions of chitosanase activity on the hydrolysis of chitosan: reaction products

1.2.6.1. Determination of reaction time, substrate and enzyme concentration on the hydrolysis of chitosan

The effect of independent variables time (*Xi*), substrate (*Xj*), and enzyme concentrations (*Xk*) on the dependent variable concentrated chitosanase activities on the chitosan hydrolysis (*Y*) was established using response surface methodology and Box-Behnken design, the latter was applied to identify the independent variable levels (Table 1). The variables were coded according to equation 3 (Abedin *et al*. 2023).

$$Xi = \frac{Xi - \left[\frac{(Xi\max + Xi\min)}{2}\right]}{\frac{(Xi\max + Xi\min)}{2}} \qquad (3)$$

where *Xi* is the coded value; *xi* is the experimental value; *xi* max and *xi* min are the maximum and minimum values, respectively. The concentrated chitosanase specific activities were adjusted by a second-order polynomial function using the SPSS program (equation 4).

$$y = \beta_0 + \sum_{i=1}^{k}\beta_i X_i + \sum_{j=1}^{k}\beta_j X_j + \sum_{k=1}^{k}\beta_k X_k + \sum\sum_{ik}\beta_{ik} X_i X_k + \sum\sum_{ij}\beta_{ij} X_i X_j + \sum_{i=1}^{k=2}\beta_{ii} X_i^2 + \sum_{j=1}^{k=2}\beta_{jj} X_j^2 + \sum_{k=1}^{k=2}\beta_{kk} X_k^2 \qquad (4)$$

where *y* is the predicted concentrated chitosanase specific activity; β_0, β_i, β_j, β_k, β_{ij}, β_{ik}, β_{ii}, β_{jj}, β_{kk} are regression coefficients of the model for the constant, linear, interaction, and quadratic effect, respectively, and *Xi, Xj, Xk* are the coded independent variables. The response surface plots were performed using STATISTICA 7.

Table 1. Box-Behnken matrix for time, enzyme, and substrate concentrations for concentrated chitosanase specific activity.

Time (min)	Enzyme (U mL^{-1})	Substrate (g L^{-1})
31.5	0.06	20
31.5	0.015	1
60	0.0375	20
3	0.0375	20
31.5	0.0375	10.5

31.5	0.0375	10.5
60	0.0375	1
60	0.06	10.5
31.5	0.015	20
31.5	0.0375	10.5
31.5	0.06	1
31.5	0.0375	10.5
3	0.015	10.5
60	0.015	10.5
3	0.06	10.5
3	0.0375	1

1.2.6.2. Determination of pH and temperature for chitosanase activity

The pH and temperature of the purified chitosanase activities were determined using the selected reaction time (15 min), enzyme (0.07 U mL^{-1}), and substrate (10 g L^{-1}) concentrations by the response surface methodology explained in section 2.6.1. The pH of the reaction media was tested in a range of 3 to 6.5, employing an acetate buffer (30 mM). The temperature was varied from 15 to 65 °C at the pH selected.

1.2.7. Characterization of reaction products: COS and chitosan

The COS obtained from the enzymatic reaction under conditions of pH and temperature previously determined in section 2.53 was analyzed by thin-layer chromatography (TLC) using a silica gel plate (HX745188, Merck, Darmstadt, Germany) that was eluted with a methanol: water (7:3) mobile phase. Subsequently, it was developed using a mixture of silver nitrate (3 g) and acetone (500 mL). The plate was allowed to dry for subsequent addition with NaOH (10 N, 50 mL) in ethanol (450 mL) (Gal, 1968).

The hydrolysis products were lyophilized and subsequently solubilized in 1 µL methanol: water mixture (7:5) and mixed with 2 µL of the matrix (25 g L^{-1} of 2,5-dihydroxybenzoic acid (DHB) in acetonitrile, containing 0.1% v v^{-1} of trifluoroacetic acid). The samples were analyzed using a MALDI-TOF/TOF Autoflex speed (Bruker Daltonics, San Jose, USA). The acquisition of the spectra was carried out in positive mode using a reflector-type detector with a stopping range of 200-3500 m z^{-1}, equipped with a Smart Beam-II solid-state laser (Bruker Daltonics, San Jose, US) and an ionization source voltage of 19 kV (Rojas-Osnaya *et al.,* 2020). The degree of acetylation (DA) in COS was calculated using the theoretical DA

value of the species from degree of polymerization (DP) of 3 to 6 (DA_{th}), and the intensity of the ion (I) obtained from MALDI-TOF/TOF analysis (Trombotto *et al.* 2008) according to equation 5.

$$DA(\%) = \frac{\sum_i DA_{th}(\%) \times (I)}{\sum_i (I)} \qquad (5)$$

Molecular weight determination of chitosans produced by enzymatic hydrolysis was carried out by intrinsic viscosity (Mv). Chitosans were dissolved in a solution of acetic acid (2%) and sodium acetate (0.2 M) at concentrations of 0.5, 1, 2, 3 and 4 g L^{-1}. Mv was determined using an Oswald-type viscometer of 0.4 mm diameter at 25°C, using the Mark-Houwink-Sakurada equation (equation 6)

$$\eta = KM_v^a \quad (6)$$

where: M_v is the viscometric molecular weight; K is 1.38×10^{-5} L g^{-1}, and a is 0.85 (Kjøniksen *et al.* 1997).

For the determination of the DA of the chitosans produced by enzymatic hydrolysis, samples were dissolved in D_2O acidified with HCl (1.16 mg mL^{-1}) and analyzed by proton nuclear magnetic resonance (^1H NMR) spectroscopy in a Bruker AVANCE-III 500 spectrometer (San Jose, US) at 200 MHz using as dissolvent DCl/D_2O, DA was calculated according to the integration of signals on the spectra (Aranday-García *et al.* 2017).

1.2.8. Statistical analysis

Statistical analysis of the experimental data was performed using analysis of variance and Tukey-Kramer's multiple comparisons of means, as implemented in SPSS software version 22.0 (IBM Corp., Armonk, US). The significant statistical differences in means were considered at $p \leq 0.05$ and are presented as different letters among chitosan characterization before and after sterilization, culture conditions, saturation with ammonium sulfate, pH, and temperature of the enzymatic reaction.

1.3. Results and discussion

1.3.1. Effect of chitosan concentration in the media on the fungal growth and production of extracellular chitosanases.

Chitosan before and after sterilization was characterized, and no significant differences were detected after heat treatment; only a significant reduction of ash content was determined due to the demineralization for the acidic condition and temperature (Table 2).

Table 2. Physicochemical characterization of chitosan before and after sterilization.

Sample	Chitosan	Chitosan after sterilization
Protein (% dry basis)	0.37 ± 0.04^{a}	0.3 ± 0.04^{a}
Ash (% dry basis)	15.15 ± 0.28^{a}	7.38 ± 0.14^{b}
Fat (% dry basis)	0.13 ± 0.09^{a}	0.12 ± 0.02^{a}
Degree of acetylation (%)	18.56 ± 0.39^{a}	18.15 ± 0.47^{a}
Mv (kDa)	121.42 ± 26.74^{a}	130.74 ± 4.68^{a}

Different letters between indicate significant differences between treatments, as determined by Tukey-Kramer's multiple comparisons of means ($p < 0.05$).

The chitosan was assimilated as the sole carbon source; the results of total protein, an indirect measurement of fungal growth, provided significant evidence that *L. lecanii* produced the necessary machinery for chitosan assimilation as a sole carbon source (Figure 1). The highest production rate was estimated for the medium supplemented with 5 g L^{-1} of chitosan (0.121 h^{-1}); however, the medium supplemented with 10 g L^{-1} produced higher total protein content (1.564 mg mL^{-1}) than the medium supplemented with 5 g L^{-1} (1.167 mg mL^{-1}). The lowest total protein content was observed at 15 g L^{-1} (0.928 mg mL^{-1}), which can be attributed to oxygen limitation, as k_La was 4.7-fold lower than that at 10 g L^{-1} (6.3 h^{-1}) (Figure 1A, Table 3). Chitosanases are extracellular enzymes (Brzezinski, 2011); therefore, it was not necessary to disrupt the cells, only the biomass was separated, and the supernatant contained the enzyme. The secreted chitosanases hydrolyzed chitosan with the release of reducing sugars in the broth (COS with reducing ends or the monomers, GlcN and GlcNAc), indicating the *L. lecanii's* ability to assimilate chitosan present in the culture medium as a sole carbon source. The highest reducing sugar concentration was recorded at 144 h, with culture

supplemented with 10 g L^{-1} and 125 rpm (0.3 ± 0.008 mg mL^{-1}), which is in agreement with the fungal growth (P_{max} 2.321 ± 0.195 mg mL^{-1}) (Figure 1B, Table 3).

The chitosanase production in a culture with added chitosan 10 g L^{-1} was significantly higher than in 5 and 15 g L^{-1} submerged cultures, which was directly attributed to the fungal growth. The specific chitosanase activity at 10 g L^{-1} was 1.16 and 1.28 fold higher than that obtained at 5 and 15 g L^{-1}, respectively (Table 3). The plausible explanation was the higher viscosity of the chitosan culture at 15 g L^{-1} (43.2 ± 0.3 cP) compared to those at 5 and 10 g L^{-1}, 18.7 ± 0.12 and 29.6 ± 0.23 cP, respectively. Since the viscosity is a factor that affects oxygen transfer and also favors the presence of heterogeneous, unmixed zones within the bioreactor, it negatively impacts fungal growth and, thus, enzyme production (Figure 1). Dispersed mycelia in a stirred tank bioreactor may increase medium viscosity during the submerged culture, thereby reducing fungal growth and enzyme production (Michelin *et al,* 2013).

Nevertheless, a decrease in viscosity was observed after 168 h, which was more closely related to the chitosan concentration in the media and its hydrolysis rather than the mycelial growth (Figure 1, Table 3). The reduction of viscosity in the broth was from 18.7± 0.12 cP to 12.4± 0.28 cP for 5 g L^{-1}; 29.6 ± 0.23 cP to 24.7 ± 0.11 for 10 g L^{-1}, and 43.2 ± 0.3 cP to 22.21± 0.22 cP for 15 g L^{-1}. It is worth noting that no pellet formation occurred, which has been reported not to increase culture broth viscosity (Michelin *et al.,* 2013). Therefore, based on growth and chitosanase production, 10 g L^{-1} was selected for further experimentation, with constant aeration (1 vvm). The agitation rate was increased from 100 rpm to 125 rpm and 150 rpm (Figure 1A and 1C). The augmentation of the agitation rate increased k_La from 6.3 at 100 rpm to 7.51 and 7.32 h^{-1} at 125 rpm and 150 rpm, respectively. The growth was also affected by the highest P_{max} at 125 rpm. Similarly, the volumetric chitosanase activity was higher at 125 rpm than at 150 rpm (Figure 1, Table 3). Therefore, this agitation rate and 10 g L^{-1} were chosen for the 50 L scale-up.

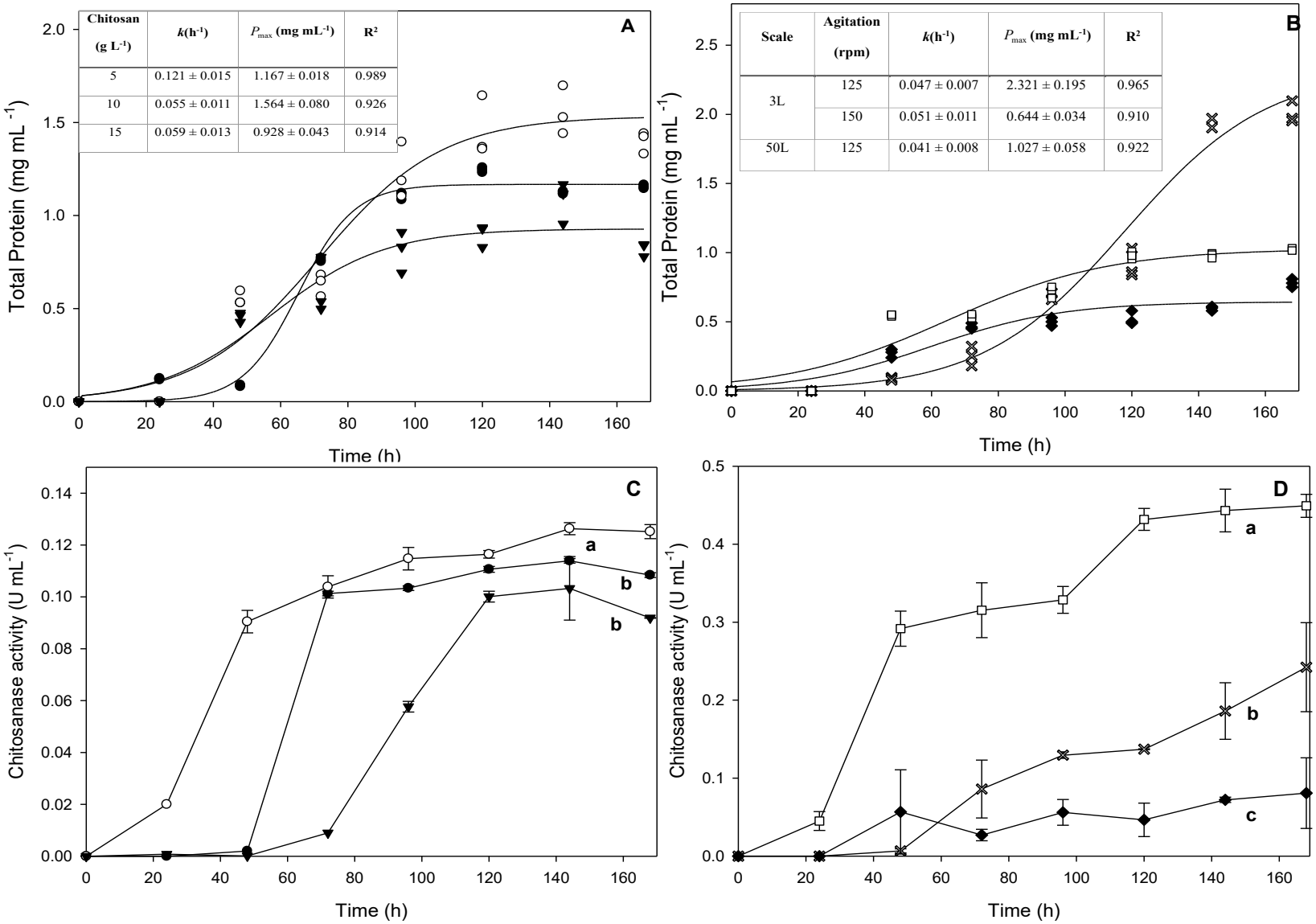
A
Chitosan (g L-1) | k(h-1) | Pmax (mg mL-1) | R2
5 | 0.121 ± 0.015 | 1.167 ± 0.018 | 0.989
10 | 0.055 ± 0.011 | 1.564 ± 0.080 | 0.926
15 | 0.059 ± 0.013 | 0.928 ± 0.043 | 0.914
Total Protein (mg mL -1)
Time (h)
B
Scale | Agitation (rpm) | k(h-1) | Pmax (mg mL-1) | R2
3L | 125 | 0.047 ± 0.007 | 2.321 ± 0.195 | 0.965
3L | 150 | 0.051 ± 0.011 | 0.644 ± 0.034 | 0.910
50L | 125 | 0.041 ± 0.008 | 1.027 ± 0.058 | 0.922
Total Protein (mg mL -1)
Time (h)
C
a
b
b
Chitosanase activity (U mL-1)
Time (h)
D
a
b
c
Chitosanase activity (U mL-1)
Time (h)

Figure 1. Time course of total protein as indirect measurement of growth, and chitosanase activities of submerged culture of *L. lecanii* at pH 6 and 28°C employing chitosan with DA 18.6% as sole carbon source at concentrations of 5 g L^{-1}(●), 10 g L^{-1}(○) and 15 g L^{-1} (▼) and 100 rpm in 3L bioreactor (A); 10 g L^{-1} at 125 rpm (✖) and 150 rpm (◆) in 3L bioreactor at 125 rpm (□) in 50L bioreactor (B); chitosanase activity at 100 rpm (C), chitosanase activity in 3L and 50L scales (D). The protein concentration data were fitted to the logistic model

1.3.2. Scale-up of chitosanase production in 50L bioreactor.

Chitosanase scaled-up bioprocess is essential to produce LMWC and COS, especially when commercial chitosanases are unavailable. Among the methods used for scaling up aerobic bioprocesses, maintaining a constant k_La is commonly employed, considering the oxygen transfer limitations due to its low solubility in water (Michelin *et al.,* 2013). In the present study, the k_La of the 3 L bioprocess, with 10 g L^{-1} of chitosan added to the medium and operating at 125 rpm, was selected for scaling up from 3 L to the pilot plant of 50 L. Scaling from the laboratory to the pilot plant with a ratio of 1:13.7 was performed, yielding k_La values of 7.51 and 7.83 for the 3 L and 50 L bioreactors, respectively. Similarly, the OTR presented differences between the 3L and 50L scales, at 1.56 mmol $L^{-1}h^{-1}$ and 1.66 mmol $L^{-1}h^{-1}$, respectively. Although the operating parameters for aeration and agitation remained constant during the scale-up from 3 to 50 L, the observed increase in k_La and OTR can be attributed to changes in the reactor geometry and hydrodynamic regime, which favored greater gas-liquid dispersion efficiency, a larger interfacial area, and an effective increase in the mass transfer coefficient.

Several factors affect volumetric activity, including k_La, substrate concentration, pH, temperature, biomass, and shear stress. In this regard, the volumetric activity was particularly relevant due to the 50L bioreactor's higher operating volume, which was 2.4-fold that of the 3L culture. The increase observed in the k_La and OTR values indicates better aeration, which favors homogeneity in the culture and oxygen transfer at the gas-liquid interface, with the consequent augmentation of chitosanase activities (Table 3).

The estimated growth parameters between reactor scales are shown in Figure 1. The *k* was lower in 50L than in 3L, indicating that the growth of *L. lecanii* was slightly affected by the working volume. As well, the Pmax (maximum protein concentration) was lower in the 50L

bioreactor than in the 3L bioreactor by 0.5 fold. Therefore, adequate scaling was achieved for this fermentation system; despite the reduction in fungal growth, the specific chitosanase activity was significantly higher in 50L, at 0.202 U mg^{-1}, than in 3L, at 0.123 U mg^{-1}.

Table 3. Reducing sugars and chitosanase activities in 144 h submerged cultures of *L. lecanii* using Czapeck medium with added chitosan (DA 18.6 %) at pH 6 and 28°C, and k_La determinations in bioreactors of 3 and 50 L.

Scale	Chitosan (g L^{-1})	rpm	k_La (h^{-1})	Reducing sugar (mg mL^{-1})	Chitosanase activity (U mL^{-1})	Specific chitosanase activity (U mg^{-1})
3L	5	100	5.89 ± 0.13^{c}	0.226 ± 0.002^{c}	0.114 ± 0.001^{bc}	0.106 ± 0.001^{b}
	10	100	6.3 ± 0.33^{bc}	0.254 ± 0.005^{bc}	0.126 ± 0.002^{bc}	0.146 ± 0.018^{ab}
	15	100	1.32 ± 0.45^{d}	0.203 ± 0.028^{c}	0.103 ± 0.012^{c}	0.096 ± 0.005^{b}
	10	125	7.51 ± 0.41^{ab}	0.300 ± 0.008^{b}	0.186 ± 0.066^{b}	0.123 ± 0.050^{b}
	10	150	7.32 ± 0.32^{ab}	0.217 ± 0.001^{c}	0.072 ± 0.003^{c}	0.150 ± 0.013^{ab}
50L	10	125	7.86 ± 0.04^{a}	0.860 ± 0.053^{a}	0.443 ± 0.027^{a}	0.202 ± 0.012^{a}

Different letters between columns indicate significant differences between treatments, as determined by Tukey-Kramer's multiple comparisons of means ($p < 0.05$).

1.3.3. Purification of chitosanases

The EC was subjected to the salting-out process with $(NH_4)_2SO_4$. The highest enzymatic activity in the pellet after precipitation was achieved at 60% and 80% saturation, with significant differences observed between 20% and 40% (Figure 2). Therefore, the saturation percentage was established at 60% based on the highest amount of recovered enzyme.

Later on, SEC was used to separate proteins by their molecular sizes (Figure. 3A). The fractions collected of SEC with chitosanase activity, 19 and 20, were ultrafiltrate in a 10 kDa molecular weight cutoff membrane. The retentate was injected into an anionic exchange column in a FPLC. The fraction 20 obtained after AEC displayed chitosanase activity and was then collected (Figure 3B) and subjected to SDS-PAGE (Figure 3C).

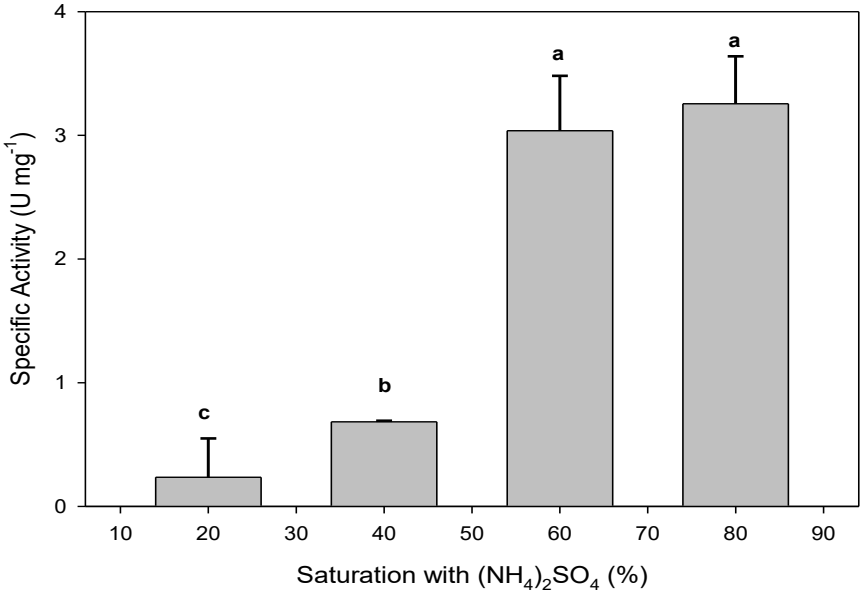

Figure 2. Precipitation of chitosanases present in the EC with $(NH_4)_2SO_4$ (%) at several percentages of saturation, different letters indicate a significant difference between treatments by Tukey Kramer multiple comparisons of means ($p \leqslant 0.05$).

Molecular weights of fungal chitosanases *Gongronella butleri* of 47 kDa (Seki *et al*., 2019) and *Mucor circinelloides* (Struszczyk *et al.,* 2009) of 42-43 kDa have been reported; these results are similar to those obtained in the present work, where the chitosanases showed a molecular mass of 44 kDa. However, so far, there are no reports of chitosanases obtained from *L. lecanii*. It is worth noting that another protein band at 31 kDa was detected, which may be due to an isoform of chitosanase (Figure 3C). The expression of chitosanase isoforms has been reported in the endophytic fungus *Pochonia chlamydosporia*, which is used in the biocontrol of nematodes when chitosan is present in the medium. This chitosanase isoform may be involved in the degradation of the supplemented chitosan medium, whereas other isoforms are expressed to rupture biopolymers in fungal cells or nematode egg walls (Sambles *et al.,* 2022). The production of chitosanase isoforms might be related to the

antagonistic process, as de Santana *et al*. (2015) also reported the production and purification of chitosanases, 35 and 45 kDa, from the entomopathogenic fungus *Metarhizium anisopliae*.

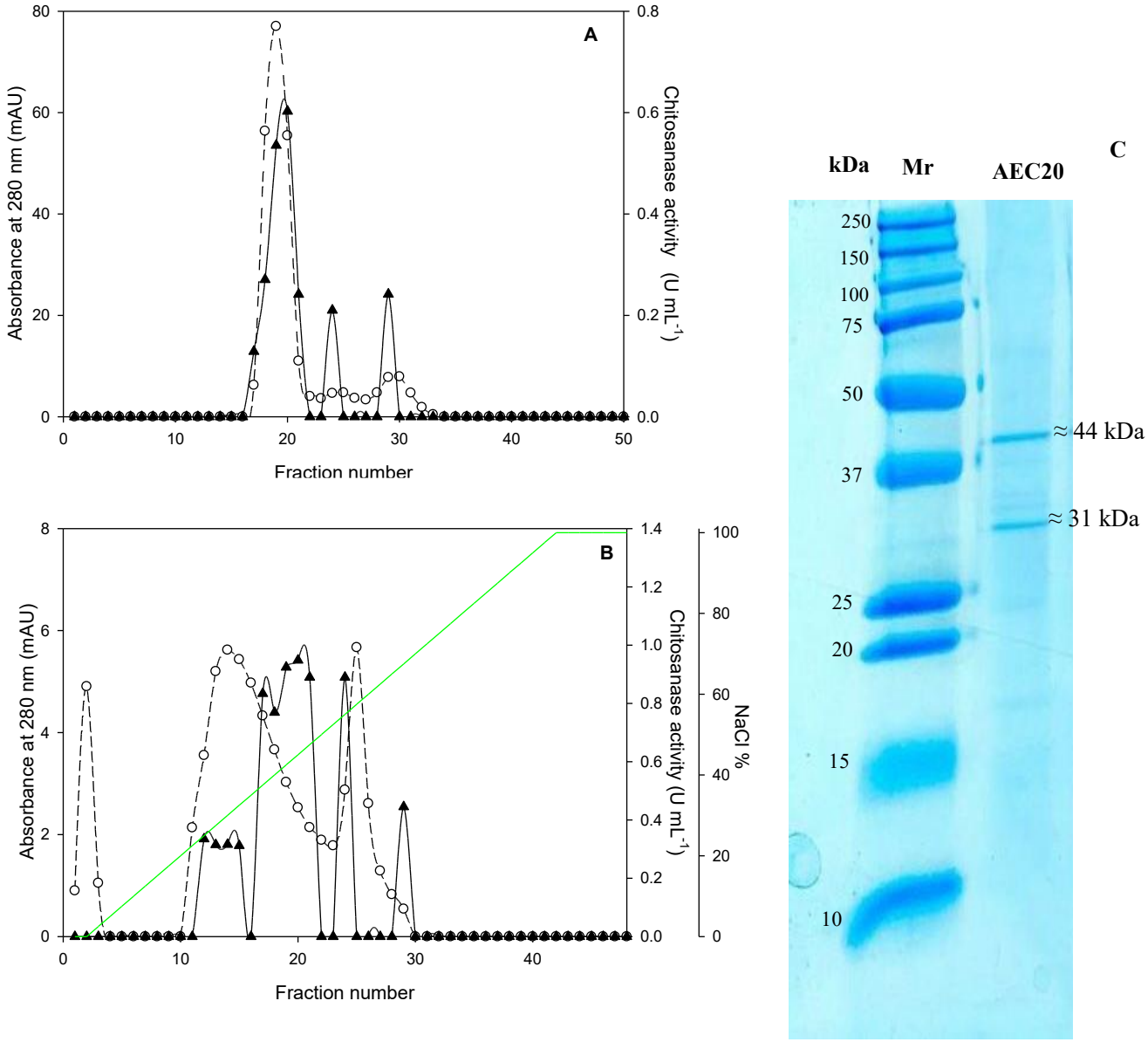

Figure. 3 Chromatograms of fractions injected on SEC eluted with Tris-HCl (0.05 M) buffer spiked with NaCl (0.15 M) at pH 7.8 (A), retentate of SEC fractions 19 and 20 injected into AEC eluted with a gradient of 0-100% NaCl (1 N) (B), SDS-PAGE stained with Coomassie blue of fractions obtained from AEC fraction 20 (C). Absorbance (○); chitosanase activity (▲).

Table 4 presents the purification steps employed to obtain chitosanases from *L. lecanii*. It can be observed that as the purification progressed, the specific activity increased, reaching a final value of 25.97 U mg^{-1} of protein and a purification factor of 319.7. The enzyme recovery (14.82%) was higher than that reported for chitosanases from *Mucor circinelloides* (4.6%) (Struszczyk *et al.,* 2009) and *Penicillium oxalicum* (3.2%) (Cao *et al.,* 2022). The specific activity of the chitosanase was higher than that of *Aspergillus fumigatus* (8.8 U mg^{-1} of protein) (Hirano *et al*. 2012), but lower than other extracellular chitosanases, such as *Gongronella butleri* with 64.6 U mg^{-1} of protein (Seki *et al.,* 2019).

Table 4. Purification stepwise of chitosanases from *L. lecanii* produced in 50 L submerged culture at pH 6 and 28°C.

Purification step	**Volume (mL)**	**Total Protein (mg)**	**Total Activity (U)**	**Specific Activity (U mg^{-1})**	**Purification Factor**	**Recovery (%)**
EC	1350	2099.40	170.52	0.081	1.00	100
$(NH_4)_2SO_4$ Precipitation	60	22.42	76.56	3.41	42.04	44.90
SEC (fractions 19 and 20)	45	2.953	27.12	9.18	113.07	15.90
AEC (Purified chitosanase)	23	0.973	25.28	25.97	319.71	14.82

Zymograms were performed under semi-native conditions, using 4-methylumbelliferyl-*N*-acetyl-β-*D*-glucosamine and glycol chitosan as substrate. As shown in Figure 4, the release of the methylumbelliferyl group, resulting from the cleavage of the GlcNAc bond, caused fluorescence when observed under UV light, thereby corroborating *N*-acetyl glucosaminidase activity (Rojas-Osnaya *et al.*, 2020). On the other hand, glycol chitosan, a deacetylated substrate, allows us to identify the type of chitosanase subclass present in the cultures, employing Congo red staining to visualize the bands. This dye interacts with the (1→4)-β-*D*-glucan bonds in the glycol chitosan (Lee *et al.,* 2014). It can be observed in the zymogram with glycol chitosan that the clear zones in the gel are due to the cleavage of the bond between two glucosamine units, which prevents the interaction of Congo red with the glycol chitosan.

The chitosanases hydrolyzed the bond between GlcNAc-GlcN, as shown with 4-methylumbelliferyl-*N*-acetyl-β-*D*-glucosamine as substrate, as well as the bond between GlcN-GlcN when glycol chitosan was the substrate (Thadathil and Velappan, 2014; Xu *et al.,* 2022). Therefore, the chitosanases produced by *L. lecanii* ATCC 26854 in chitosan-supplemented submerged cultures are not a subclass II, and accordingly with their activities can belong to subclass I or III.

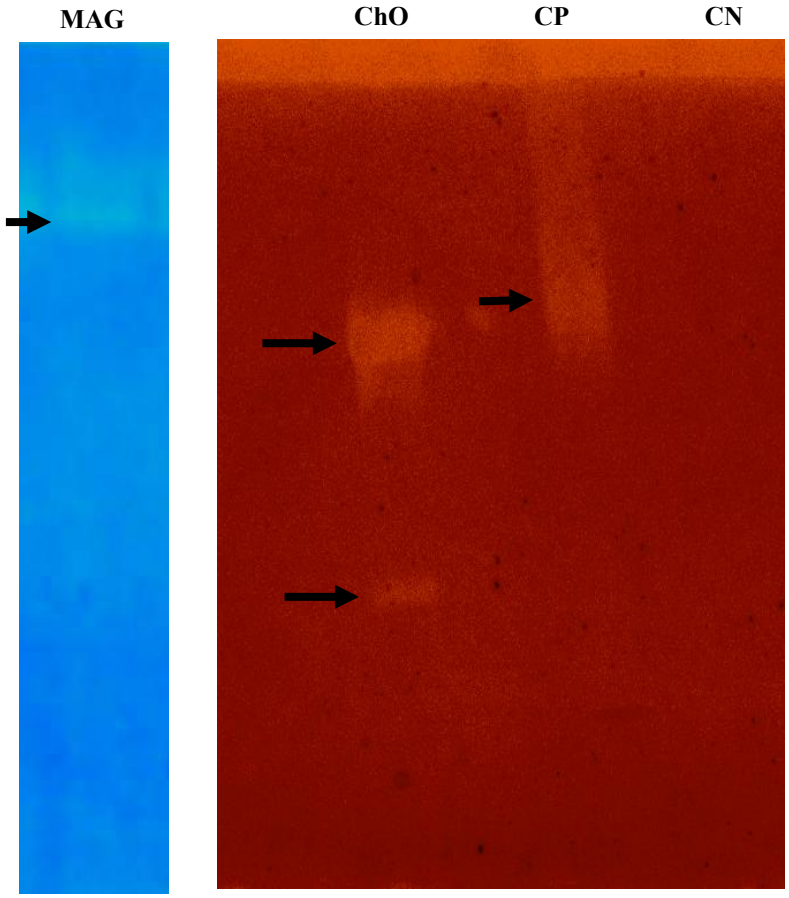

Figure 4. Zymogram of chitosanase activity in SDS-PAGE under semi-denaturing conditions employing as substrate 4-methylumbelliferyl *N*-acetyl-β-*D*-glucosamine (MAG), glycol chitosan: chitosanase from *L. lecanii* (ChO), chitinase from *Streptomyces griseus* as negative control (CN), and cellulase from *Trichoderma longibranchiatum* as positive control (CP). The hydrolysis reaction was carried out in acetate buffer (50 mM, pH 6) at 50°C for 1 hour.

1.3.4. Establishment of reaction conditions for chitosanase activity

1.3.4.1. Estimation of reaction time, substrate, and enzyme concentrations on the hydrolysis of chitosan

The concentrated chitosanase was used for the establishment of reaction time, enzyme, and substrate concentrations using the response surface methodology. Surface plots are shown in Figure 5, in which the least significant effects were the squared variables of time and substrate. While the linear and interaction of time with enzyme and substrates effects were significant, except for the interaction of substrate and enzyme, which was not included in the quadratic model (Table 5). It can be seen in Figure 5 that the highest specific activities were in the range of 5 to 15 min, 9 to 18 g L^{-1}, 0.05 to 0.07 U mL^{-1}, and for time, substrate, and enzyme concentrations, respectively. To ensure the best performance of the purified chitosanase, further experimentation on hydrolysis was carried out over a range of pH and temperature values, with the reaction conditions of 15 min, 10 g L^{-1}, and 0.07 U mL^{-1}, which were detected with the highest level of specific activities.

Table 5. Estimated coefficients, standard errors, t- and p-values for the model of concentrated chitosanase on chitosan hydrolysis with reaction time, enzyme, and substrate concentrations.

Parameter	Coefficient	Standard Error	t-value	p-value
Constant	1.035	.323	3.199	.003
Time	-.035	.009	-3.763	.001
Enzyme	-50.581	13.747	-3.680	.001
Substrate	.166	.026	6.506	.000
Time Enzyme	.470	.134	3.499	.001
Time Substrate	-.001	.000	-3.647	.001
Time2	.000	.000	3.024	.004
Enzyme2	635.311	170.884	3.718	.001
Substrate2	-.004	.001	-3.071	.004

R=0.931, R2=.866

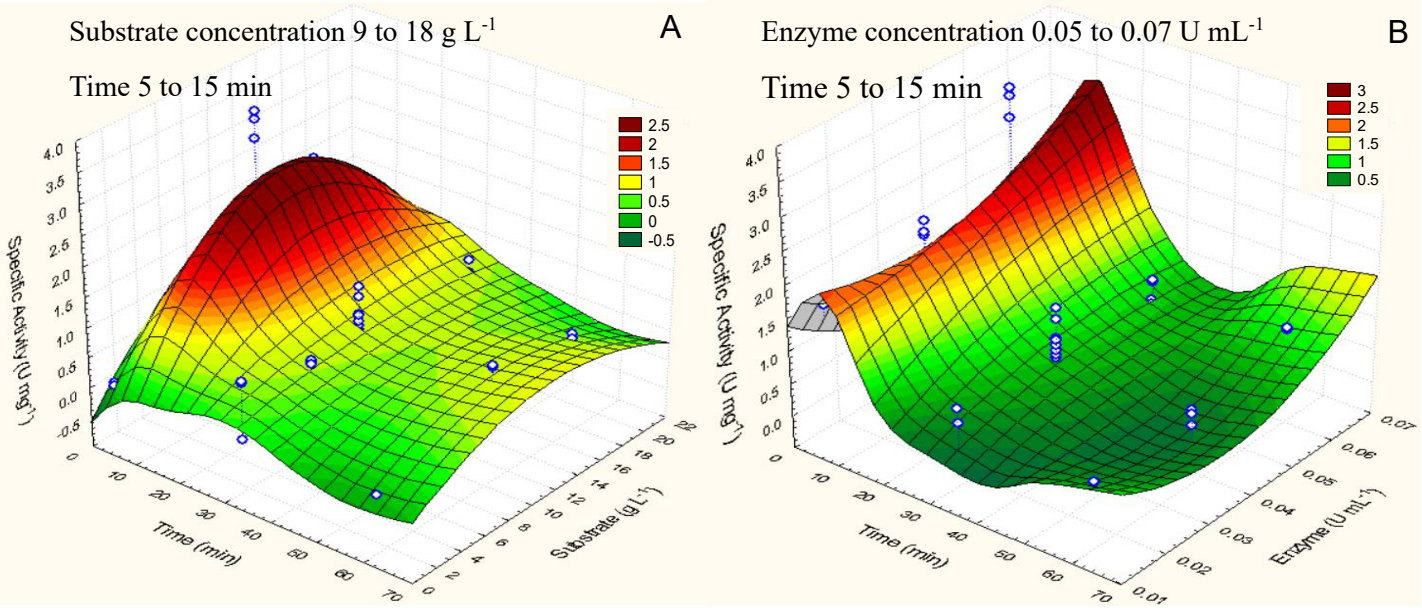

Figure 5. Response surface plots for concentrated chitosanase with variations of substrate concentration and time (A) and enzyme concentration and time (B).

The effect of pH (Figure 6A) on enzymatic activity indicates that at acidic pH, there was no activity, likely due to the protonation of amino acids in the active site, such as aspartate and glutamate, which resulted in the loss of catalytic activity (Xu *et al*., 2022). In contrast, the enzymatic activity displayed a maximum increase at pH 6, but the low availability of chitosan at pH 7 due to its insolubility explained a decreasing trend in chitosanase activity. The amino groups are deprotonated and form strong hydrogen bonds, leading to precipitation at pH 7 (Chang *et al*., 2015). Similarly, other reports on optimum pH of enzyme activity were near 6 for chitosanase of *Aspergillus fumigatus* ATCC13073 (Hirano *et al.,* 2012), pH 6, *Mucor circinelloides* 5.5-6.0 (Struszczyk *et al,.* 2009), *Fusarium oxysporum* 5.6 (Abedin, et al. 2023), *Penicillium oxalicum* 5.5 (Cao *et al.,* 2022), *Gongronella sp.* JG 5.6 (Wang *et al.,* 2008). The temperature was evaluated at pH 6. The optimum temperature of *L. lecanii* chitosanase was observed at 50°C; above this temperature, the activity decreased significantly. Other fungal chitosanases, such as those from *Fusarium oxysporum* (Abedin *et al*., 2023) *and Gongronella sp.* JG 5.6 55-60°C (Wang *et al*., 2008), *Penicillium oxalicum* 60°C (Cao *et al*., 2022), presented a similar optimum temperature near 50°C (Wang *et al*., 2008; Abedin *et al.,* 2023).

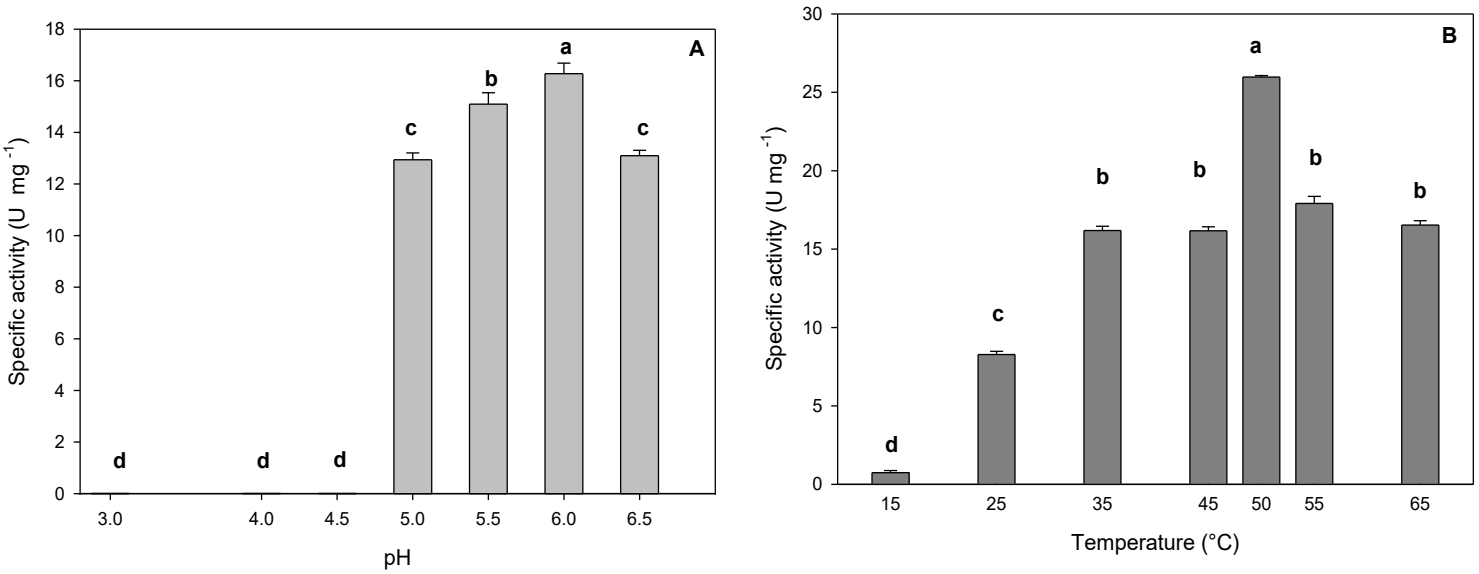

Figure 6. Effect of pH (A) and temperature (B) on the hydrolytic activity of purified chitosanases from *L. lecanii*, different letters indicate significant differences between treatments by Tukey Kramer multiple comparisons of means ($p<0.05$).

1.3.5 Characterization of chitosan hydrolysis products by the action of chitosanases.

The hydrolysis products of chitosan resulting from the action of purified chitosanases of *L. lecanii* under optimal conditions of temperature and pH were an insoluble fraction consisting of LMWC with a yield of 23.14% and a soluble fraction comprised of COS in a yield of 75.83% in dry mass. Similar yields of COS production have been reported for the chitosanase from *Gynuella sunshinyiii*, with a 71% yield (Gonçalves *et al.,* 2021). Higher yield was achieved by *L. lecanii* than those produced by the action of cellulase, pepsin, lipase, and chitosanase on chitosan 46%, 52%, 42%, and 46%, respectively. In the same study, LMWCs were obtained with a yield of 49%, 48%, 50%, and 45%, respectively (Roncal *et al.,* 2007).

The hydrolysis can be controlled by pH and temperature, and also by the chitosanase concentration, which depends on the degree of purification, as shown in the TLC analysis (Figure 7). The presence of bands in the upper part of the plate evidenced the production of COS of small molecular weights. In the case of the negative control, the spots in the lower part can be due to the chitosan used as a substrate. On the other hand, dark spots can be observed in the ChO and CP samples, indicating enzymatic activity over the chitosan, which releases COS with a low degree of polymerization. Despite being lighter, these spots can be

observed in the partially purified samples, which is evidence of the capacity of chitosanase class I to hydrolyze chitosan even when it is not pure. Moreover, the detection of COS in TLC at 5, 10, 15, and 20 min showed the chitosanase stability at optimal conditions of pH 6 and 50°C.

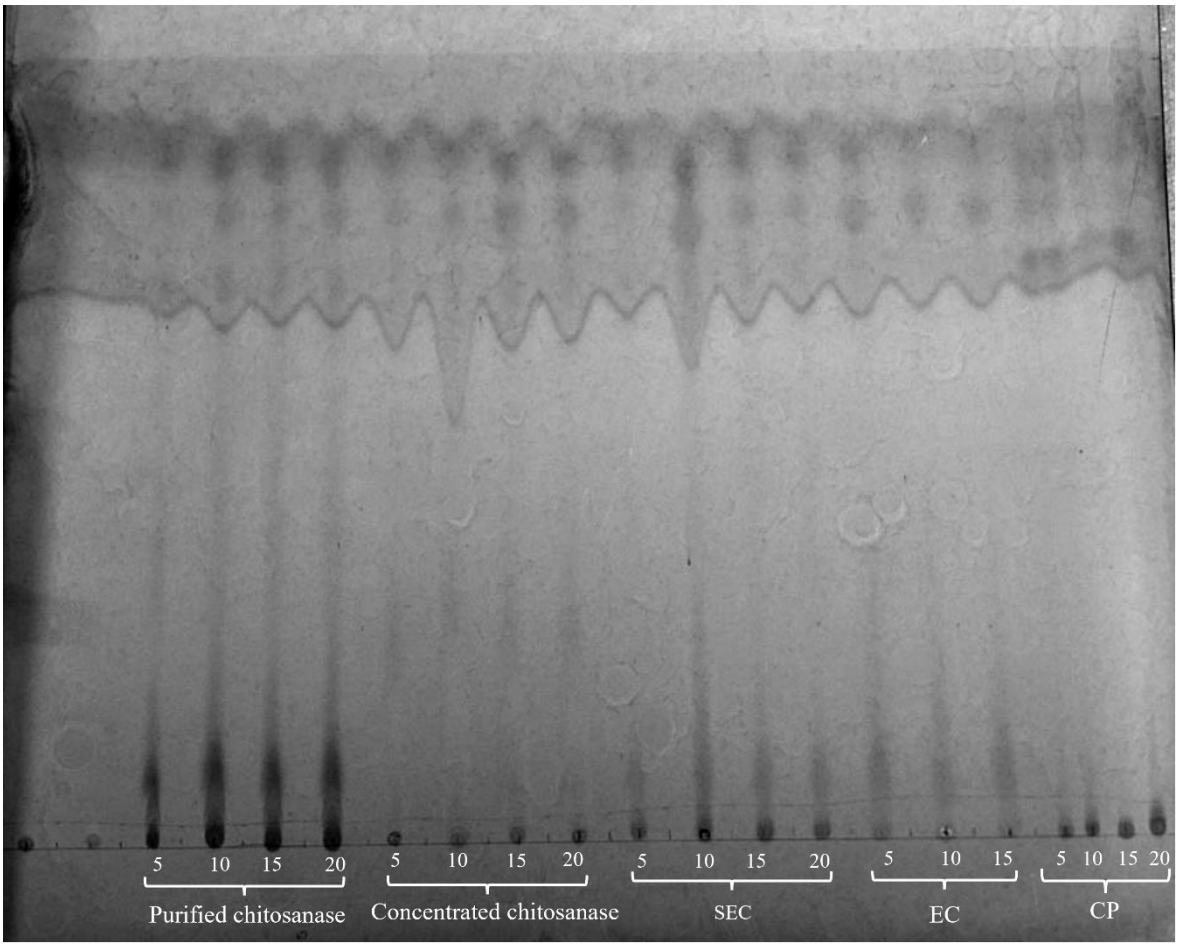

Figure 7. TLC of hydrolysis products: purified chitosanase, crude enzyme (EC), concentrated chitosanase, chitosanase obtained from SEC (SEC), cellulase from *Trichoderma longibranchiatum* as positive control (CP), promoting the reaction at pH 6, incubated at 50°C at 5, 10, 15, and 20 min.

The m z^{-1} spectra confirmed the presence of peaks characteristic of COS with a DP between DP 2-6 (Figure 8A) produced by enzymatic hydrolysis of chitosan (DA 18.6%) by subclass I chitosanase from *L. lecanii* at reaction conditions of 15 min, pH 6, and 50°C. Chitosanase subclass I hydrolyzed chitosan to homo or partially acetylated heterooligomers of GlcNAc and GlcN with DA of 29.78%, while the COS produced using chemical method were fully

deacetylated (Figure 8B). An important consideration is that the MALDI-TOF is a semiquantitative technique, which has been reported to be inaccurate when relative intensity measurements are used to determine concentration ratios in peptide analysis, and is strongly influenced by the molecular milieu of the analyzed sample (Szájli *et al.,* 2008). However, according to Trombotto *et al*. (2008), there was a good correlation between the DA determined by MALDI-TOF MS and ^{1}H NMR analysis, which suggests that the MALDI-TOF MS can also be used as a quantitative analytical method for the determination of the average DA of mixtures of low DP COS. In this study, the determination of DA of COS by MALDI-TOF mass spectrometry was carried out considering DP 3 to 6, avoiding COS with DP 2 for the effects of matrix peaks. Previous reports studied the use of the enzymatic degradation of 85% deacetylated chitosan to produce chitobiose, chitotriose, and chitotetraose by an endo-type chitosanase of *Gongronella sp.* JG DP2-4 (Wang *et al.,* 2008), likewise for the endochitosanase isolated from *Penicillium oxalicum* that was more active in hydrolyzing chitosan with a high degree of deacetylation (95-87%) to COS with DP 2-5 (Cao *et al.,* 2022). It is worth noting that the scales of chitosanase production in these reports are laboratory scale, so COS production may be limited due to the volume of chitosanase production, making it difficult to evidence its use as a possible alternative to conventional methods.

The time course of chitosan enzymatic hydrolysis on the molecular weight products was analyzed using substrate chitosan with a molecular weight of 121.42 ± 26.74 kDa and chitosanases at different purification stages (EC, PP, SEC, and purified). According to Gonçalves *et al*. (2021), COS are smaller than 3.9 kDa with DP≤20, while medium molecular weight chitosan is in the range of 100 to 1000 kDa, and LMWC is within <100 kDa. Herein, as shown in Figure 8A, there was a significant effect of the enzyme purification on the hydrolysis of medium molecular weight chitosan (120 kDa) to produce chitosan (8.89-10 kDa).

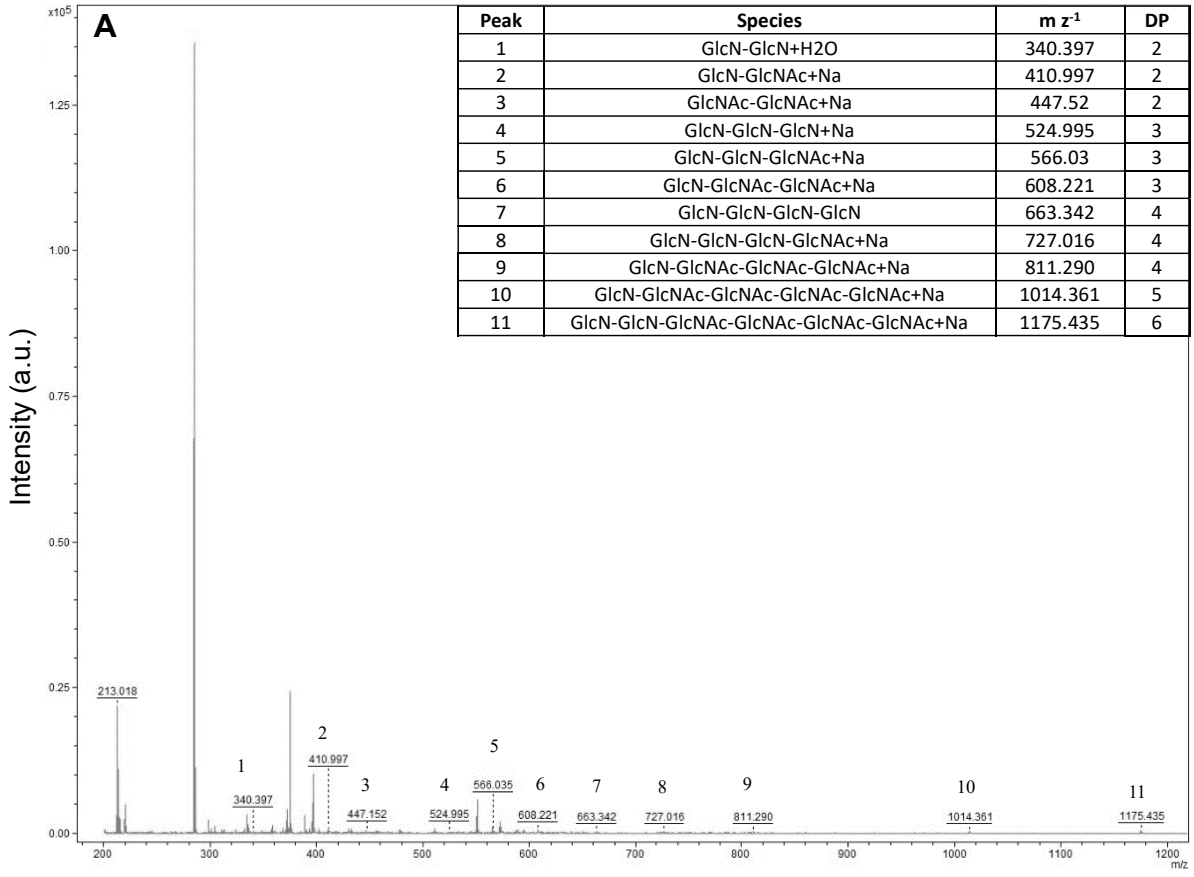

Peak	Species	m z^{-1}	DP
1	GlcN-GlcN+H2O	340.397	2
2	GlcN-GlcNAc+Na	410.997	2
3	GlcNAc-GlcNAc+Na	447.52	2
4	GlcN-GlcN-GlcN+Na	524.995	3
5	GlcN-GlcN-GlcNAc+Na	566.03	3
6	GlcN-GlcNAc-GlcNAc+Na	608.221	3
7	GlcN-GlcN-GlcN-GlcN	663.342	4
8	GlcN-GlcN-GlcN-GlcNAc+Na	727.016	4
9	GlcN-GlcNAc-GlcNAc-GlcNAc+Na	811.290	4
10	GlcN-GlcNAc-GlcNAc-GlcNAc-GlcNAc+Na	1014.361	5
11	GlcN-GlcN-GlcNAc-GlcNAc-GlcNAc-GlcNAc+Na	1175.435	6

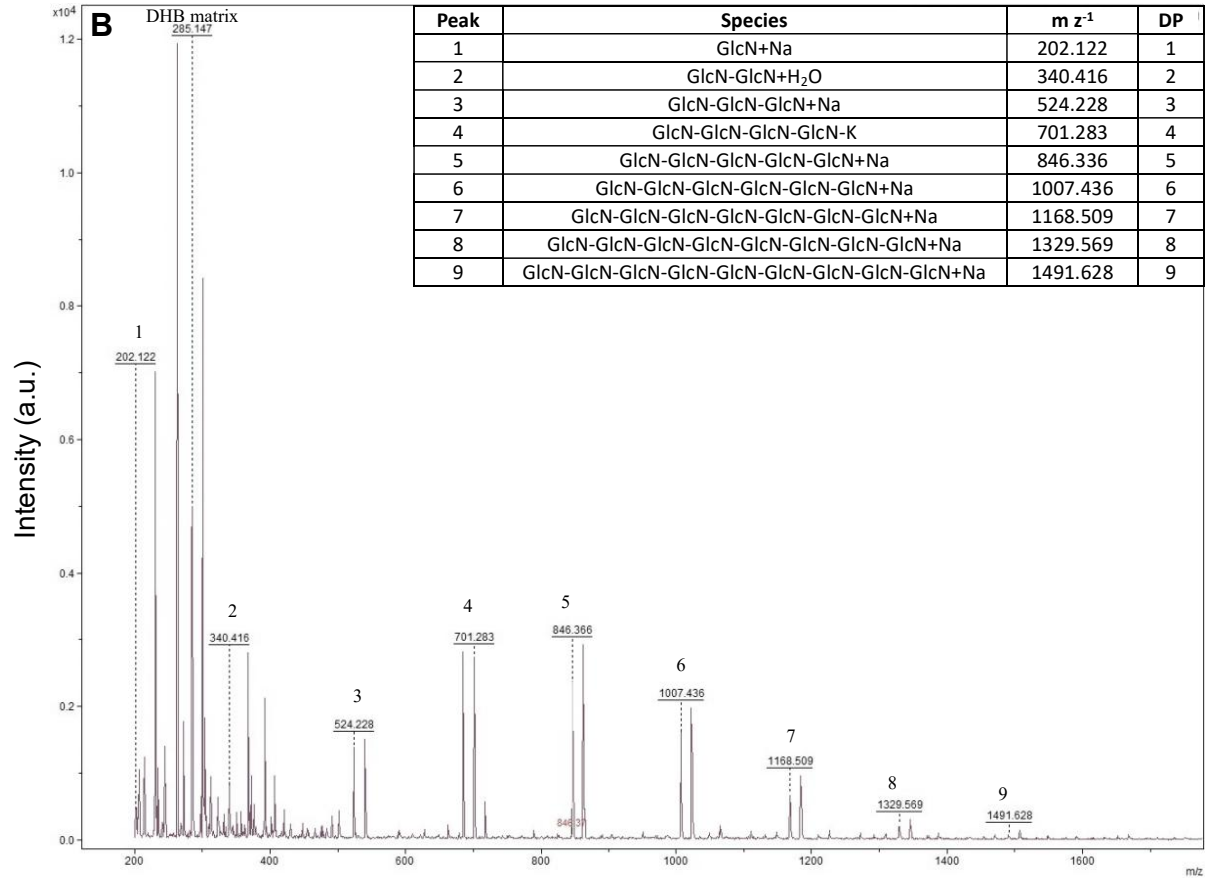

Peak	Species	m z^{-1}	DP
1	GlcN+Na	202.122	1
2	GlcN-GlcN+H_2O	340.416	2
3	GlcN-GlcN-GlcN+Na	524.228	3
4	GlcN-GlcN-GlcN-GlcN-K	701.283	4
5	GlcN-GlcN-GlcN-GlcN-GlcN+Na	846.336	5
6	GlcN-GlcN-GlcN-GlcN-GlcN-GlcN+Na	1007.436	6
7	GlcN-GlcN-GlcN-GlcN-GlcN-GlcN-GlcN+Na	1168.509	7
8	GlcN-GlcN-GlcN-GlcN-GlcN-GlcN-GlcN-GlcN+Na	1329.569	8
9	GlcN-GlcN-GlcN-GlcN-GlcN-GlcN-GlcN-GlcN-GlcN+Na	1491.628	9

Figure 8. MALDI-TOF spectra of the chitosan (0.8% w v^{-1}) hydrolysis products after 15 min of reaction (A) and commercial COS (B).

In addition, the DA (Figure 9B) was measured in the LMWC, which presents an increase in the acetylated fraction of 43.50 ± 0.27%, compared with the initial substrate, the chitosan of DA 18.6 ± 0.39%. The ability of chitosanases to cleave the bond between GlcNAc and GlcN confirmed that *L. lecanii* chitosanase belongs to class I (Thadathil and Velappan, 2014), explaining the augmentation of DA in the LMWC. The presence of the acetyl group can represent an advantage due to its high reactivity; such is the case of antimicrobial activity, where chitosan with a higher degree of acetylation is more effective due to better availability of free amino groups, The antimicrobial mechanism consists in the action of the polycationic nature, which is due to the presence of amino groups an could be a key feature of its ability to interact with the negatively charged surface components of many microorganisms, causing extensive alterations in the negatively charged cell surface, leading to leakage of intracellular constituents resulting in cell death (Ganan *et al*., 2009). COS presents a biocompatible material for wound healing, as a hypocholesterolemic agent (Thadathil and Velappan, 2014).

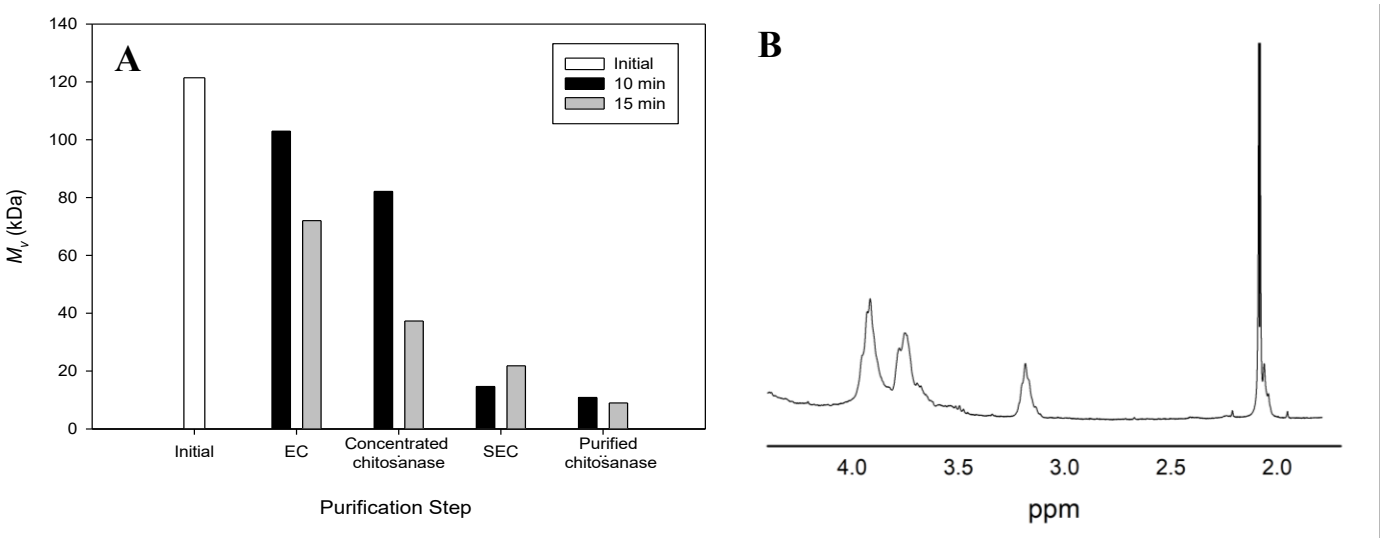

Figure 9. *Mv* of chitosans after reaction at pH 6 and 55°C with purified chitosanases at several purification steps: initial (white) and after hydrolysis 10 min (black) and 15 min (gray) (A). Nuclear proton magnetic resonance (1H NMR) spectra of LMWC obtained with purified chitosanases from *L. lecanii* after 15 min of reaction (B).

Chitosans with low molecular weights are of interest because decreasing the size of the polymer chains improves their solubility and biological properties, thereby increasing the number of applications, such as serving as antibacterial agents in animals (Chang *et al*. 2015), antioxidants (Thomas *et al.*, 2023), and as drug nanocarriers (Niu *et al.,* 2019).

Among the advantages of using enzymatic hydrolysis to produce chitosans in this study is that this method is solvent-free, resulting in a considerably lower environmental footprint. In addition, the production of chitosan with a specific molecular weight can be controlled by the degree of purification of chitosanase subclass I and reaction at optimal pH and temperature, allowing the production of chitosans for a specific application.

1.4. Conclusion

This study investigates the impact of scaling up submerged culture of fungi using chitosan as the sole carbon source and inducer on the production of chitosanases. Successfully scaling up chitosanase production has significant practical implications for various industries, indicating that the specific chitosanase activity achieved in a 50L bioreactor could be cost-effective. The findings provide new evidence for the use of fungal strains in producing enzymes, oligosaccharides, and low molecular weight chitosans. Additionally, the purified chitosanase hydrolyzes chitosan into homo or partially acetylated heterooligomers, increasing the degree of acetylation. This increase may influence mucosal adhesion and antioxidant activity. Future research will focus on identifying the specific class of chitosanase produced. Moreover, studies on biological properties are necessary to evaluate the applicability of low molecular weight chitosan developed enzymatically. In conclusion, this study provides strong evidence for chitosanase production by *Lecanicillium lecanii*, offering new insights into the use of this biological control agent and paving the way for innovative approaches in biomaterials.

1.5. References

Abedin, R., Abd Elwaly, D. R., El-Salam, A., Ayat, E. (2023). Production, statistical evaluation and characterization of chitosanase from *Fusarium oxysporum* D18. Ann. Microbiol. 73(1), 1-14. https://doi.org/10.1186/s13213-023-01731-w

AOAC Official Methods of Analyses of the Association of Official Analytical Chemists; Association of Official Analytical Chemists: Washington, DC, 1977.

Aranday-García, R., Guerrero, A. R., Ifuku, S., Shirai, K. (2017). Successive inoculation of *Lactobacillus brevis* and *Rhizopus oligosporus* on shrimp wastes for recovery of chitin and added-value products. Process Biochem. 58:17-24. https://doi.org/10.1016/j.procbio.2017.04.036

Brzezinski, R. (2011) Uncoupling chitosanase production from chitosan, Bioeng. Bugs. 2:4, 226-229. https://doi.org/10.4161/bbug.2.4.16111

Cao, S., Gao, P., Xia, W., Liu, S., Wang, N. (2022). A Novel Chitosanase from *Penicillium oxalicum* M2 for Chitooligosaccharide Production: Purification, Identification and Characterization. Mol. Biotechnol. 64, 947-957. https://doi.org/10.1007/s12033-022-00461-9

Chang, S.H., Lin, H.T., Wu, G.J., Tsai, G.J. (2015). pH Effects on solubility, zeta potential, and correlation between antibacterial activity and molecular weight of chitosan. Carbohydr. Polym. 134:74-81. https://doi.org/10.1016/j.carbpol.2015.07.072

de Santana, S. C., da Silva Filho, R. C., de Oliveira, J. A., de Macedo, G. R., Padilha, F. F., dos Santos, E. S. (2015). Enhancing purification of chitosanase from *Metarhizium anisopliae* by expanded bed adsorption chromatography using Doehlert design. Biocatal. Agric. Biotechnol. 4(4), 727-736. http://dx.doi.org/10.1016/j.bcab.2015.10.005

Fenice, M., Barghini, P., Selbmann, L., Federici, F. (2012).. Combined effects of agitation and aeration on the chitinolytic enzymes production by the Antarctic fungus *Lecanicillium muscarium* CCFEE 5003. Microb. Cell Fact. 11, 12. https://doi.org/10.1186/1475-2859-11-12

Gal, A. E. (1968). Separation and identification of monosaccharides from biological materials by thin-layer chromatography. Anal. Biochem. 24, 452-461. http://doi.org/10.1016/0003-2697(68)90152-8

Ganan, M., Carrascosa, A.V., Martínez-Rodríguez, A.J. (2009). Antimicrobial activity of chitosan against Campylobacter spp. and other microorganisms and its mechanism of action. Journal of Food Protection, 72(8), 1735–1738. https://doi.org/10.4315/0362-028x-72.8.1735

Gonçalves, C., Ferreira, N., Lourenço, L. (2021). Production of low molecular weight chitosan and chitooligosaccharides (COS): A review. Polymers. 13(15), 2466. http://doi.org/10.3390/polym13152466

Hirano, K., Arayaveerasid, S., Seki, K., Adams, D. J., Mitsutomi, M. (2012). Characterization of a chitosanase from *Aspergillus fumigatus* ATCC13073. Biosci. Biotechnol. Biochem. 76(8), 1523-1528. http://doi.org/10.1271/bbb.120248

Kean, T., Thanou, M. (2010). Biodegradation, biodistribution and toxicity of chitosan. Adv Drug Deliv. Rev. 62(1), 3-11. https://doi.org/10.1016/j.addr.2009.09.004

Kjøniksen, A. L., Nyström, B., Iversen, C., Nakken, T., Palmgren, O., Tande, T. (1997). Viscosity of dilute aqueous solutions of hydrophobically modified chitosan and its unmodified analogue at different conditions of salt and surfactant concentrations. Langmuir. 13(19), 4948-4952. https://doi.org/10.1021/la9702594

Kumar, M., Dangayach, P., Pareek, N. (2020). Enhanced glucosamine production through synergistic action of *Aspergillus terreus* chitozymes. J. Clean. Prod. 262, 121363. https://doi.org/St10.1016/j.jclepro.2020.121363

Kumar, S. S., Mohideen, S. S. (2025). Low Molecular Weight Chitosan Attenuates Acrylamide-Induced Toxicity in *Drosophila melanogaster*. Toxicol. Rep. 101933. https://doi.org/10.1016/j.toxrep.2025.101933

Laemmli, U. K. (1970). Cleavage of structural proteins during the assembly of the head of bacteriophage T4. Nat. 227(5259), 680-685. http://doi.org/ 10.1038/227680a0

Lee, C. M., Lee, Y. S., Seo, S. H., Yoon, S. H., Kim, S. J., Hahn, B. S., Sim, J. S., Koo, B. S. (2014). Screening and characterization of a novel cellulase gene from the gut microflora of *Hermetia illucens* using metagenomic library. J. Microbiol Biotechnol. 24(9), 1196–1206. https://doi.org/10.4014/jmb.1405.05001

Liu, Y.L, Jiang, S., Ke, Z.M., Wu, H.S., Chi, C.W., Guo, Z.Y. (2009). Recombinant expression of a chitosanase and its application in chitosan oligosaccharide production. Carbohydr. Res. 344(6):815-819. https://doi.org/10.1016/j.carres.2009.01.027

Luo, S., Qin, Z., Chen, Q., Fan, L., Jiang, L., Zhao, L. (2020). High level production of a *Bacillus amlyoliquefaciens* chitosanase in *Pichia pastoris* suitable for chitooligosaccharides preparation. Int J Biol Macromol. 149:1034-1041. https://doi.org/10.1016/j.ijbiomac.2020.02.001

Matsumoto, Y., Saucedo-Castañeda, G., Revah, S., Shirai, K. (2004). Production of β-N-acetylhexosaminidase of *Verticillium lecanii* by solid state and submerged fermentations utilizing shrimp waste silage as substrate and inducer. Process Biochem. 39(6), 665-671. https://doi.org/10.1016/S0032-9592(03)00140-7

Michelin, M., de Oliveira Mota, A. M., de Moraes, M. D. L. T., da Silva, D. P., Vicente, A. A., Teixeira, J. A. (2013). Influence of volumetric oxygen transfer coefficient (k_La) on xylanases batch production by *Aspergillus niger* van Tieghem in stirred tank and internal-loop airlift bioreactors. Biochem. Eng. J. 80, 19-26. https://doi.org/10.1016/j.bej.2013.09.002

Miller, G. L. (1959). Use of dinitrosalicylic acid reagent for determination of reducing sugar. Anal. Chem. 31(3), 426-428. https://doi.org/10.1021/ac60147a030

Mulchandani, A., Luong, J.H., Leduy, A. (1988). Batch kinetics of microbial polysaccharide biosynthesis. Biotechnol Bioeng. 32(5):639-646. https://doi.org/10.1002/bit.260320508

Niu, S., Williams, G. R., Wu, J., Wu, J., Zhang, X., Chen, X., Li. S., Jiao., J., Zhu, L. M. (2019). A chitosan-based cascade-responsive drug delivery system for triple-negative breast cancer therapy. J. Nanobiotechnology, 17, 1-18. https://doi.org/10.1186/s12951-019-0529-4

Pan, Y., Yang, J., Wu, J., Yang, L., Fang, H. (2022). Current advances of *Pichia pastoris* as cell factories for production of recombinant proteins. Front. Microbiol. 13:1059777. https://doi.org/10.3389/fmicb.2022.1059777

Peterson, G. L. (1977). A simplification of the protein assay method of Lowry et al. which is more generally applicable. Anal. Biochem. 83(2), 346-356. https://doi.org/10.1016/0003-2697(77)90043-4

Radwan, O., Gunasekera, T. S., Ruiz, O. N. (2019). Draft genome sequence of *Lecanicillium* sp. isolate LEC01, a fungus capable of hydrocarbon degradation. Microbiol. Resour. Announc. 8(15), 10-1128. https://doi.org/10.1128/mra.01744-18

Rocha-Pino, Z., Marín-Cervantes, M., Martínez-Archundia, M., Soriano-Blancas, E., Revah, S., Shirai, K. (2013). Morphological changes, chitinolytic enzymes and hydrophobin-like proteins as responses of *Lecanicillium lecanii* during growth with hydrocarbon. Bioprocess Biosyst. Eng. 36:531-539. https://doi.org/10.1007/s00449-012-0808-z

Rojas-Osnaya, J., Rocha-Pino, Z., Nájera, H., González-Márquez, H., Shirai, K. (2020). Novel transglycosylation activity of β-N-acetylglucosaminidase of *Lecanicillium lecanii* produced by submerged culture. Int. J. Biol. Macromol. 145, 759-767. http://doi.org/10.1016/j.ijbiomac.2019.12.237

Rojas-Osnaya, J., Quintana-Quirino, M., Espinosa-Valencia, A., Bravo, A. L., & Nájera, H. (2024). Hydrophobins: multitask proteins. Frontiers in Physics, 12, 139334. http://doi.org/10.3389/fphy.2024.1393340

Roncal, T., Oviedo, A., Armentia, I.L., Fernández, L., Villarán, M.C. (2007). High yield production of monomer-free chitosan oligo-saccharides by pepsin catalyzed hydrolysis of a high deacetylation degree chitosan. Carbohydr. Res. 2007, 342, 2750-2756. http://doi.org/10.1016/j.carres.2007.08.023

Sambles, C., Suarez-Fernandez, M., Lopez-Moya, F., Lopez-Llorca, L. V., Studholme, D. J. (2022). Chitosan induces differential transcript usage of chitosanase 3 encoding gene (csn3) in the biocontrol fungus *Pochonia chlamydosporia* 123. BMC Genet. *23*(1), 101.. https://doi.org/10.1186/s12864-021-08232-7

Schneider, C. A., Rasband, W. S., Eliceiri, K. W. (2012). NIH Image to ImageJ: 25 years of image analysis. Nat. Methods. 9(7), 671-675. http://doi.org/10.1038/nmeth.2089

Seki, K., Nishiyama, Y., Mitsutomi, M. (2019). Characterization of a novel exo-chitosanase, an exo-chitobiohydrolase, from *Gongronella butleri*. J. Biosci. Bioeng. 127(4), 425-429. https://doi.org/10.1016/j.jbiosc.2018.09.009

Shinya, S., & Fukamizo, T. (2017). Interaction between chitosan and its related enzymes: A review. *International journal of biological macromolecules*, *104*, 1422-1435. https://doi.org/10.1016/j.ijbiomac.2017.02.040

Struszczyk, K., Szczesna-Antczak, M., Walczak, M., Pomianowska, E., Antczak, T. (2009). Isolation and purification of *Mucor circinelloides* intracellular chitosanolytic enzymes. Carbohydr. Polym. 78, 16-24. https://doi.org/10.1016/j.carbpol.2009.04.010

Szájli, E., Fehér, T., Medzihradszky, K.F. (2008). Investigating the quantitative nature of MALDI-TOF MS. Mol. Cell Proteomics. 7(12):2410-2418. https://doi.org/10.1074/mcp.M800108-MCP200

Thadathil, N., Velappan, S. P. (2014). Recent developments in chitosanase research and its biotechnological applications: a review. Food Chem., 150, 392-399. https://doi.org/10.1016/j.foodchem.2013.10.083

Thomas, R., Fukamizo, T., Suginta, W. (2023). Green-Chemical Strategies for Production of Tailor-Made Chitooligosaccharides with Enhanced Biological Activities. Molecules. 28, 6591. https://doi.org/10.3390/molecules28186591

Trombotto, S., Ladavière, C., Delolme, F., Domard, A. (2008). Chemical preparation and structural characterization of a homogeneous series of chitin/chitosan oligomers. Biomacromolecules. 9(7):1731-1738. https://doi.org/10.1021/bm800157x

Wang, J., Zhou, W., Yuan, H., Wang, Y. (2008). Characterization of a novel fungal chitosanase Csn2 from *Gongronella* sp. JG. Carbohydr. Res. 343, 2583–2588. https://doi.org/10.1016/j.carres.2008.08.004

Wang, Y., Li, D., Liu, M., Xia, C., Fan, Q., Li, X., Lan, Z., Shi, G., Don, W., Li, Z., Cui, Z. (2021). Preparation of active chitooligosaccharides with a novel chitosanase Aq CoA and their application in fungal disease protection. J. Agric. Food Chem. 69(11), 3351-3361. https://doi.org/10.1021/acs.jafc.0c07802

Xu, Y., Li, L., Cao, S., Zhu, B., Yao, Z. (2022). An updated comprehensive review of advances on structural features, catalytic mechanisms, modification methods and applications of chitosanases. Process Biochem. 118, 263-273. https://doi.org/10.1016/j.procbio.2022.05.001

Chapter 2: Study of hydrophobins class II as a nanocarrier of pirarubicina: evaluation in vivo and in vitro

2.1. Introduction

Anticancer drugs encapsulated in nanoparticles have been developed using various polymers, including proteins and polysaccharides, for the treatment of multiple types of cancer (Amreddy *et al*., 2018;Thakkar *et al*., 2020; Veselov *et al.,* 2022). Nanoparticles may contain macromolecular drugs (>40 kDa), exhibiting prolonged blood circulation and selective tumor accumulation due to the enhanced permeability and retention (EPR) effect (Matsumura *et al*., 1986; Tsukigawa *et al*., 2015). However, polymer conjugates of anticancer agents must be designed to release the drug specifically at the tumor site to achieve sufficient therapeutic effects. This process often requires complex chemical reactions, such as cross-linking with polymers, which are time-consuming and costly (Ezhilarasan *et al*., 2022; Li *et al*., 2023; Chakraborty *et al*., 2025). Thus, a simple and efficient method for nanoparticle preparation is essential for developing anticancer drugs, highlighting the importance of exploring the materials that form optimal anticancer nanoparticles.

Filamentous fungi secrete hydrophobins (HFB) as a physiological response to their growth and environment. HFB belong to a class of small surface-active proteins typically comprising 100-150 amino acids. A key feature of HFB is the presence of eight conserved cysteine residues, which form four intramolecular disulfide bonds, stabilizing its unique structure. Based on solubility and structure, HFB are classified as class I when they are capable of self-assembling into highly stable amyloid-like rodlets, which are insoluble in water and resistant to high temperatures. These structures can be dissolved by strong acids such as formic and trifluoroacetic acid. Opposite class II when HFB present monolayer structures and fibrils on surfaces that can be in ethanol and some detergents such as sodium dodecyl sulfate (SDS) (Sallada *et al*., 2018; Calonje *et al*., 2002; Agwora *et al*., 2025). HFB exhibit remarkable amphiphilicity, allowing them to self-assemble into highly ordered monolayers at hydrophilic-hydrophobic interfaces. HFB forms a thin and stable monolayer, enabling it to modify surface properties, such as hydrophobicity and adhesion (Sunde *et al*., 2008; Aimanianda *et al*., 2009; Zhang *et al*., 2011). These unique physicochemical properties have garnered significant interest in industrial and biomedical applications, including surface

coatings in nanotechnology, drug delivery systems, and biomaterials with tailored wettability (Valo *et al*., 2011; Reuter *et al*., 2017).

The amphiphilic nature of HFB has been leveraged to form encapsulated nanoparticles of anticancer drugs. For instance, commercial recombinant HFB class I (H Star Protein ® B) has been used as a coating agent on polylactic acid/glycolic acid copolymer (PLGA) nanoparticles (Sun *et al*., 2020) and anticancer drug-encapsulated nanoparticles (Fang *et al*., 2014), while recombinant HFB class II from *Trichoderma virens* has been used for the preparation of liposomes (Osmanagaoglu *et al*., 2024). Despite these efforts to prepare formulations using HFB alone, these studies have been primarily conducted *in vitro*, with limited evaluation *in vivo* in cancer models. Besides, the native HFB used in the present study offers the advantage of being soluble, unlike recombinant HFB produced for industrial applications, such as H Protein A and H Protein B from BASF. These recombinant proteins often form inclusion bodies, which can limit their functional properties and lead to time-consuming and ineffective refolding processes. Even with the purification of the recombinant HFB from inclusion bodies, only a partial ability to self-assemble on hydrophobic surfaces was preserved compared with wild-type hydrophobin isolated from the mushroom *Grifola frondosa* (Cheng *et al*., 2020). Therefore, it is essential to investigate the functional properties of naturally occurring HFB fungi. In this regard, *Lecanicillium lecanii* has been identified as an effective producer of hydrophobins, either in solid or submerged cultures, with high yields significantly influenced by the carbon source and cultivation method (Rocha-Pino *et al*., 2011).

Pirarubicin (4'-O-tetrahydropyranyl doxorubicin) (THP) is a semi-synthetic derivative of doxorubicin and belongs to the anthracycline class of antitumor agents, widely used in clinical cancer treatment (Umezawa *et al*., 1979; Kunimoto *et al*., 1983). Compared to doxorubicin (DOX), THP exhibits faster cellular uptake, reduced cardiotoxicity, and effectiveness against DOX-resistant tumors (Kunimoto *et al*., 1984; Koh *et al*., 2002). However, THP lacks tumor-selective delivery like other small-molecule drugs, leading to side effects and dose-limiting cardiotoxicity. To address these limitations, we have explored various nanocarriers for THP, including styrene-maleic acid copolymer, 2-*N*-(hydroxypropyl)

methacrylamide polymer, and serum albumin (Tsukigawa *et al*., 2015; Nakamura *et al*., 2016; Hasegawa *et al*., 2024).

In this study, we prepared THP nanoparticles using HFB as a nanocarrier (TNPs). Additionally, glucosamine (GlcN) was incorporated into these nanoparticles to create glucosamine-containing THP nanoparticles (GlcN-TNPs). GlcN, a glucose analog, is recognized by GLUT1 on tumor cell membranes and transported into cells, thereby enhancing the intertumoral accumulation of chemotherapeutic agents via receptor-mediated internalization (Airley *et al*., 2010; Amann *et al*., 2011). Numerous studies have demonstrated that GlcN exerts anticancer activity by modulating biological pathways related to cell death, apoptosis, cell proliferation, and angiogenesis (Oh *et al*., 2007; Zahedipour *et al*., 2017; Pawar *et al*., 2017). Furthermore, GlcN has been shown to reduce drug toxicity, particularly cardiotoxicity, in novel polymer-drug conjugates. These properties make GlcN an ideal targeting ligand for modifying micelles to achieve tumor targeting, inhibit tumor growth, and reverse drug resistance.

Thus, we compared the anticancer activity of hydrophobin THP nanoparticles with glucosamine-containing THP nanoparticles and free THP against C26 cells and tumor-bearing mice.

2.2. Experimental

2.2.1. Materials

Glucosamine hydrochloride was purchased from Sigma-Aldrich (St. Louis, US), RPMI-1640 and Dulbecco modified Eagle medium were purchased from FUJIFILM (Wako Pure Chemical Corporation, Osaka, Japan), Cell Counting Kit-8 was purchased from DoJinDo Molecular Technology Inc. (CCK-8, Kumamoto, Japan), and other chemicals used were of high purity. All solutions were prepared using deionized or distilled water.

2.2.2. Hydrophobin characterization

Hydrophobins class II (HFBII) were produced in submerged cultures of *Lecanicillium lecanii* using biological chitosan as a carbon source in a stainless steel stirred tank bioreactor with a 50 L capacity, with Czapeck medium supplemented with 10 g L^{-1} of chitosan (degree of

acetylation, 18.6%), at 1 volume of air volume of liquid^{-1} min^{-1}, 125 rpm, and 28°C. HFBII was purified from biomass, which was resuspended in Tris-HCl (10 mM) SDS (2%) pH 9 for 2 h at 25°C, subsequently centrifuged at 14,534 x g at 4°C for 15 min (Thermo Scientific, Osterode, Germany), supernatant fraction was mixed with KCl (2M) in ratio 1:0.5 to removed SDS, followed by centrifugation at 14,534 x *g* at 4°C for 15 min. Subsequently, the supernatant was precipitated by the electrobubbling process at 300 mA in Tris-HCl (10 mM) solution at pH 9 (Rocha-Pino *et al*., 2011). The collected foam was subjected to centrifugation at 14,534 x *g* at 4°C for 10 min. The precipitated fraction was concentrated using ultrafiltration units with a 3 kDa molecular weight cutoff membrane (Merck, Darmstadt, Germany). Afterward, the retentate was subjected to a freeze-drying process (Freezone 2.5 Plus, LabConco, Kansas City, Missouri, US) and stored at 4°C until use. HFBII was characterized by electrophoresis using one-dimensional acrylamide gels under denaturing conditions (SDS-PAGE), as proposed by Laemmli (1970). Precision Plus Protein Standard Unstained (Bio-Rad, Hercules, US) was used as a reference. Gels were stained with Coomassie Blue R-250 (Bio-Rad, Hercules, CA, USA) and analyzed using ImageJ 1.41 (National Institutes of Health, USA) [35]; the data were expressed as the mean of three independent measurements and reported as mean ± standard deviation. HFBII surface charge was analyzed by dynamic light scattering (DLS) at 25°C (ELZ1000 series, Otsuka Electronics Co., Ltd., Osaka, Japan), the data were expressed as the mean of three independent measurements and reported as mean ± standard deviation.

Surface activity was assessed by measuring the change in contact angle on Teflon and glass surfaces, reflecting changes in the material's hydrophobicity properties. Teflon was subjected to a thorough cleansing process involving deionized water and ethanol, while the glass underwent treatment with nitric acid (5% vv^{-1}) and was washed with deionized water (Rocha-Pino *et al*., 2011). HFBII solutions with concentrations ranging from 10 to 60 µg mL^{-1} were deposited onto surfaces and subsequently treated with 1 µL of deionized water. Contact angle (θ) was observed using a horizontal light microscope (Intel Qx3, Intel Corporation, Santa Clara, US). The contact length (*b*) and height (*h*) of the water drop were analyzed using ImageJ 1.41 software, as shown in Equation 7.

$$\theta = 2\tan^{-1}(2h/b) \qquad \textbf{(7)}$$

Circular dichroism (CD) measurements of HFBII were performed in water: ethanol solution (40:60) at 100 μg mL^{-1} using a Jasco model J-720 spectropolarimeter (Tokyo, Japan) with a Jasco J32CDQ10 cell at 25°C in the far UV CD range (190-250 nm). CD analysis was carried out by Dichro Web using the K2D method (Whitmore *et al*., 2008).

2.2.3. HFBII solubilization

Phosphate buffer (0.2 M) at pH 5.5, 6, 6.5, 7, 8, and 9. NaOH (0.5 M) was used to adjust the pH for HFBII solubilization under vigorous agitation for 15 min at 25°C. Once completely solubilized, it was adjusted to pH 8 using HCl (1 M). Particle size and polydispersity index (PDI) were determined (5 mg mL^{-1}) in phosphate buffer (0.2 M) through DLS at a temperature of 25°C (ELS-Z2, Otsuka Electronics Co., Ltd., Japan).

2.2.4. Synthesis and purification of TNPs nanoparticles.

HFBII solution (2 mg mL^{-1}) was added dropwise under stirring conditions of 1150 rpm and 25 °C. A pirarubicin solution (1:0.25 molar ratio HFBII: THP) was added dropwise. The THP solution was previously solubilized in dimethyl sulfoxide (4.5 % of the formulation's total volume) and dispersed in phosphate buffer (0.2 M), pH 8, followed by stirring at 25 °C for 25 min to promote particle formation.

2.2.5. Synthesis and purification of GlcN-TNPs.

A solution of GlcN (1 mg mL^{-1}) in phosphate buffer (0.2 M) pH 7.4 was mixed with a solution of HFBII (2 mg mL^{-1}). Subsequently, a solution of pirarubicin was added dropwise to the HFB-GlcN mixture at a molar ratio of 1:0.25 HFBII: THP under conditions of 25°C and 1150 rpm. GlcN-TNPs were stirred for 25 min to promote particle formation.

Both treatments (TNPs and GlcN-TNPs) were purified by column chromatography using Sephadex G-50 fine to separate molecules by size in the range of 1 to 30 kDa (GE Healthcare, Tokyo, Japan) and eluted with ultrapure water to separate the free THP. The recovered fraction was subjected to a dialysis process using 8 kDa molecular-weight cut-off membranes (Millipore, Bedford, MA, USA) for 12 h at 4°C. The nanoparticles were freeze-dried and subsequently stored at 4°C until use.

2.2.6. Nanoparticles characterization.

The zeta potential, particle size, and polydispersity index (PDI) of NPs were determined in a phosphate buffer (0.2 M) through DLS at a temperature of 25°C (ELS-Z2, Otsuka Electronics Co., Ltd., Japan). Fourier Transform Infrared (FTIR) Spectroscopy with the Attenuated Total Reflectance (ATR) detector device method was performed using a Spectrum 100 (PerkinElmer, Boston, MA, US) in a scanning rate of 4000-550 cm^{-1}. Data acquisition was carried out with 16 scans per sample at a resolution of 1 cm^{-1} to analyze the chemical structures of the NPs and their components.

Atomic force microscopy (AFM) analysis was carried out on a sample (6 mg) dissolved in deionized water (50 µL). Solution (15 µL) was dispersed on the surface of a 12 mm highest grade mica disk (Ted Pella Inc.) NPs were dried at room temperature, and mica discs were mounted on magnetic discs for analysis in air using tapping mode with an Innova scanning probe microscope (Veeco Instruments Inc.). Sample was scanned at a rate of 1 Hz and with 512 lines using an Innova Scanning Probe microscope (Veeco Instruments Inc., USA) equipped with a Nanodrive 8.02 controller and a high-resolution scanning probe, SHR150 (Budget Sensors). The probes have a tip radius of 1 nm and display average force constants of 5 N m^{-1}, with a resonance frequency of 75-225 kHz, which are compatible with high-resolution soft tapping mode operation. Morphology of NPs was visualized by transmission electron microscopy (TEM). A 20 µL of NPs suspension (phosphate buffer 0.2 M pH 7) was deposited on a mesh carbon-coated copper grid, samples were further dried for 24 h at 25°C and visualized by a high-resolution transmission electron microscope (HRTEM) (JEM-2100F, JEOL, Tokyo, Japan)

Protein determination was carried out using Quick-CBB plus FUJIFILM (Wako Pure Chemical Corporation, Osaka, Japan) according to the manufacturer's instructions; bovine serum albumin solution was used as the standard.

Concentration of the THP released (D_R) was determined by fluorescence intensity with an excitation wavelength of 480 nm and an emission of 590 nm. (FP-6600: JASCO, Hachioji, Japan) (Tsukigawa *et al*., 2015). Employing a curve of free THP from 7 to 150 µg mL^{-1}. The THP release (D_R%) was determined considering D_R and the total concentration of drug (C_{TD}) using equation 8.

$$D_R(\%) = D_R / C_{TD} \times 100 \qquad \textbf{(8)}$$

THP release from the NPs (0.5 mg mL^{-1}) was evaluated in PBS for 12 h at pH 5, 6.5, 7.4 at 37 °C. THP release experiments were also carried out at the storage conditions of pH 7.4 and 4°C. In a typical procedure, each sample was sonicated for 1 min and then centrifuged at 14,534 × g for 5 min. The concentration of the THP released (DR) was determined by fluorescence intensity with an excitation wavelength of 480 nm and an emission of 590 nm. The calibration curve of free THP was prepared with concentrations 0 to 7 µg mL^{-1} (FP-6600: JASCO, Hachioji, Japan).

HPLC measured GlcN content, employed a column Shodex Asahipak NH2P 50 4E (5 µm particle size, 4.6mm i.d.× 250 mm) (Showa Denko K.K, Minato-Ku, Japan) equipped with a guard column NH2P 50G 4A (5 µm particle size, 4.6mm i.d.×10 mm) (Showa Denko K.K, Minato-Ku, Japan), acetonitrile (70% v v^{-1}) was used as a mobile phase with a constant flow rate of 0.8 mL min^{-1} at 28°C with an injection volume of 20 µL. GlcN signals were identified by a refractive index detector. A standard curve of D-glucosamine hydrochloride was prepared using concentrations of 1, 2.5, 5, 10, 16 and 20 mg mL^{-1}. For the D-glucosamine hydrochloride stock solution, 1 g was dissolved in 25 mL of distilled water, and after complete dissolution, the solution was mess up to 50 mL with acetonitrile. All determinations were conducted in triplicate.

Entrapment efficiency (*EE*) and loading capacity (*LC*) of nanoparticles were calculated employing the total amount of drug (T_D), free drug (F_D), and total weight of nanoparticles (W_T) according to equations 9 (Jamshidi *et al*., 2024).

$$EE(\%) = (T_D - F_D)/T_D \times 100 \qquad \textbf{(9)}$$

2.2.7. *In vitro* cytotoxicity assay.

The cytotoxicity of the NPs was evaluated using the murine colon adenocarcinoma cell line, C26. Colon cell culture was grown using DMEM low glucose containing 100 U/mL penicillin and 100 µg/mL streptomycin (P/S) and supplemented with 10 % fetal bovine serum (FBS). The cells were incubated at 37°C, 5% CO_2, and 95% relative humidity.

C26 colon cells ($3x10^3$ cells mL^{-1}) were seeded on a 96-well plate and incubated for 12 h at 37°C and 5% CO_2. After incubation, different final concentrations (0.01-100 µg mL^{-1}) of free THP or THP equivalent (TNPs and GlcN-TNPs) were added to the plate. The *in vitro* cytotoxic effect was analyzed after 48 h of incubation by measuring the cell viability using the Cell Counting Kit-8 (CCK8) was purchased from DoJinDo Molecular Technology Inc. (Kumamoto, Japan) and the absorbance was measured at 450 nm. The IC_{50} was determined using GraphPad Prism (GraphPad Software, Inc., San Diego, CA, USA).

2.2.7.1. Intracellular uptake of THP

C26 cells ($2x10^5$ cell mL^{-1}) were seeded on 6-well plates. After a 24 h incubation at 37°C, 5% CO_2, and 95% relative humidity, 10 µg mL^{-1} of free THP or THP equivalent was added to examine internalization profiles. Cells were incubated at 4 and 37 °C for 30 min. Once the incubation time had elapsed, 1% (w v^{-1}) SDS was added to promote cell lysis. The contents of the wells were recovered and sonicated for 1 min, followed by centrifugation at 12,000 x *g* for 5 min. Supernatant f was used to determine THP and protein content as described in section II.2.5.

2.2.7.2. Intracellular pathways of THP

To obtain a better understanding of intracellular uptake of THP and NPs, C26 cells ($1x10^6$ cells) were seeded in poly-lysine-coated glass-bottom culture dishes in growth medium (DMEM). After 12 h of incubation, Lysotracker and Hoechst 33342 (Sigma-Aldrich, St. Louis, US) were added to the medium, and the dishes were incubated for 30 min. Later, the medium was changed to RPMI 1640 without phenol red. Free THP or THP equivalent was added at 10 µg mL^{-1} and examined using confocal laser microscopy, with an excitation wavelength of 647 nm and emission of 668 nm for Lysotracker, and excitation of 352 nm and emission of 461 nm for Hoechst under control conditions of 37 °C and 5% CO_2.

To elucidate the pathways involved in the cellular uptake of TNPs, C26 cells ($2 x 10^5$ cell mL^{-1}) were seeded in 6-well plates. After overnight incubation, inhibitors were added: 5-(*N*-ethyl-N-isopropyl)-amiloride (EIPA) (30 µg mL^{-1}), Filipin III (10 µg mL^{-1}), Chlorpromazine (20 µg mL^{-1}), Cytochalasin-D (5.58 µg mL^{-1}) in a pre-incubation time of 40 min, free THP or THP equivalent was added until a final concentration of 10 µg $mL^{-1,}$ and incubated for 1

h. THP and protein extraction and quantification were carried out as described in section II.2.5.

2.2.8. *In vivo* antitumor activity

All animal experiments were carried out in accordance with the Laboratory Protocol for Animal Handling of Sojo University (Kumamoto, Japan). Murine colon adenocarcinoma C26 cells ($1x10^7$ cells mL^{-1}) were implanted subcutaneously in the dorsal skin of male BALB/cCrSlc mice 5 weeks old. When the tumor grew to 5-9 mm in diameter, mice were administered 3 doses (2.5 mg THP eq. Kg^{-1}) of free THP or THP equivalent on 15 d, 18 d, and 21 d after cell inoculation by intravenous injection at a volume of 0.2 mL per mouse. Mouse weight, tumor volume, and survival rate were monitored. Tumor volume (TV) (mm^3) was measured by the width (W) and length (L) of the tumor on the dorsal skin, calculated by equation 10.

$$TV = \left(W^2 \times L\right)/2 \qquad \textbf{(10)}$$

2.2.9. *In vivo* acute toxic study

To demonstrate the cytotoxic effect of THP, a single i.v. doses of 5, 15, and 30 mg of free THP or THP equivalent per Kg of healthy 5-week-old male mice were administered, and changes in mouse weight and survival rate were monitored.

2.2.10. Statistical analysis.

Statistical analysis of the experimental data was evaluated using Tukey-Kramer's multiple comparisons of means in SPSS software version 22.0 (IBM Corp., Armonk, US); significant statistical differences were considered at a p-value of <0.05.

2.3. Results and Discussion

2.3.1. Hydrophobin characterization

HFBs in filamentous fungi have been reported as mediators for adhesion of hyphae and spores on host surfaces (i.e., insect cuticle) (Rocha-Pino *et al*., 2011). HFBs class I consist of 100-125 amino acid residues and can be glycosylated, while HFBs class II are shorter, containing 50-100 amino acid residues (Agwora *et al*., 2025). The recombinant HFB II has

molecular weights of 6.6 kDa and 6.4 kDa for *Trichoderma reesei* and recombinant *Trichoderma virens* in *Pichia pastoris*, respectively (Osmanagaoglu *et al*., 2024). A HFBs class II isolated from *Verticillium fungicola*, a closely related fungus of *Lecanicillium lecanii*, presented a molecular weight of 7 kDa (Calonje *et al*., 2002), while *L. lecanii* HFBII, produced and purified in this study, presented a molecular weight of 5.8 ± 0.1 kDa (Figure 10A).

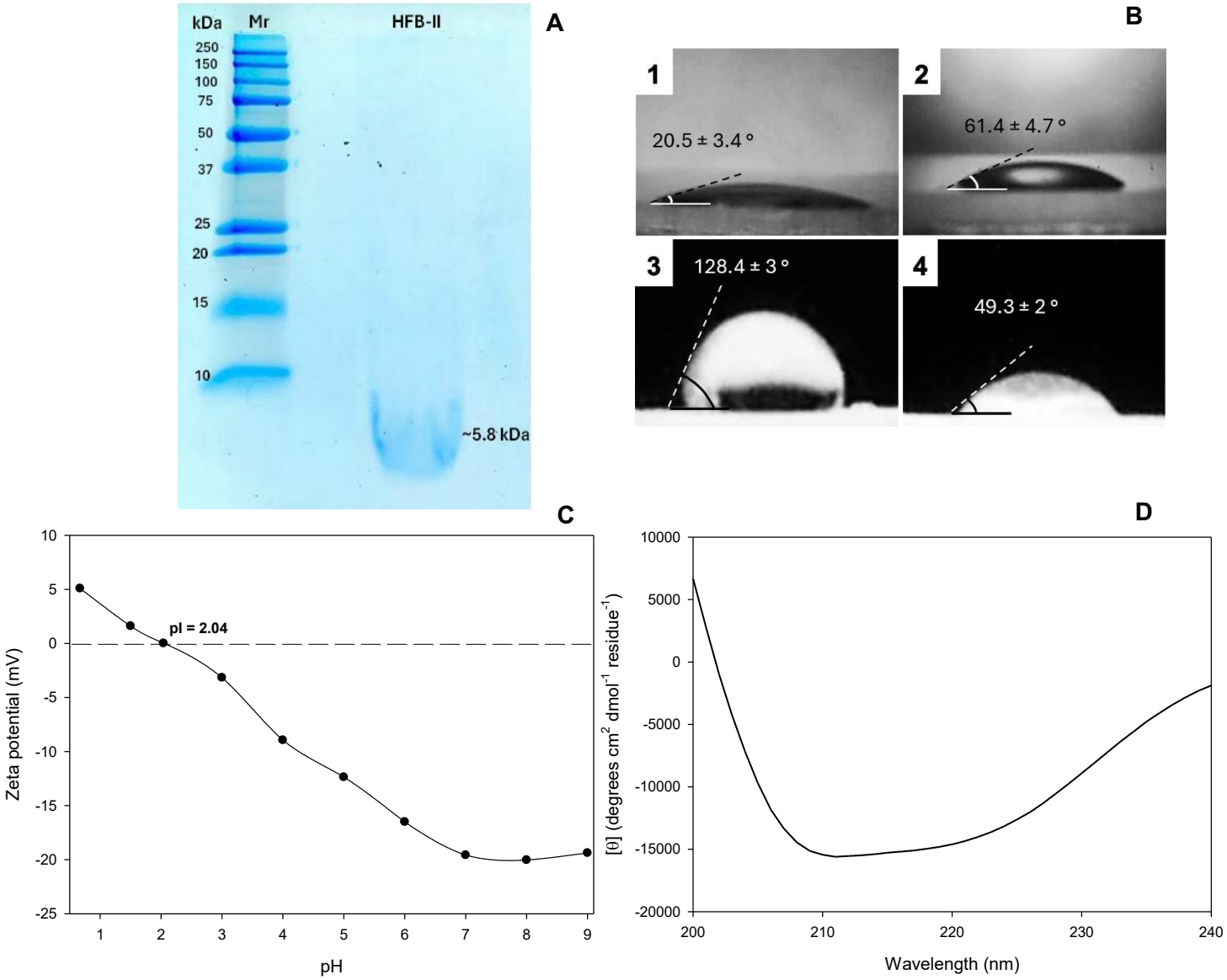

Figure 10. SDS-PAGE of HFBII stained with Coomassie blue R-250 (A). Contact angle measurements of water droplets at 26°C (B): on glass without treatment (1) and with HFB-II coating (2); on Teflon without treatment (3) and HFBII coating (50 µg mL^{-1}) (4). Zeta

potential of HFBII (1 mg mL^{-1}) dissolved in phosphate buffer (0.2 M) at 25°C (C), far-UV CD spectra of 16 µM of HFBII at 25°C in phosphate buffer (0.2 M) pH 8 (D).

Surface activity of HFBII (50 µg mL^{-1}) was tested on a hydrophilic surface (glass), resulting in a change in contact angle from 20.5 ± 3.4° to 61.4 ± 4.7°. On a hydrophobic surface, Teflon , the contact angle was modified from 128.4° ± 3° to 49.3 ° ± 2.1°, representing a 60.9% decrease in contact angle when 50 µg mL^{-1} HFBII was used as a coating. Contact angle values >90° describe a hydrophobic surface; while values <90° refer to a hydrophilic surface (Wösten *et al*., 2000). HFBs were able to modify the hydrophobicity of Teflon to a hydrophilic surface (<90°) (Figure 10B). This behavior is attributed to the intrinsic ability of hydrophobins to spontaneously self-assemble at interfaces into ordered monolayers (Class II) or amyloid-like rodlet films (Class I), driven primarily by hydrophobic interactions. Upon assembly, hydrophobins form a stable molecular coating that reorients surface-exposed functional groups, thereby redefining the surface physicochemical properties in response to the surrounding environment.

Zeta potential analysis revealed that the isoelectric point (pI) was 2.04, indicating that the HFBII became less soluble and reduced its interaction with water molecules. HFBII has a net negative partial charge at neutral and basic pH (Figure 10C). HFBII are surface-active proteins that can form flexible structures as needle-like aggregates (Wösten *et al*., 2000).

The poor solubility in water for recombinant HFB class II has been reported as challenging due to the loss of protein refolding, which directly affects functional properties such as amphiphilicity (Osmanagaoglu *et al*., 2024). Therefore, the solubility of HFB is a critical consideration for nanoparticle formation. Herein, the native HFBII from *L. lecanii* was fully solubilized at pH 9 in phosphate buffer and pH 10 in NaOH, exhibiting monodisperse behavior due to its complete solubility. In contrast, at phosphate buffer pH 5 and 6, the presence of high-particle-size species was attributed to the formation of aggregates during a partial solubilization stage, which is in accordance with their pI, where solubility is enhanced at alkaline pH (Figure 11C).

Results of CD analysis estimated the structural contents of α-helix in 60%, β-sheet 6% and a random coil 33%. Minimums were observed at 215 and 220 nm, which corresponds to β-strand and α-helical structures, respectively (Figure 10D). Results showed that HFBII

behaves as a molten globule; this flexible conformation is key for the self-assembly at air-water or hydrophobic interfaces (Sallada *et al*., 2018; Sunde *et al*., 2008). This behavior has

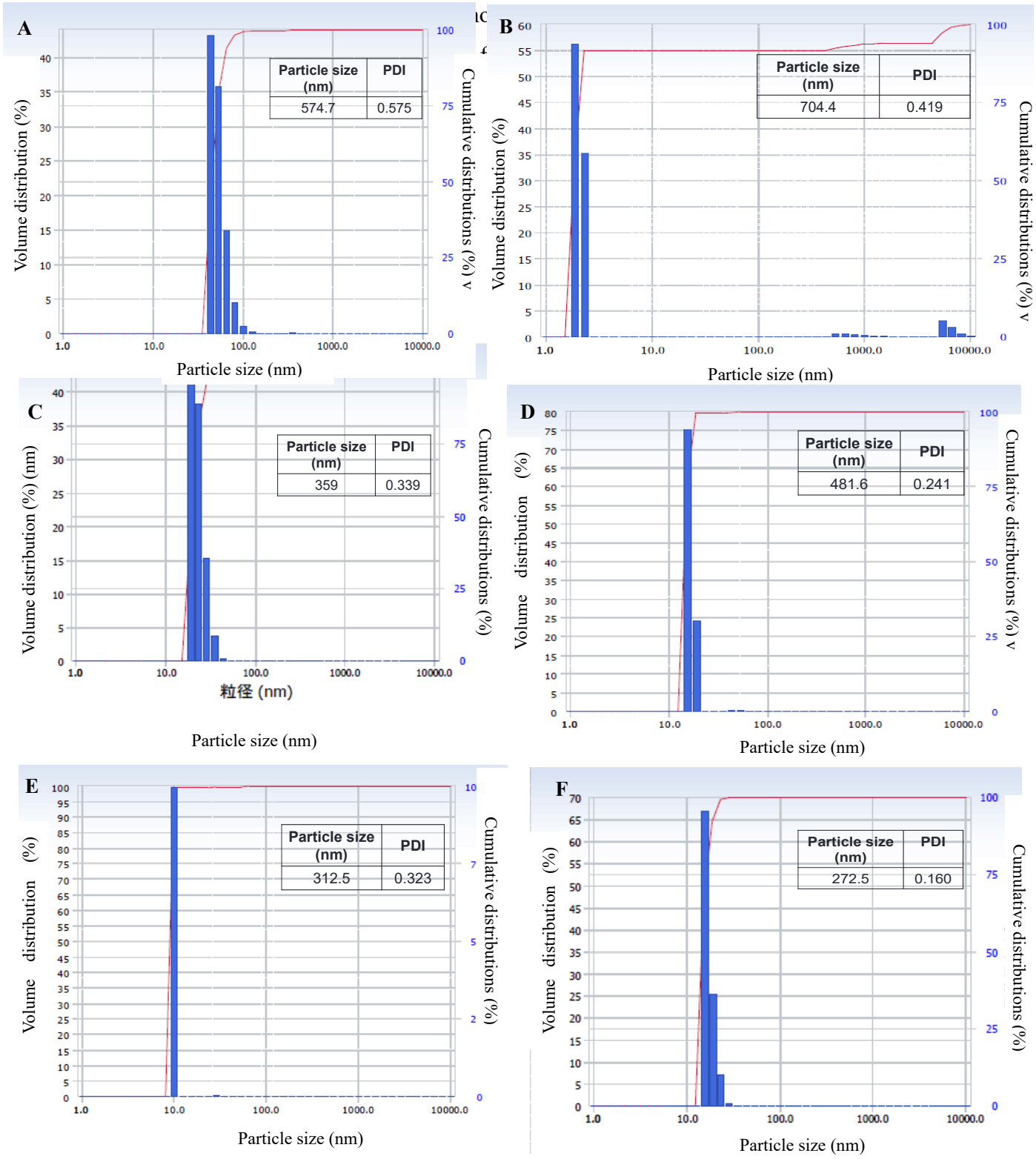

Figure 11. HFBII (5 mg mL^{-1}) size dissolved in phosphate buffer (0.2 M) at pH 5 (A), pH 6 (B), pH 7 (C), pH 8 (D), pH 9 (E), and NaOH (0.5 M) (F) was analyzed by DLS at 25°C.

2.3.2. Nanoparticles synthesis and characterization.

NPs were synthesized using a simple method with an easy purification process, which includes chromatography and dialysis for eliminating free components (THP, GlcN, and HFB). In the present study, TNPs were formulated by HFB: THP (1:0.25 molar ratio), and GlcN-TNPs were added with GlcN (1 mg mL^{-1}). Characterization of these formulations was conducted as described in Table 6. The size and polydispersity are characteristics of paramount importance for the quality of nanoparticles (Li *et al*., 2023). A PDI of 0.05 indicates a uniform sample or a highly monodisperse standard, while a value of 0.5 or higher indicates a highly polydisperse system, i.e., presents more than one particle size population. It is widely accepted that values of around 0.3 and below are most suitable for polymeric nanoparticle material systems in drug delivery applications, such as those exhibited by TNPs and GlcN-TNPs, which involve a relatively homogeneous system (Mohanraj *et a*l., 2006; Danaei y *et al*., 2018).

Table 6. Physicochemical characterization of nanoparticles (0.5 mg mL-1) dissolved in phosphate buffer (0.2M) at pH 7, analyzed at 25°C

Nanoparticles	Zeta potential (mV)	Mean size (nm)	PDI	THP loading (wt%)	Protein content (%)	AG content (%)
TNPs	-19.67±0.13	87.43 ± 2.05	0.279 ± 0.014	2.37 ± 0.03	7.02 ± 0.06	0
AG-TNPs	-17.07 ± 0.93	188.30 ± 8.85	0.17 ± 0.02	1.22 ± 0.12	10.20 ± 0.36	37.69 ± 4.9

The kidney rapidly eliminates particles with a small size, such as those measuring <10 nm in diameter, while large-sized particles are primarily deposited in the lungs, liver, or spleen (Li *et al*., 2023). In contrast, some reports indicate that molecules with diameters of 200 nm or less can be accumulated in tumors due to the EPR effect (Matsumura *et al.,* 1986). AFM of freeze-dried NPs measures the geometric size of individual particles; the results showed TNPs sizes between 57 and 75 nm (Figure 13A). Likewise, GlcN-TNPs had sizes ranging from 98 to 185 nm (Figure 12B). DLS results of TNPS in phosphate buffer at pH 7.4 indicated

a mean size of 87.43 ± 2.05 nm. For GlcN-TNPs, the size increased to 188.30 ± 8.85 nm (Table 6, Figure 12). The increase in hydrodynamic size detected by DLS can be attributed to the hydrodynamic diameter, which comprises not only the particle core but also its solvation layer (Wösten *et al*., 2000). Additionally, the TEM image shows NPs morphology, with the presence of spherical particles with a size of around 100 nm for TNPs and GlcN-TNPs, and there is no presence of aggregation. According with this findings, they present an adequate size for their use as a nanocarrier, since it has been documented that the nanoparticles with a diameter of less than 150 nm have the capacity to traverse the fenestrated capillaries that are a hallmark of tumorous regions (Mohanraj *et al*., 2006).

Zeta potential denotes the repulsive force exerted by the particles. TNPs and GlcN-TNPs produced in the present work exhibit a negative charge at pH 7 (-19.67 and -17.07 mV, respectively) (Table 6). It has been reported that values around (+/-) 30 mV evidence stability, thus preventing particle aggregation (Mohanraj *et al*., 2006). Additionally, Makimoto et al. (2021) have proposed that a critical factor in the selective accumulation of NPs in tumors is the electrical charge; a neutral or marginally negative charge reduces uptake by reticuloendothelial cells, thereby enhancing tumor accumulation.

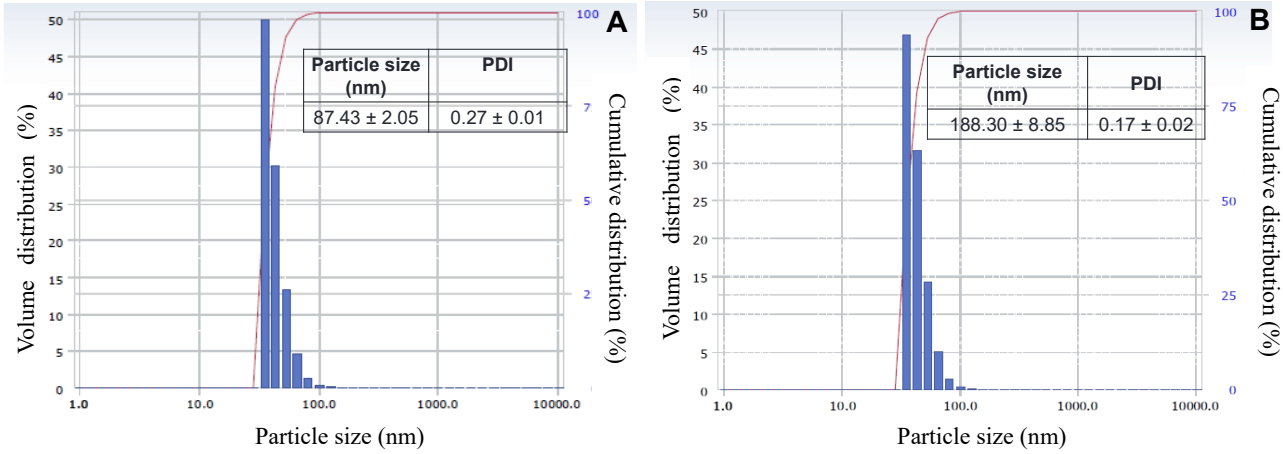

Figure 12. Particle size distribution of 0.5 mg mL^{-1} of TNPs (A) and AG-TPNs (B) dissolved in phosphate buffer (0.2 M) pH 7.4, analyzed by DLS at 25°C.

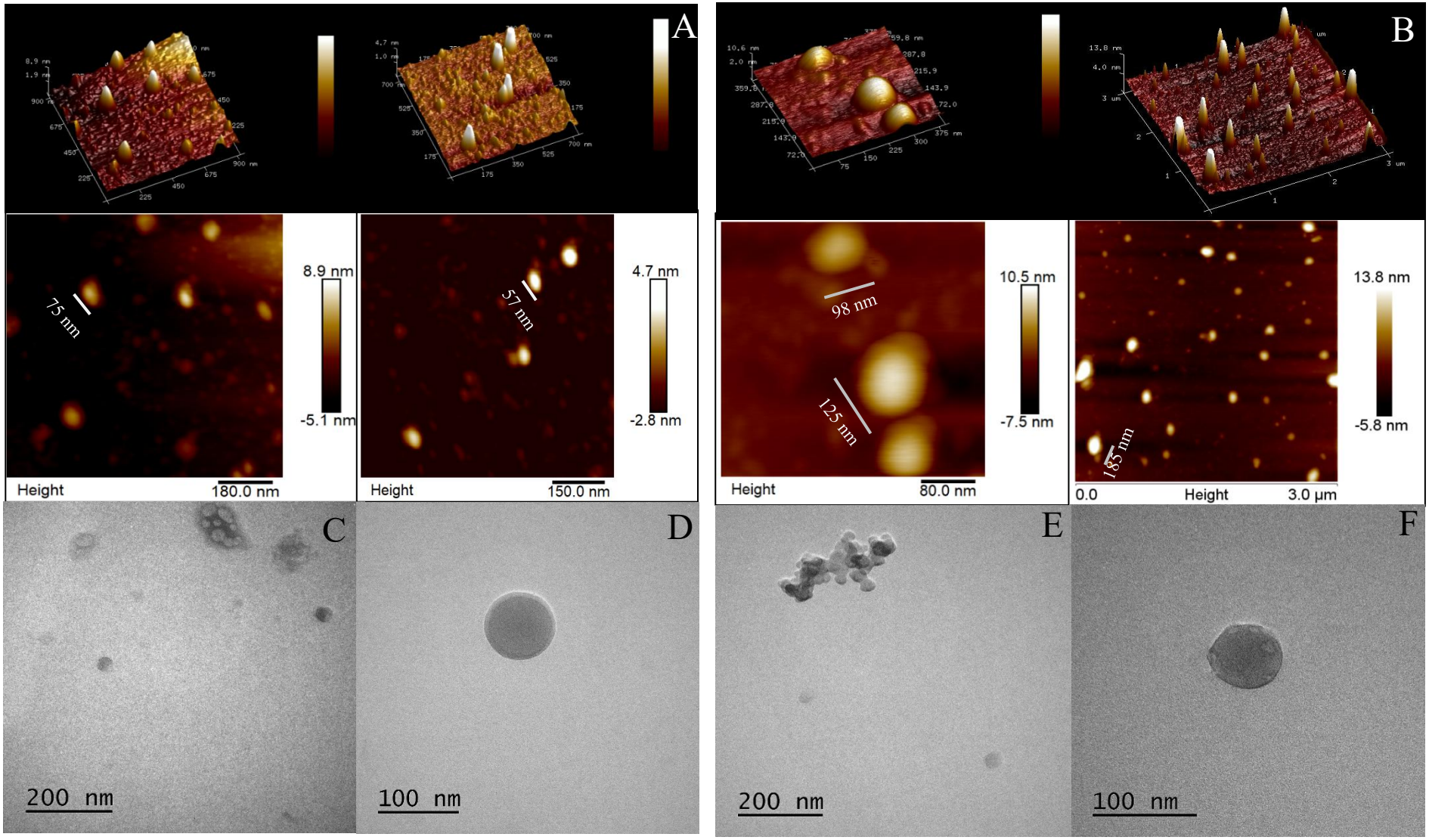
A
B
75 nm
8.9 nm
-5.1 nm
Height
180.0 nm
57 nm
4.7 nm
-2.8 nm
Height
150.0 nm
98 nm
125 nm
10.5 nm
-7.5 nm
Height
80.0 nm
185 nm
13.8 nm
-5.8 nm
0.0
Height
3.0 µm
C
200 nm
D
100 nm
E
200 nm
F
100 nm

Figure 13. AFM of TNPs (A) and GlcN-TNPs (B) in powder (6 mg) at 26°C, analyzed in air using tapping mode, TEM of TNPs at 20,000 x (C) and 40,000 x (D), and GlcN-TNPs at 20,000 x (E) and 50,000 x (F) in phosphate buffer (0.2 M) pH 7.

FTIR analysis (Figure 14) shows a shift near 3300 cm^{-1} assigned to O-H stretching vibration groups of HFBII and the absorption bands of amide I C=O stretching 1650 cm^{-1} (Sunde *et al*., 2008), and amide II N-H 1539 cm^{-1} for GlcN, due to hydrogen bonding and other interactions with THP. THP showed a sharp stretch around 1730 cm^{-1}, which is also observed due to nanoparticle formation in GlcN-TNPs and TNPs.

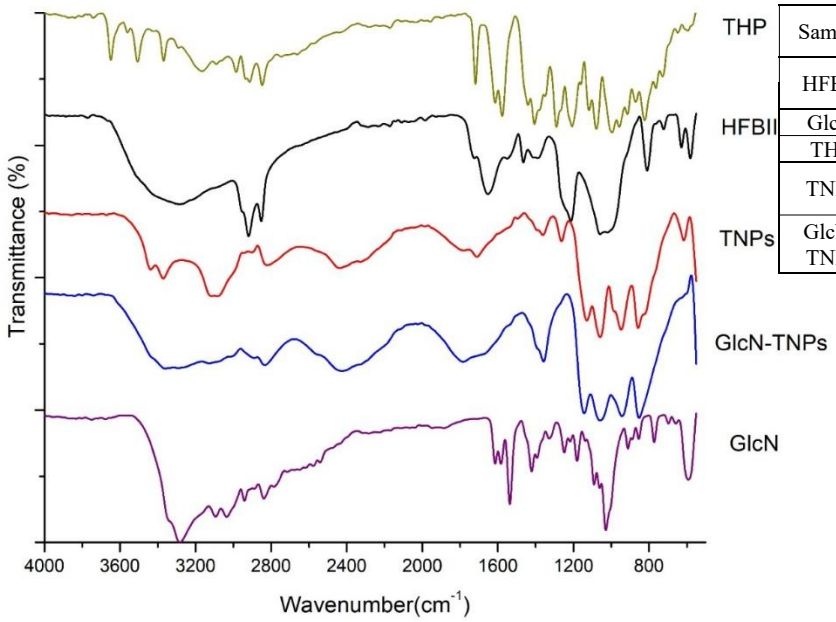

Sample	Frequencies (cm^{-1})	Functional group
HFBII	3300	O-H and N-H stretching vibration
	1650	C=O stretching vibration
GlcN	1539	N-H in-plane bending vibration
THP	1720	C=O stretching vibration
TNPs	3280.6	O-H and N-H stretching vibration
	1722.5	C=O stretching vibration
GlcN-TNPs	3280.6	O-H and N-H stretching vibration
	1718.5	C=O stretching vibration

Figure 14. ATR FTIR spectra of THP, HFBII, TNPs, GlcN-TNPs, and GlcN at 25°C.

The effect of pH on the release of THP at 37 ◦C was determined (Figure 15). The release of THP from NPs at pH 5, 6.5, and 7.4 corresponds to the pH present within lysosomes, tumor environment, and physiological conditions in the body, respectively (Hillaireau et al., 2009; Kennedy et al., 2020) The data of the THP released from TNPs were fitted using a first-order kinetic model (R2 > 0.8), estimating the release rates, k, at pH 5, 6.5, and 7.4 of 0.01, 0.006, and 0.004 h -1, respectively (Figure 15A). The release half-life (t½) was determined using the estimated first-order equation for pH 5, 6.5, and 7.4, which are 70.09 h, 111.63 h, and 155.31 h, respectively. The t½ represents the time required for 50% of the THP released from NPs. Similarly, when TNPs were at pH 5, t ½ was reduced by 2.2-fold in comparison to pH

7.4. This suggests that THP is retained mainly within the TNPs, with only limited release in the systemic circulation or in normal organs; nevertheless, THP released occurred at acidic pH when it interacts with the tumor and lysosomal environment. It is worth noting that at all pH levels, a *DR(%)* < 10% was observed up to 12 h, which describes good stability due to HFBII. HFBII could form a less water-soluble complex, so the drug release was very slow (Mohanraj *et al*., 2006). Moreover, the introduction of GlcN resulted in higher *k*, particularly at acidic pH values of 5 and 6.5. Reports demonstrate that particles with GlcN are better released in acidic conditions, promoting THP release.

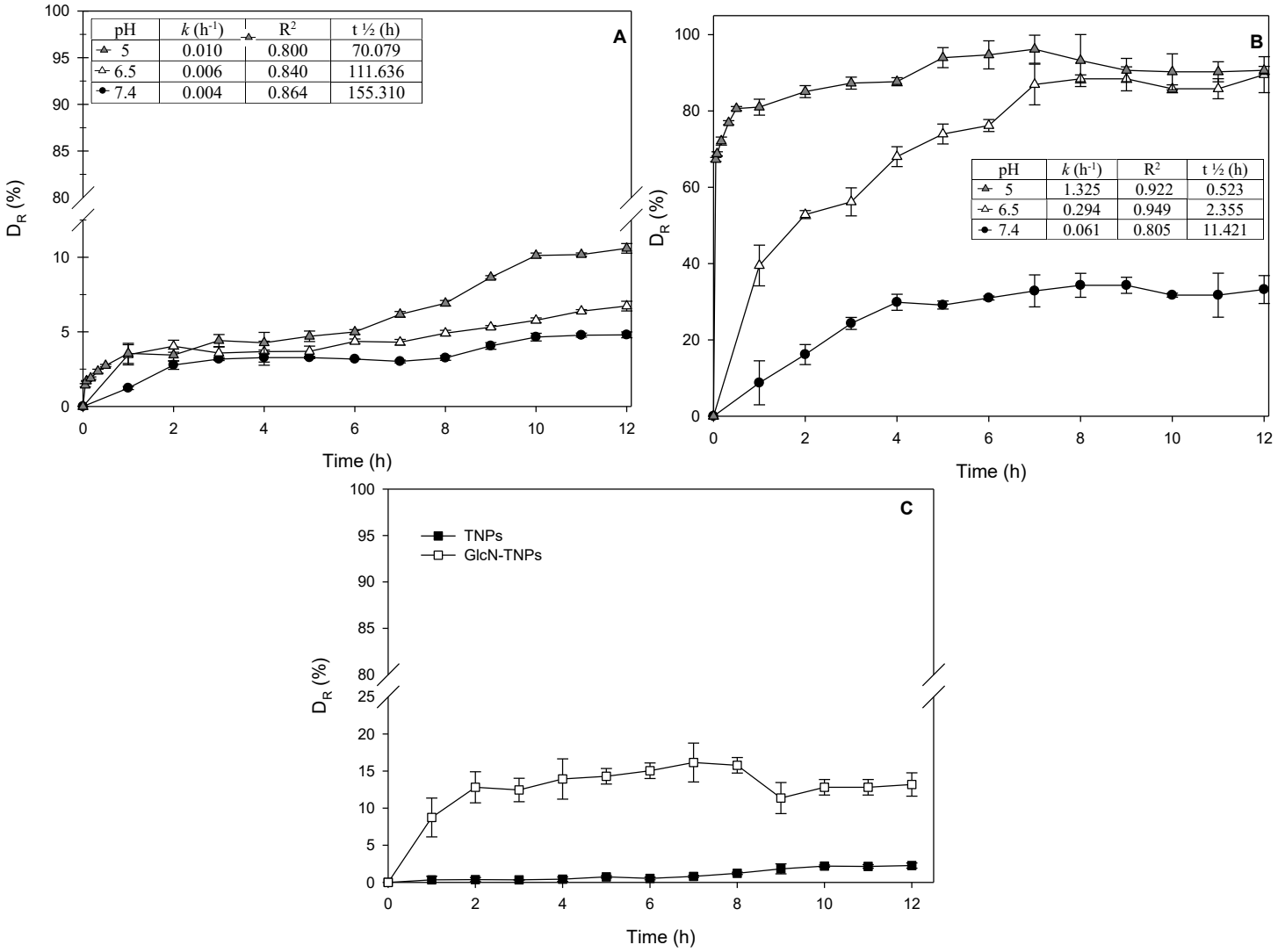

Figure 15. Time course of THP release from TNPs (A) and GlcN-TNPs (B) at 37°C, varying pH, 5, 6.5 and 7.4; and TNPs and GlcN-TNPs pH 7.4 at 4°C (C).

2.3.3. *In vitro* cytotoxicity assay

To analyze cell cytotoxicity, adenocarcinoma C26 colon cells were incubated in DMEM medium supplemented with P/S (1%) and FBS (10%), at varying concentrations of NPs and free THP, for 48 h at 37°C and 5% CO_2. The Cell Counting Kit-8 (CCK-8) contains tetrazolium salt 2-(2-methoxy-4-nitrophenyl)-3-(4-nitrophenyl)-5-(2,4-disulfophenyl)-2H-tetrazolium, which is bioreduced by cellular dehydrogenases to form an orange dye. The amount of formazan produced is directly proportional to the number of viable cells.

In this study, HFBII exhibits a cytotoxic effect against C26 cells; however, the anticancer mechanism by which HFB's action is mediated has not been thoroughly studied. Nevertheless, a few reports of cytotoxicity have been found (Fang *et al*., 2014; Osmanagaoglu *et al*., 2024; Khalesi *et al*., 2020). HFBII has been reported to have a cytotoxicity effect against T47D cells (IC_{50} 131 µM) (Khalesi *et al*., 2020) and MCF7 cells (IC_{50} 62.40 µM) (Osmanagaoglu *et al*., 2024).

In the present work, the IC_{50} values for THP alone were 0.25 µg mL^{-1} and for THP equivalent in TNPs and GlcN-TNPs were 1.12 µg mL^{-1} and 0.98 µg mL^{-1}, respectively (Figure 16). It indicates that the addition of GlcN to the formulation enhances its effect. GlcN-TNPs presented a 1.14-fold lower IC_{50} than TNPs, indicating their higher efficacy. Osmanagaoglu et al. (2024) report an IC_{50} of 0.46 µM (0.26 µg mL^{-1}) for DOX-HFB particles against MCF7 at 72 h. The difference in this behavior might be that MCF7 has been shown to be more sensitive to the anthracycline drug family than C26 cells (Jamshidi *et al*., 2024). As shown in Figure 16, GlcN-TNPs enhanced the cytotoxicity of THP against C26 cells under physiological conditions (pH 7.4) after 48 h, significantly lowering the IC_{50} compared with TNPs. GlcN itself has anticancer activity, affecting pathways related to apoptosis, proliferation, and angiogenesis (Pawar *et al*., 2017; Oh *et al*., 2007).

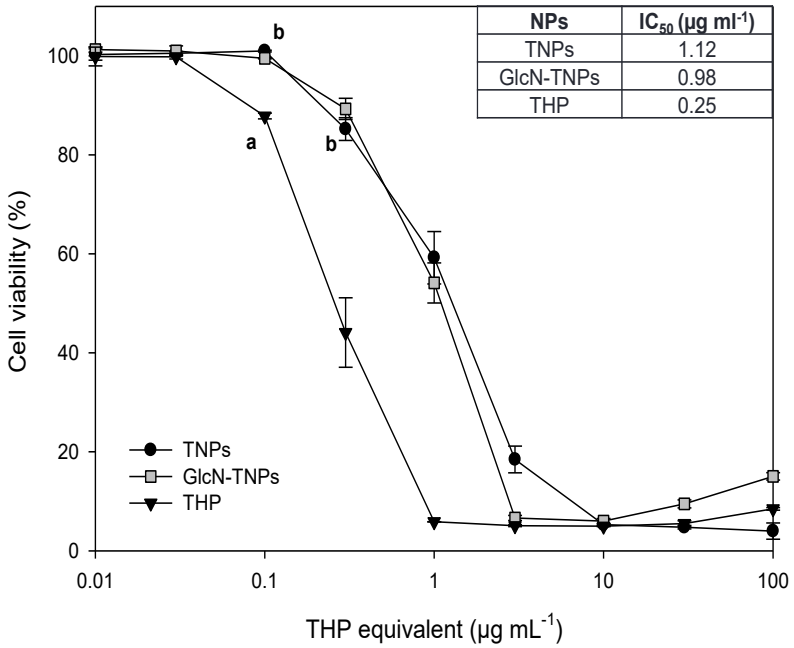

Figure 16. C26 cell viability incubated at 37 °C, 5% CO2 for 48 h in the presence of TNPs, GlcN-TNPs, and free THP. Different letters indicate significant difference ($p<0.05$) by Tukey-Kramer multiple mean comparison test; All values represent the mean ± standard deviation of the mean (n=4).

2.3.4. Intracellular uptake of THP

There are no reports on the internalization mechanism by which HFBII is incorporated into the cells. In this regard, the incubation temperature (4°C) was decreased to inhibit energy-dependent endocytosis, as shown in Figure 17A, which provides evidence that the cell uptake of THP in the TNPs and GlcN-TNPs involved endocytosis (Figure 17). Moreover, the uptake of GlcN-TNPs was markedly higher than that of TNPs, indicating the enhanced cellular internalization mediated by glucosamine modification. In the case of the free drug, even when the endocytosis process was stopped, THP continued to be taken up by the cells due to passive diffusion. The uptake mechanism involves endocytosis and passive diffusion (Kunimoto *et al*., 1984).

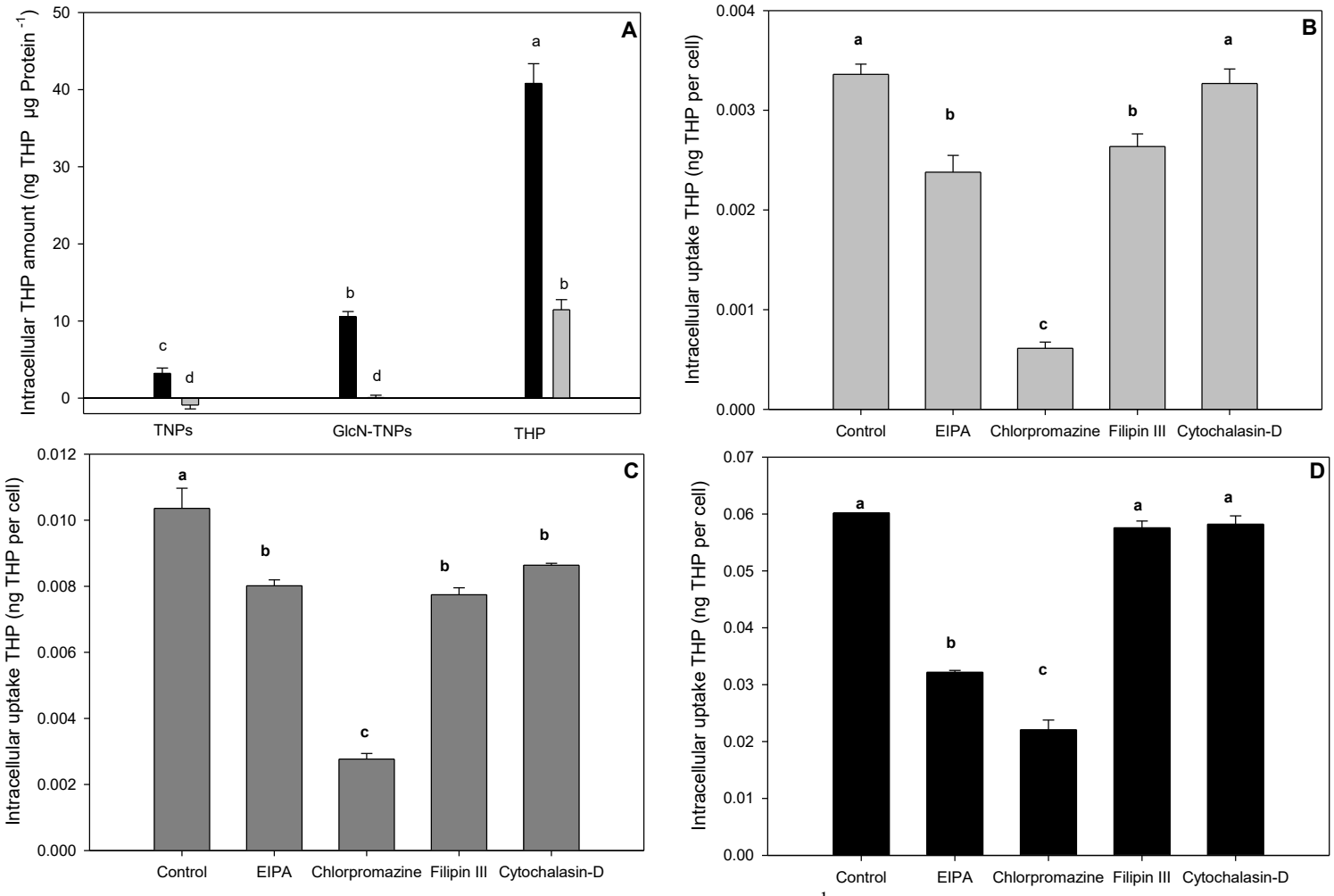

Figure 17. Intracellular uptake of free THP or NPs (10 µg mL^{-1}) at 37 (black) and 4°C (grey) for 30 min incubation; all values represent the mean± standard deviation (n=4) (A), Intracellular uptake of TNPs (B), GlcN-TNPs (C), and free THP (D). All assays were conducted with free THP or THP equivalent of 10 µg mL^{-1} at 37°C in the presence and absence of endocytosis inhibitors. Different letters indicate significant difference ($p<0.05$) by Tukey-Kramer multiple mean comparison test (n= 3).

The internalization study was conducted in the presence of different endocytosis inhibitors with known pathways. Filipin III for caveolin-mediated endocytosis, chlorpromazine for clathrin-mediated endocytosis, EIPA as a selective inhibitor of macropinocytosis, and Cytochalasin-D blocks micropinocytosis and disrupts actin polymerization (Hillaireau *et al*., 2009).

Figure 17B shows that endocytosis, mainly clathrin-mediated, is the dominant pathway for the cellular uptake of TNPs. In contrast, GlcN-TNPs appear to utilize additional routes, such as caveolin-mediated endocytosis and macropinocytosis (Figure 17C). GlcN could promote cellular internalization through micropinocytosis and actin polymerization. Moreover, GlcN is taken up via the glucose transporter GLUT1, a hypoxia-related protein associated with tumor progression and often found in peri-necrotic cancer regions (Airley *et al*., 2010; Amann *et al*., 2011). Thus, GLUT1 might provide an additional entry route, further enhancing the cellular uptake of the drug.

2.3.5. Intracellular pathways of THP

Intracellular localization of NPs was assessed using Hoechst 33342 and LysoTracker, which specifically stain the nucleus and lysosomes, respectively (Figure 18). TNPs showed perinuclear localization within lysosomes after internalization. HFBs are stabilized by disulfide bonds (Sallada *et al*., 2018). Glutathione is an agent that can reduce disulfide bridges to thiol groups, and it has been reported to be in higher concentrations in cancer cells than in normal cells (Kennedy *et al*., 2020). This mechanism could be associated with the THP release from NPs in cancer cells, especially for GlcN-TNPs that were observed surrounding the nucleus (Figure 18). In addition to the THP interaction with DNA (Kunimoto *et al*., 1983), GlcN might O-glycosylate nuclear and cytosolic proteins, affecting the phosphorylation of STAT3, which is required for its activation. STAT 3 is essential for proliferation, survival, angiogenesis and immune response of cancer cells (Chesnokov *et al*., 2009).

The extracellular acidic environment in colon cancer cells, with a pH of 6.5 (Hillaireau *et al*., 2009; Kennedy *et al*., 2020), is another factor that might allow the release of THP. In this regard, the combination of redox potential and pH may act as other release mechanisms (Kunimoto *et al*.,1983).

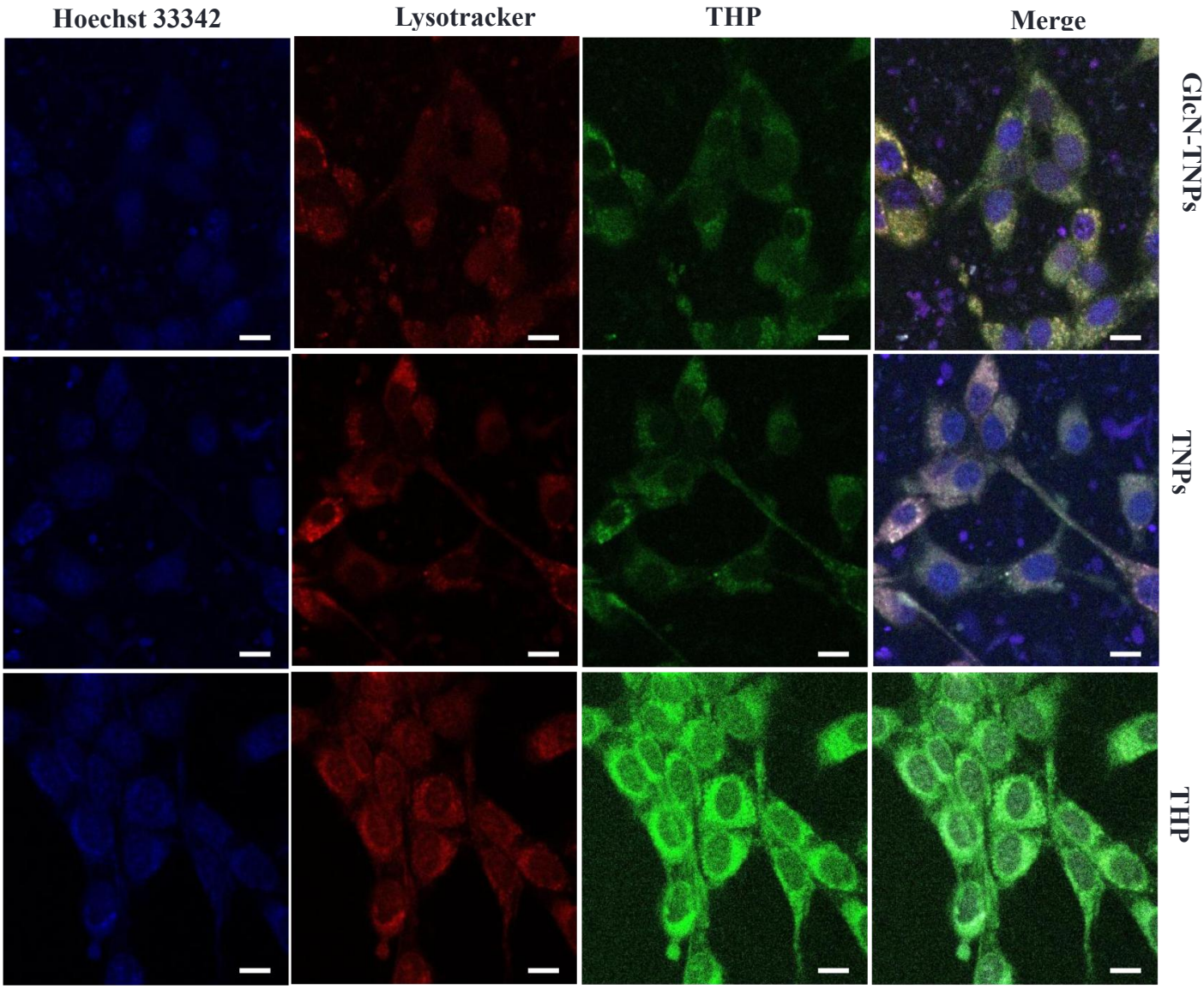

Figure 18. Confocal fluorescence of intracellular THP uptake of free THP or THP equivalent (10 µg mL^{-1}) at 30 min of incubation under controlled conditions of 37 °C and 5% CO_2, dyeing Hoechst 33342 and Lysotracker for identification of nucleus and lysosomes, respectively, scale bars correspond to 20 µm.

2.3.6. *In vivo* antitumor activity

The present study is the first to report *in vivo* results for the natural macromolecule HFB class II and GlcN. Antitumor effect of nanoparticles was determined in mice bearing colon adenocarcinoma tumors, which were administered (i.v.) a total dose of 7.5 mg of free THP

or THP equivalent per Kg of mouse body weight reparted in three doses (Figure 19A). The tumor size was significantly reduced when GlcN-TNPs were administered, followed by TNPs treatment and free THP. GlcN-TNPs exhibited superior anticancer properties and the use of HFBII as a THP carrier denotes its ability to act as a biomaterial in drug delivery (Figure 19B). GlcN inhibits the ubiquitin proteosome pathway, which regulates tumor-growth-associated proteins; some types of cancer are sensitive to proteosome inhibitors. GlcN might increase the modification of intracellular proteins with *O*-linked-β-*N*-acetylglucosamine, affecting protein-protein interaction, activity and degradation (Zahedipour *et al*., 2017). In addition, it has been reported that HFBs from conidia of airborne fungi were immunologically inert, with no induction of dendritic cell or alveolar macrophage maturation and activation observed, nor did they activate helper T-cell immune responses in an *in vivo* study (Aimanianda *et al*., 2009). Thus, HFBs prevent immune recognition, which may reduce interactions with components of biological fluids, thereby avoiding the elimination of NPs.

Antitumor effect was enhanced in GlcN-TNPs, 40% of the mice did not show tumor recurrence during the observation period, 40 days, suggesting that GlcN plays a critical role in this effect. Although several mechanisms for anticancer activity have been postulated for GlcN, such as the suppression of tumor cell proliferation through the inhibition of the G1-S transition in the cell cycle, these mechanisms might contribute to the non-recurring tumor effect (Zahedipour *et al*., 2017).

Additionally, the increase in antitumor activity (GlcN-TNPs) can also be attributed to higher internalization (Figure 17); a greater number of uptake particles results in a higher percentage of THP. Figure 19C also shows that there was no drastic change in weight loss in mice when TNPs and GlcN-TNPs were administered.

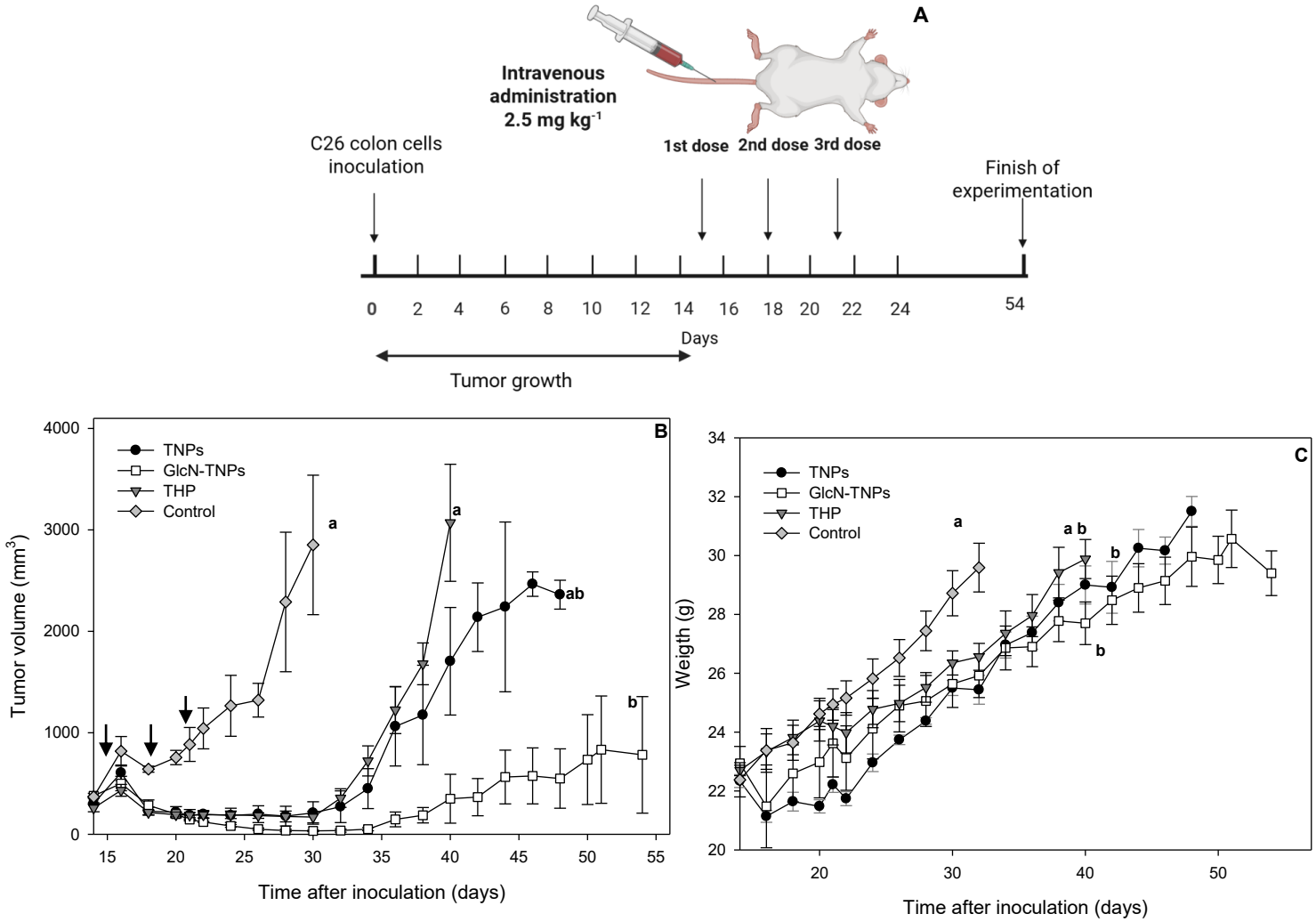

Figure 19. Administration of a total dose of 7.5 mg of free THP or THP equivalent per Kg of mouse mass (A), *in vivo* antitumor activity in mice with C26 adenocarcinoma (n = 5) (B), toxicity of treatment (C). Different letters indicate significant differences ($p<0.05$) by Tukey-Kramer multiple mean comparison test; All values represent the mean ± standard deviation of the mean (n=5), arrows indicate intravenous administration.

To identify the acute toxic dose of NPs, single intravenous injections of different concentrations of free THP or THP equivalent (5, 15, and 30 mg Kg^{-1}) were administered to healthy mice. Data showed that those mice treated with free THP at 15 and 30 mg Kg^{-1} died one day after administration, a behavior attributed to the cytotoxic effects of the free drug (Koh *et al*., 2002).

The survival rates of mice treated with GlcN-TNPs at 5 mg Kg^{-1} and 15 mg Kg^{-1} were significantly higher than those treated with TNPs or free THP (Figure 20A). Pawar *et al*. (2017) similarly reported reduced DOX toxicity using an *N*-acetyl glucosamine polymer conjugate, achieving a survival rate above 70% compared with less than 50% for the DOX solution. Our study, the survival rate for GlcN-TNPs was 100% and 77% at 5 and 15 mg Kg^{-1}, respectively (Figure 20A). GlcN and *N*-acetyl glucosamine bind to glycan receptors, resulting in drug accumulation at tumor site (Zahedipour *et al*., 2017). These amino sugars have a high affinity for the C-type of lectin receptors, which are overexpressed in cancer cells due to the increased glucose uptake to meet their energy demands (Pawar et *al*., 2017).

However, administration of GlcN-TNPs at 30 mg/kg caused fatal outcomes in mice (Figure 20A). As shown in Figure 20B, changes in body weight also reflected the toxicity profiles. Mice treated with free THP (15 or 30 mg/kg) showed a marked decrease in body weight for up to 5 days after administration, followed by partial recovery. In contrast, mice treated with TNPs or GlcN-TNPs showed no significant weight loss, indicating minimal toxicity to healthy cells. This biocompatibility is attributed to HFBII and GlcN, which not only exhibit anticancer properties but also significantly reduce the cytotoxicity of free THP.

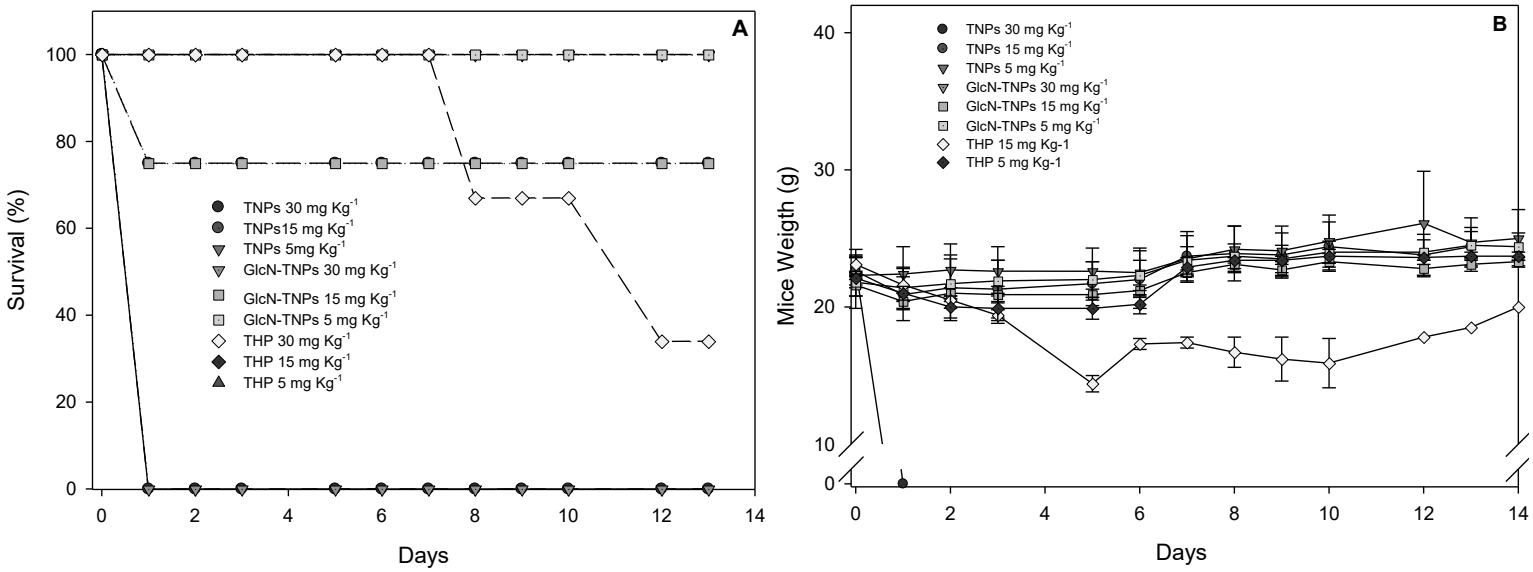

Figure 20. Survival rate of C26 tumor mice after unique i.v. administration of free THP or THP equivalent (5, 15, and 30 mg Kg^{-1}) (A), change in body weight of mice after treatment (B). Values represent the mean ± standard deviation (n= 3-4).

2.4. Conclusions

TNPs and GlcN-TNPs presented suitable characteristics as a promising system for nanomedicine, such as particle size, polydispersity distribution, stability at physiological conditions and biocompatibility. A thorough evaluation of the C26 cells revealed that GlcN-TNPs demonstrated significantly superior anticancer activity to TNPs. *In vivo* models also demonstrated that the administration of HFBII NPs resulted in a significantly higher antitumor effect against colon adenocarcinoma than free THP. Furthermore, GlcN enhanced this antitumor activity without adverse effects, as evidenced by the weight profile and percentage of survival. Nanoparticles of hydrophobins class II from *Lecanicillium lecanii* and glucosamine developed in the present study were highly efficient and selective.

2.5. References

Thakkar, S., Sharma, D., Kalia, K., Tekade, R. K. (2020). Tumor microenvironment targeted nanotherapeutics for cancer therapy and diagnosis: A review. Acta Biomater, 101, 43-68. https://doi.org/10.1016/j.actbio.2019.09.009

Veselov, V. V., Nosyrev, A. E., Jicsinszky, L., Alyautdin, R. N., Cravotto, G. (2022). Targeted delivery methods for anticancer drugs. Cancers, 14(3), 622. https://doi.org/10.3390/cancers14030622

Amreddy, N., Babu, A., Muralidharan, R., Panneerselvam, J., Srivastava, A., Ahmed, R., Mehta, M., Munshi, A., Ramesh, R. (2018). Recent advances in nanoparticle-based cancer drug and gene delivery. Adv Cancer Res, 137, 115-170. https://doi.org/10.1016/bs.acr.2017.11.003

Matsumura, Y., Maeda, H. (1986). A new concept for macromolecular therapeutics in cancer chemotherapy: mechanism of tumoritropic accumulation of proteins and the antitumor agent smancs, Cancer Res, 46(12 Pt 1), 6387-92.

Tsukigawa, K., Liao, L., Nakamura, H., Fang, J., Greish, K., Otagiri, M., Maeda H. (2015). Synthesis and therapeutic effect of styrene-maleic acid copolymer-conjugated pirarubicin, Cancer Sci, 106(3), 270-8. https://doi.org/10.1111/cas.12592

Li, H., Dai,W., Xiao, L., Sun, L., He, L. (2023) Biopolymer-Based Nanosystems: Potential Novel Carriers for Kidney Drug Delivery. Pharmaceutics 2023, 15, 2150. https://doi.org/10.3390/pharmaceutics15082150

Chakraborty, D. D., Chakraborty, P., Mondal, A. (2025). An insight into cancer nanomedicine based on polysaccharides. Int J Biol Macromol, 290, 138678. https://doi.org/10.1016/j.ijbiomac.2024.138678

Cheng, Y., Wang, B., Wang, Y., Zhang, H., Liu, C., Yang, L., ... & Wang, Z. (2020). Soluble hydrophobin mutants produced in Escherichia coli can self-assemble at various interfaces. Journal of Colloid and Interface Science, 573, 384-395.https://doi.org/10.1016/j.jcis.2020.04.012

Ezhilarasan, D., Lakshmi, T., Mallineni, S. K. (2022). Nano-based targeted drug delivery for lung cancer: therapeutic avenues and challenges. Nanomedicine, 17(24), 1855-1869. https://doi.org/10.2217/nnm-2021-0364

Calonje, M., Bernardo, D., Novaes-Ledieu, M., García Mendoza, C. (2002). Properties of a hydrophobin isolated from the mycoparasitic fungus Verticillium fungicola. Can J Microbiol., 48(11):1030-4. https://doi.org/10.1139/w02-098.

Agwora D., Gufu B., Marik T., Papp T., Vágvölgyi C., Kredics L., Tyagi C. (2025). Structural elucidation of four fungal hydrophobins belonging to classes I and II: Results from Alphafold and accelerated molecular dynamics simulations. Comput Struct Biotechnol J. 12(27):1067-1080. https://doi.org/10.1016/j.csbj.2025.03.015.

Sallada, N. D., Dunn, K. J., Berger, B. W. (2018). A structural and functional role for disulfide bonds in a class II hydrophobin. Biochemistry, 57(5), 645-653. https://doi.org/10.1021/acs.biochem.7b01166

Sunde, M., Kwan, A. H., Templeton, M. D., Beever, R. E., Mackay, J. P. (2008). Structural analysis of hydrophobins. Micron, 39(7), 773-784. https://doi.org/10.1016/j.micron.2007.08.003

Zhang, X.L., Penfold, J., Thomas, R.K., Tucker, I.M., Petkov, J.T., Bent, J., Cox, A., Grillo, I. (2011). Self-assembly of hydrophobin and hydrophobin/surfactant mixtures in aqueous solution. Langmuir, 27(17), 10514-10522. https://doi.org/10.1021/la2020226

Aimanianda, V., Bayry, J., Bozza, S. Kniemeyer, O. Perruccio, K., Ramulu Elluru, S., Clavaud, C., Paris, S., Brakhage, A.A., Kaveri, S.V., Romani, L., Latgé, J.P. (2009). Surface hydrophobin prevents immune recognition of airborne fungal spores. Nature, 460, 1117-1121, https://doi.org/10.1038/nature08264

Valo, H., Kovalainen, M., Laaksonen, P., Häkkinen, M., Auriola, S., Peltonen, L., Linder, M., Järvinen, K., Hirvonen, J., Laaksonen, T. (2011). Immobilization of protein-coated drug nanoparticles in nanofibrillar cellulose matrices—Enhanced stability and release. J. Control. Release, 156(3), 390-397. https://doi.org/10.1016/j.jconrel.2011.07.016

Reuter, L.J., Shahbazi, M.A., Mäkilä, E.M., Salonen, J.J., Saberianfar, R., Menassa, R., Santos, H.Á., Joensuu, J.J., Ritala, A. (2017). Coating nanoparticles with plant-produced transferrin–Hydrophobin fusion protein enhances their uptake in Cancer cells. Bioconjug. Chem., 28(6), 1639-1648. https://doi.org/10.1021/acs.bioconjchem.7b00075

Sun, L., Xu, H., Xu, J.H., Wang, S.N., Wang, J.W., Zhang, H.F., Jia, W.R., Li, L.S. (2020). Enhanced antitumor efficacy of curcumin-loaded PLGA nanoparticles coated with unique fungal hydrophobin. AAPS Pharmscitech, 21(5), 171. https://doi.org/10.1208/s12249-020-01698-w

Fang, G., Tang, B., Liu, Z., Gou, J., Zhang, Y., Xu, H., Tang, X. (2014). Novel hydrophobin-coated docetaxel nanoparticles for intravenous delivery: in vitro characteristics and in vivo performance. Eur. J. Pharm. Sci., 60, 1-9. https://doi.org/ 10.1016/j.ejps.2014.04.016

Osmanagaoglu, F. H., Ekmekcioglu, A., Ozcan, B., Bayram Akcapinar, G., Muftuoglu, M. (2024). Preparation and characterization of hydrophobin 4-coated liposomes for doxorubicin delivery to cancer cells. Pharmaceuticals, 17(11), 1422. https://doi.org/10.3390/ph17111422

Rocha-Pino, Z., Vigueras, G., Shirai, K. (2011). Production and activities of chitinases and hydrophobins from Lecanicillium lecanii. Bioprocess Biosyst. Eng., 34(6), 681-686. https://doi.org/10.1007/s00449-011-0517-z

Umezawa, H., Takahashi, Y., Kinoshita, M., Naganawa, H., Masuda, T., Ishizuka, M., Tatsuta, K., Takeuchi, T. (1979). Tetrahydropyranyl derivatives of daunomycin and adriamycin. J. Antibiot., 32(10), 1082-1084. https://doi.org/10.7164/antibiotics.32.1082

Kunimoto, S., Miura, K., Takahashi, Y., Takeuchi, T., Umezawa, H. (1983). Rapid uptake by cultured tumor cells and intracellular behavior of 4'-O-tetrahydropyranyladriamycin. J. Antibiot., 36(3), 312-317. https://doi.org/ 10.7164/antibiotics.36.312

Koh, E., Ueda, Y., Nakamura, T., Kobayashi, A., Katsuta, S., Takahashi, H. (2002). Apoptosis in young rats with adriamycin-induced cardiomyopathy—comparison with pirarubicin, a new anthracycline derivative. Pediatr Res. 51(2) 256-9. https://doi.org/ 10.1203/00006450-200202000-00021

Kunimoto, S., Miura, K., Umezawa, K., Xu, C.Z., Masuda, T., Takeuchi, T., Umezawa, H (1984). Cellular uptake and efflux and cytostatic activity of 4'-O-tetrahydropyranyladriamycin in adriamycin-sensitive and resistant tumor cell lines. J Antibiot , 37(12), 1697-1702. https://doi.org/10.7164/antibiotics.37.1697

Nakamura, H., Koziolová, E., Chytil, P., Tsukigawa, K., Fang, J., Haratake, M., Ulbrich, K., Etrych, T., Maeda, H. (2016). Pronounced Cellular Uptake of Pirarubicin versus That of Other Anthracyclines: Comparison of HPMA Copolymer Conjugates of Pirarubicin and Doxorubicin, Mol Pharm, 13(12) 4106-4115. https://doi.org/ 10.1021/acs.molpharmaceut.6b00697

Hasegawa, T., Tsukigawa, K., Commey, K., Sakuragi, M., Imoto, S., Taguchi, K., Nishi, K., Otagiri, M., Yamasaki, K. (2024). Preparation and in Vitro Characterization of Fatty-Acid Modified Pirarubicin Nanosuspensions Stabilized by Albumin. Chem. Pharm. Bull. (Tokyo), 72(1):21-27. https://doi:10.1248/cpb.c23-00701

Airley, R., Evans, A., Mobasheri, A., Hewitt, S.M. (2010). Glucose transporter Glut-1 is detectable in peri-necrotic regions in many human tumor types but not normal tissues: Study using tissue microarrays, Ann Anat, 192(3), 133-8. https://doi.org/10.1016/j.aanat.2010.03.001

Amann, T., Kirovski, G., Bosserhoff, A.K., Hellerbrand, C. (2011). Analysis of a promoter polymorphism of the GLUT1 gene in patients with hepatocellular carcinoma, Mol Membr Biol, 28(3), 182-6. https://doi.org/10.3109/09687688.2011.554447

Zahedipour, F., Dalirfardouei, R., Karimi, G., Jamialahmadi, K. (2017). Molecular mechanisms of anticancer effects of Glucosamine. Biomed. Pharmacother, 95, 1051-1058.http://dx.doi.org/10.1016/j.biopha.2017.08.122

Pawar, S., Mahajan, K.,Vavia, P. (2017) In Vivo Anticancer Efficacy and Toxicity Studies of a Novel Polymer Conjugate N-Acetyl Glucosamine (NAG)–PEG–Doxorubicin for Targeted Cancer Therapy. AAPS PharmSciTech 18, 3021-3033. https://doi.org/10.1208/s12249-017-0787-0

Oh, H.J., Lee, J.S., Song, D.K., Shin, D.H., Jang, B.C., Suh, S.I., Park, J.W., Suh, M.H., Baek, W.K. (2007). D-glucosamine inhibits proliferation of human cancer cells through inhibition of p70S6K, Biochem Biophys Res Commun, 360(4) 840-5. https://doi.org/10.1016/j.bbrc.2007.06.137

Meng, F., Hennink, W.E., Zhong, Z. (2009). Reduction-sensitive polymers and bioconjugates for biomedical applications, Biomaterials, 30(12) 2180-98. https://doi.org/10.1016/j.biomaterials.2009.01.026

Laemmli, U. K. (1970). Cleavage of structural proteins during the assembly of the head of bacteriophage T4. Nat., 227(5259), 680-685. http://doi.org/ 10.1038/227680a0

Schneider, C. A., Rasband, W. S., Eliceiri, K. W. (2012). NIH Image to ImageJ: 25 years of image analysis. Nat. Methods., 9(7), 671-675. https://doi.org/ 10.1038/nmeth.2089

Whitmore, L., Wallace, B.A. (2008) Protein secondary structure analyses from circular dichroism spectroscopy: Methods and Reference Databases. Biopolymers 89: 392-400.

Jamshidi, Z., Dehghan, R., Nejabat, M., Abnous, K., Taghdisi, S. M., Hadizadeh, F. (2024). Dual-targeting CD44 and mucin by hyaluronic acid and 5TR1 aptamer for epirubicin delivery into cancer cells: Synthesis, characterization, in vitro and in vivo evaluation. Heliyon, 10(2). https://doi.org/10.1016/j.heliyon.2024.e24833

Wösten, H. A., de Vöcht, M. L. (2000). Hydrophobins, the fungal coat unravelled. Biochim. Biophys. Acta – Rev. Biomembr., 1469(2), 79-86. https://doi.org/10.1016/S0304-4157(00)00002-2

Mohanraj, V. J., Chen, Y. (2006). Nanoparticles-a review. Trop. J. Pharm. Res., 5(1), 561-573. https://doi.org/10.4314/tjpr.v5i1.14634

Danaei, M., Dehghankhold, M., Ataei, S., Hasanzadeh Davarani, F., Javanmard, R., Dokhani, A., Khorasani, S., Mozafari, M.R. (2018). Impact of particle size and polydispersity index on the clinical applications of lipidic nanocarrier systems. Pharmaceutics, 10(2),57. https://doi.org/10.3390/pharmaceutics10020057

Makimoto, A., Fang, J., Maeda, H. (2021). Development of a selective tumor-targeted drug delivery system: Hydroxypropyl-acrylamide polymer-conjugated pirarubicin (P-THP) for pediatric solid tumors. Cancers, 13(15), 3698. https://doi.org/10.3390/cancers13153698

Khalesi, M., Mamashli, F., Goliaei, B., Moosavi-Movahedi, A. A., Derdelinckx, G. (2020). Class II Hydrophobin HFBII: A Potential Carrier for Antitumor Agents. Curr. Bioact. Compd, 16(1), 80-84. https://doi.org/10.2174/1573407214666180420092631

Hillaireau, H., Couvreur, P. (2009). Nanocarriers' entry into the cell: relevance to drug delivery. Cell. Mol. Life Sci, 66(17), 2873-2896. https://doi.org/10.1007/s00018-009-0053-z

Kennedy, L., Sandhu, J. K., Harper, M. E., Cuperlovic-Culf, M. (2020). Role of glutathione in cancer: from mechanisms to therapies. Biomolecules, 10(10), 1429. https://doi.org/10.3390/biom10101429

Chesnokov, V., Sun, C., Itakura, K. (2009). Glucosamine suppresses proliferation of human prostate carcinoma DU145 cells through inhibition of STAT3 signaling. Cancer Cell Int. 9(1), 25. https://doi:10.1186/1475-2867-9-25

Chapter 3: Emulsions of hydrophobins class I and II from *Lecanicillium lecanii* with jatropha oil as a biolubricant for cutting fluids.

3.1. Introduction

Metalworking industry relies heavily on working fluids (MWFs), especially water-miscible oil emulsions (WMOs). However, conventional formulations based on mineral oils and petroleum-derived emulsifiers are not biodegradable. Additionally, the management of mineral oil waste represents a source of contamination in ecosystems, where the burning of these oils is accompanied by the release of metals with health implications, such as zinc, generating hazardous waste (Narayana *et al*., 2022). In response to these problems, alternatives have been developed using vegetable oils and ecological emulsifiers based on coconut, castor, palm, and jatropha oils, which have demonstrated performance comparable to commercial products, offering a more sustainable and ecological option.

Jatropha oil (JO) is a non-edible vegetable oil that has been reported as an alternative for the development of biolubricants due to its chemical and tribological characteristics. Tribological characteristics describe the behavior of interacting surfaces in relative motion, encompassing friction, wear, and lubrication. These characteristics are governed by surface chemistry, roughness, contact mechanics, and the presence of lubricating films, which collectively determine energy dissipation and material loss (Narayana *et al*., 2022). In biological systems, controlling tribological properties is critical to improving efficiency, durability, and performance by minimizing friction coefficients and reducing wear under applied loads and sliding conditions.

JO is composed of fatty acids such as arachidonic acid, linoleic acid, behenic acid, oleic acid, and lauric acid (32.7%, 26.6%, 25.2%, 11.2%, and 4.2%, respectively) (Aguilar-Rosas *et al*., 2022). It also has a low coefficient of friction, a key parameter in its use as a lubricant (Narayana *et al*., 2022).

Hydrophobins (HFB) are small proteins with the ability to modify the hydrophobicity of surfaces. Their production by filamentous fungi has been reported to play a key role in the growth and development of these organisms (Wösten and de Votch, 2000).

HFBs have been divided into classes I and II, based on their hydrophilic characteristics, solubility, and structures formed during self-assembly (Wösten and de Votch, 2000). HFB Class I (HFBI) are produced by ascomycete and basidiomycete fungi, forming highly stable structures called rodlets that are insoluble in water and resistant to temperatures up to 100°C. In contrast, HFB class II (HFBII) are only produced by ascomycetes with an amino acid residue content between 50-100. They are soluble in aqueous solutions containing sodium dodecyl sulfate (SDS) and are characterized by not forming rodlet-type structures, which is why the assemblies they form are more unstable than those formed by class I (Terauchi *et al*., 2022).

The characteristics of these proteins, due to their amphiphilic properties, self-assembly, and surface activity, have led to a variety of applications, such as in oil recovery (Rocha-Pino e*t al.,* 2018), as an emulsifying and surfactant agent in food (Alamprese *et al.,* 2022), in medicine as a drug carrier (Barani *et al.,* 2022), and as anti-fouling agents (Kulkarni *et al.,* 2022).

3.2. Experimental method

3.2.1. Materials

All reagents used in this study were of analytical grade.

3.2.2. Production of Hydrophobins

Submerged cultures (50 L) of chitosan (10 g L^{-1}) were used as a carbon source, inoculated with a suspension of *L. lecanii* ATCC 26854 spores (10^7 spores mL^{-1}) at 28°C, pH 6, 125 rpm, and 1 volume of air per volume of medium (vvm) (Hernández-Alcántara *et al*., 2025).

3.2.3. Purification of HFBs

Biomass obtained by centrifuging the crude extract (CE) was resuspended in Tris-HCl (10 mM) supplemented with SDS (2%) at pH 9 under agitation for 2 h for HFBI extraction. It was then centrifuged at 10,000 rpm at 4°C for 15 min (Thermo Scientific, Osterode, Germany). Precipitate was washed with deionized water to remove excess SDS, resuspended in concentrated formic acid, and sonicated in an ice bath for two 30-second cycles. The

mixture was neutralized with NaOH (50%) and then centrifuged at 10,000 rpm at 4°C for 10 minutes.

The pellet was resuspended in Tris-HCl (100 mM) at pH 9 for precipitation by electrobubbling at 300 mA; the foam collected was centrifuged at 10,000 rpm for 10 minutes at 4 °C. The precipitate was solubilized in trifluoroacetic acid for subsequent evaporation with air for 24 hours (Rocha-Pino *et al*., 2018).

On the other hand, to obtain HFBII, the supernatant obtained from washing the biomass with Tris-HCl and SDS was mixed with KCl (2M) in a 1:0.5 ratio to remove the SDS. It was then centrifuged at 10,000 rpm for 15 min. Supernatant was washed with deionized water to remove excess of SDS, for subsequent electrobubbling at 300 mA; the collected foam was centrifuged at 10,000 rpm for 10 minutes at 4 °C (Rocha-Pino *et al*., 2018).

3.2.4. Characterization of HFBs

Surface activity of HFBs was determined using Teflon and glass as hydrophobic and hydrophilic surfaces, respectively. Solutions of HFBI and II were placed on the clean surfaces at concentrations of 10, 25, 30, 40, 50, and 60 µg ml^{-1} and left to dry for 12 h. Hydrophobicity was determined by measuring the contact angle of a water drop (20 µL) on the surfaces (Rocha-Pino *et al.,* 2018) and analyzed using ImageJ 1.41 software (National Institutes of Health, USA).

Molecular weight of the HFBs was analyzed by electrophoresis with 5% polyacrylamide gels and 17% separation at 175 V, under denaturing conditions (SDS-PAGE) as proposed by Laemmli (1970). Using Precision Plus Protein Standard Unstained (Bio-Rad, Hercules, US) as a broad-range molecular weight standard, the gels were stained with Coomassie Blue R-250 (Bio-Rad, Hercules, CA, USA) and silver (Bio-Rad, USA), and then analyzed using ImageJ 1.41 software.

Charge analysis was performed using a Zetasizer Nano-ZS instrument (Malvern Panalytical, UK). HFBI and II (100 µg mL^{-1}) were dissolved in KCl (10 mM) at pH between 2-9, using HCl or KOH (0.1 M) for pH adjustment (Terauchi *et al*., 2022).

Secondary structure was determined by dissolving HFBI andII (at 100 µg mL^{-1}) in ethanol:water at a ratio of 40:60, using a Jasco model J-720 spectropolarimeter (Tokyo, Japan)

with a Jasco J32CDQ10 cell at 25°C in the far UV CD range (190-250 nm) (Kulkarni *et al*., 2022). CD analysis was carried out by Dichro Web using the K2D method (Whitmore *et al*., 2008).

3.2.5. Emulsions with Jatropha Oil

Based on the concentration determined to modify the hydrophobicity of the materials, emulsions of HFBI and II (100 µg mL^{-1}) were prepared with jatropha oil (JO) in a 3:1 ratio. Mixture was homogenized at 9,500 rpm for 7 min, rested for 1 min, followed by a second mixing at 13,500 rpm for 3 min using an Ultraturrax T25 (IKA, Staufen, Germany). The stability of the emulsion was characterized in an accelerated coagulation process by centrifugation at 4,000 x g for 15 min at 25°C. Subsequently, the total volume of the emulsion and the creaming index (CI) were calculated using equation 11.

$$IC = \frac{100\ x\ Hs}{HE} \qquad (11)$$

Where HE and Hs represent the total height of the emulsion and serum layer, respectively (Aguilar-Rosas *et al*., 2022).

A sample (1 mL) of emulsion was separated for subsequent observation under an optical microscope to determine the particle size. For this purpose, the ImageJ 1.41 program was used, where the polydispersity index (PDI) was calculated using equation 12.

$$IPD = (\frac{\sigma}{d})^2 \qquad (12)$$

where IPD is the square of the standard deviation (σ) divided by the mean diameter of the emulsion (d) (Raval *et al.,* 2019).

3.2.6. Friction tests

Emulsions formulated from HFBI and II (100 µg mL^{-1}) with JO in a 3:1 ratio were tested for use as biolubricants. These were subjected to friction tests in a 4-ball machine, under conditions of room temperature (26 °C), 392 N, at a speed of 1200 ± 60 rpm for 10 minutes. Coefficient of friction was determined using a customized Arduino, and the friction mark was measured using an optical microscope (Aguilar-Rosas *et al.,* 2022).

3.2.7. Shear tests

Emulsions formulated from HFBI and II (100 μg mL^{-1}) with JO were compared to a commercial semi-synthetic oil-based emulsion MWF CIM-STAR® (10% w/v). These formulations were tested in a dry machining process in turning operations.

Machining operations were carried out on AISI 1018 steel bars (C-0.15e 0.20%, Mn- 0.60e 0.900%, S-0.050%, P-0.050%, hardness 116 ± 2 HB) measuring Ø 25.4 x 120 mm on a 5 HP lathe (Pinacho SP 200) under constant cutting parameters of 70 m min^{-1} as cutting speed, 860 RPM, 0.15 mm rev^{-1} as feed, and 0.5 mm as cutting depth. The emulsions were stirred before the machining test to ensure homogeneity.

Emulsions were applied at a constant flow rate of 4e-5 m^3 h^{-1} using the minimum quantity lubrication (MQL) technique with constant parameters of air pressure, nozzle distance, and nozzle diameter of 0.4 MPa, 20 mm, and 0.4 mm, respectively. The cutting forces (cutting force (Fx), radial force (Fy), and feed force (Fz)) were measured using a piezoelectric dynamometer (kISTLER type 9121), a dual model amplifier (kISTLER type 5814B1), and a data acquisition device (NI-USB 182 6008) together with Lab-View software. The temperatures during the cutting process were measured using a thermal imaging camera (FLIR TG). The surface finish of the part was measured in terms of surface roughness, Ra, using a roughness tester (Surfcom 130A) after each cutting operation. Roughness was measured in the longitudinal direction along the machined area of each part, taking the average of three measurements with a displacement of 120° from the previous measurement (Aguilar-Rosas *et al*., 2022).

3.2.8. Microbiological analysis

Microbiological growth was determined in accordance with Mexican Official Standards NOM-092-SSA1-1994 for the count of aerobic mesophiles in standard agar at 35°C, NOM-113-SSA1-1994 for the determination of total coliforms by incubation on brilliant green agar plates at 35°C, and NOM-111-SSA1-1994 for the count of molds and yeasts on potato dextrose agar at 25°C.

3.2.9. Statistical analysis

Statistical analysis of the experimental data was performed using analysis of variance and Tukey-Kramer multiple comparisons of means, using SPSS software version 22.0 (IBM Corp., Armonk, US). Statistically significant differences in means were considered at $p \leq 0.05$, presented as different letters between contact angle conditions, variation.

3.3. Results and discussion

3.3.1. Production and purification of HFB

HFBI and II were produced and purified from biomass present in submerged cultures of *L. lecanii* with chitosan as a carbon source (Figure 21A). The production of these proteins is necessary for aerial growth and spore dispersal in filamentous fungi. Other biological functions have been reported, such as hyphal adhesion, where the common point is interaction with surfaces (Wösten and de Votch, 2000; Schor *et al*., 2016). Likewise, the production of these surface-active proteins acts as protection for the mycelium to prevent it from drying out (Rocha Pino *et al.,* 2018).

In *L. lecanii* cultures, a higher yield of HFB class I was obtained compared to type II (Figure 21B). This behavior may be associated with their biological function, where HFBIIs are related to a greater ability to reduce surface tension, while HFBIs are key in the sporulation process of the fungus (Mustalahti *et al.,* 2013). Thus, higher HFBI production may be a biological response to the growth of *L. lecanii*. Similar results have been reported by Rocha-Pino *et al.* (2018), where higher production of HFBI compared to HFBII is obtained in solid medium cultures using polyurethane foam squares as a support, with HFI and HFBII yields of 9.5% and 2.5%, respectively, which is lower than the results obtained in the present study for HFBI (36.46 ± 2.36%) and HFBII (19.53 ± 0.45%) with molecular masses of 8.7 and 5.8 kDa, respectively.

The hydrophobicity of materials is an important parameter for evaluating the ability of proteins to interact with surfaces. In this regard, the surface activity of HFBs was determined by the contact angle on a Teflon (PTFE) and glass surface, at concentrations ranging from 0 to 60 $\mu g\ mL^{-1}$ (Table 7).

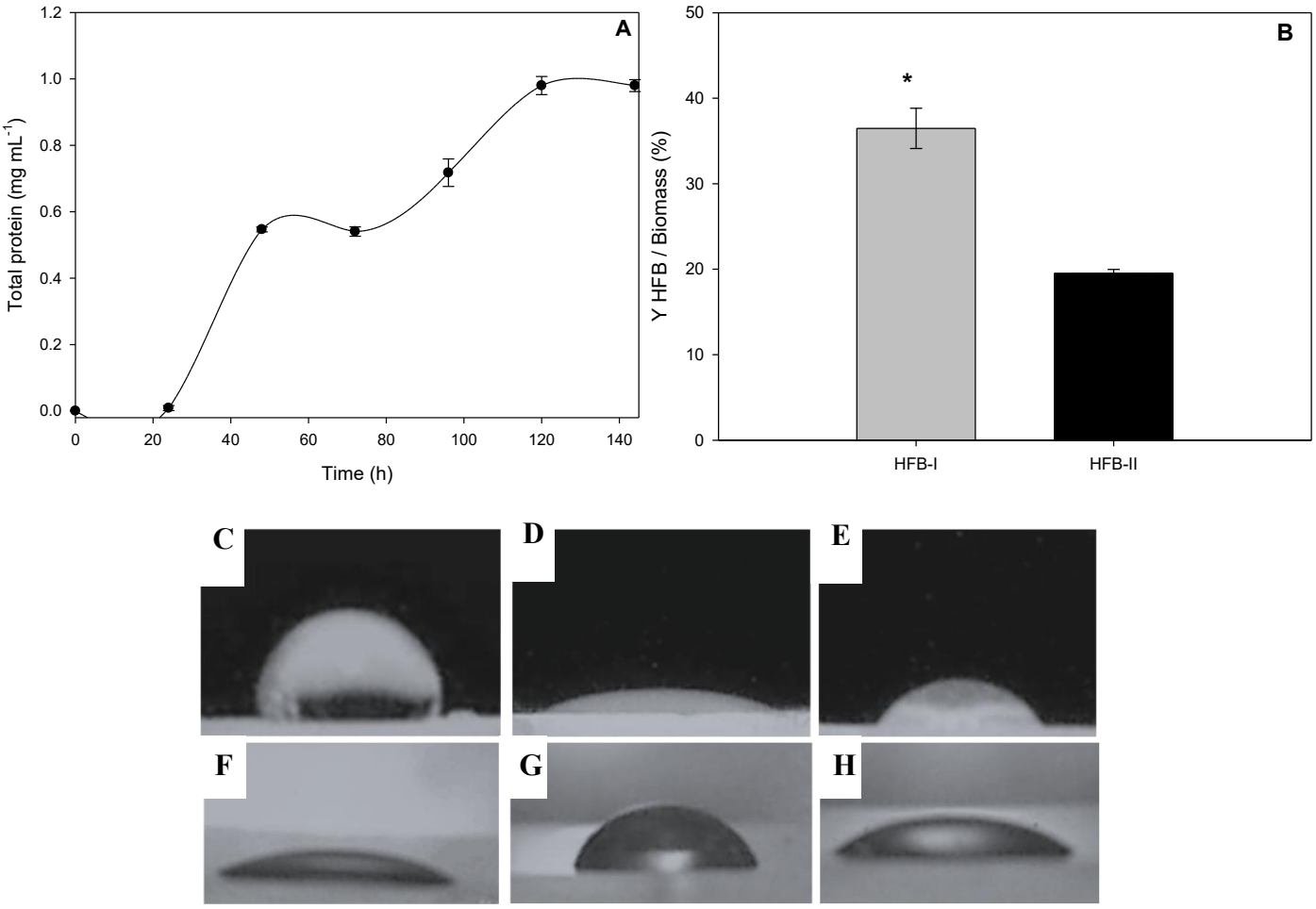

Figure 21. Biomass production in submerged cultures of *L. lecanii* with chitosan as a carbon source at 28°C, pH 6, 125 rpm, and 1 vvm (A). Yield obtained in the extraction of HFBs from *L. lecanii* biomass (B). Measurement of the contact angle on an untreated Teflon surface (C), on a Teflon surface with HFBI (D) and with HFBII (E), on an untreated glass surface (F), on a glass surface with HFBI (G) and with HFBII (H) at 25°C. Symbols (*) indicate a significant difference using Student's t-test.

Surfaces were classified according to this parameter, where a contact angle greater than 90° is considered hydrophobic, while, conversely, a contact angle less than 90° represents a hydrophilic surface (Ragesh *et al*., 2014). Surfaces coated with HFBI achieved a greater change compared to class II surfaces, reducing the contact angle on Teflon (PTFE) by 65.8% using 50 μg mL^{-1} (Figure 21D). Similar behaviors have been reported by Rocha-Pino *et al*. (2018), where the same concentration of HFBI, obtained in solid cultures with chitin,

achieved a 52% reduction in the contact angle. Regarding the ability to modify hydrophilic surfaces (glass), HFBI (50 μg mL^{-1}) can modify a hydrophilic surface to hydrophobic with contact angle values of 89.7 ± 2.6°, compared to an untreated glass surface (24.58 ± 4.4°) (Table 7). On the other hand, it is observed that the hydrophobic effect due to coating with HFBII requires a higher concentration of HFB, which is consistent with the report by Winandy *et al*. (2018), in which a coating with hydrophobin class II from *Trichoderma reesei* forms less stable layers on glass surfaces. However, in the present study, HFBs class I and II from *L. lecanii* showed a marked hydrophobic and hydrophilic effect on glass and Teflon surfaces, respectively, a behavior that is attributed to their well-reported self-assembly characteristics (Wösten and de Votch, 2000).

Table 7. Contact angle on glass and Teflon surfaces coated with HFB class I and II of *L. lecanii* at 25°C.

Sample	**Protein concentration (μg mL^{-1})**	**Φ (°) in Glass**	**Φ (°) in Teflon**	**Decrease in Teflon (%)**
Control	0	24.58 ± 4.4 [a]	127.3 ± 3.6 [a]	0
HFBI	10	63.6 ± 1.4 [b]	108.6 ± 2.4 [b]	14.6
	25	62 ± 3.6 [b]	101.5 ± 2.6 [b]	20.2
	30	60.6 ± 3.2 [b]	100.2 ± 3.1 [b]	21.2
	40	61.7 ± 1.6 [b]	97.4 ± 2.8 [b]	23.4
	50	89.7 ± 2.6 [c]	43.5 ± 3 e	65.8
	60	77.3 ± 4.8 [d]	70.5 ± 4.4 [d]	44.6
HFBII	10	46.6 ± 4.1	84.3 ± 3.6 [b]	33.09
	25	53.4 ± 1.5	67.8 ± 3.9 [d]	45.9
	30	53.2 ± 4.6	55.8 ± 2.9 [e]	55.4
	40	57 ± 3.1	53.8 ± 8.6 [e]	57.01
	50	62.8 ± 4.2	46.2 ± 1.7 [e]	62.9
	60	67.9 ± 3.6	49.5 ± 5[e]	60.3

*Different letters indicate significant differences using Tukey-Kramer multiple comparison test ($p<0.05$), values represent mean ± standard deviation n=5.

Isoelectric point (pI) is defined as the pH at which the protein has a net zero charge. Generally, proteins are less soluble at their pI, promoting aggregation and precipitation in solutions. It was observed that the pI was determined at pH 7.3 for HFBI (Figure 22A), so solubility decreases as the pH approaches this value; in this case, it is favored in acidic pH, adopting a positive charge. This behavior has been reported by Basheva *et al*., (2011) in HFBII from *Trichoderma reesei*, where, as it approaches its pI, the proteins aggregate, thus decreasing their solubility (pI 6.5).

In contrast, HFBII had a pI of around pH 2.1, so alkaline conditions are favorable, where a partial net negative charge occurs under these conditions.

Circular dichroism is a technique capable of distinguishing between the predominant type of structure. Minima between 208 and 220 nm can be observed, which are significant and correspond to α/β structures (Figure 22B). Likewise, a minimum between 250 and 215 nm characteristic of β-sheet structure has been reported (Kulkarni *et al*., 2022). Following the classification proposed by Manavalan *et al.,* (1983), HFBI and II have α/β structures with intermingled segments of α-helix and β-sheet. Differences in structure between the two classes can be seen in the size and displacement in the minimum zone. HFBI exhibits behavior characteristic of β-sheets. It has been reported that the marked stability of this class is due to the large, disordered loop that contains a greater number of β-sheets in the hydrophobic zone compared to HFBII. In contrast, HFBIIs are composed of one α-helix and four β-sheets, which promote the formation of a central structure called a "barrel." (Kulkarni *et al*., 2017; Schor *et al*., 2016).

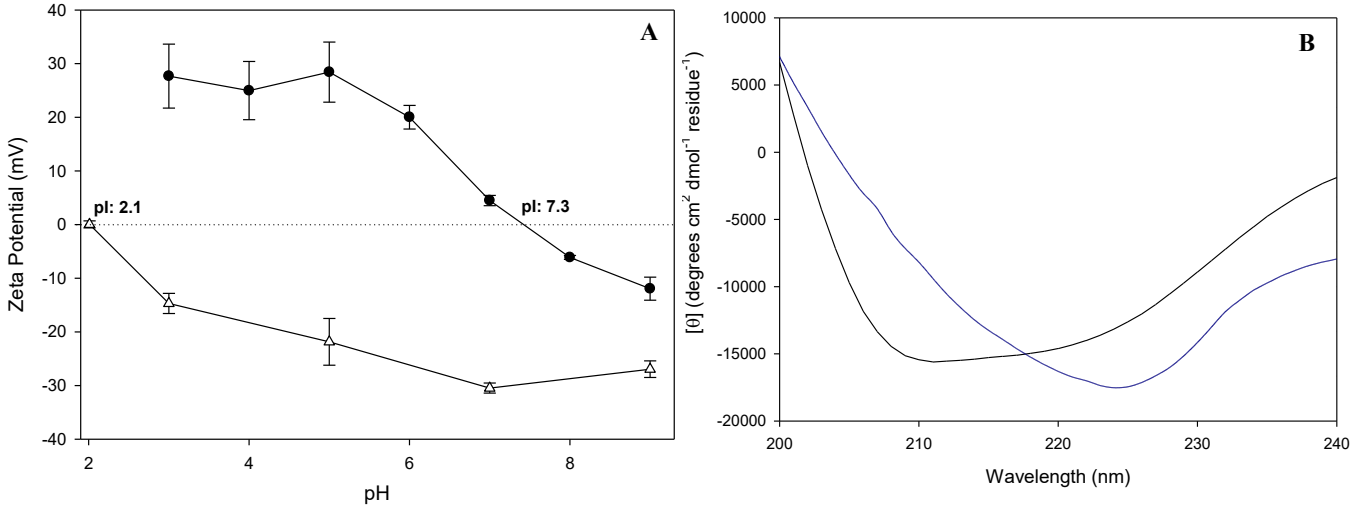

Figure 22. Determination of the zeta potential of HFBI (●) and HFBII (△) dissolved in KCl (10 mM) at 25°C (A) and DC spectrum of far UV of HFBI (blue) and II (black) (100 µg mL^{-1}) dissolved in ethanol:water in a 4:6 ratio at 26°C (B).

3.3.2. HFB-JO emulsions

Emulsions were formulated with HFBI and II (100, 200, 300, 400, and 500 µg mL^{-1}) (Figure 23) based on JO oil, the results showed evidence of a minimum creaming index (CI) of between 24.48 and 26.63% for HFBI and II, respectively, at concentrations of 100 µg mL^{-1} HFBI emulsions were superior, and it has been reported that HFBI has greater efficiency in stabilizing oil emulsions (Mustalahti *et al*., 2013). The CI is a parameter of emulsion stability; the higher the creaming index, the lower the stability (Alamprese, C *et al*., 2022).

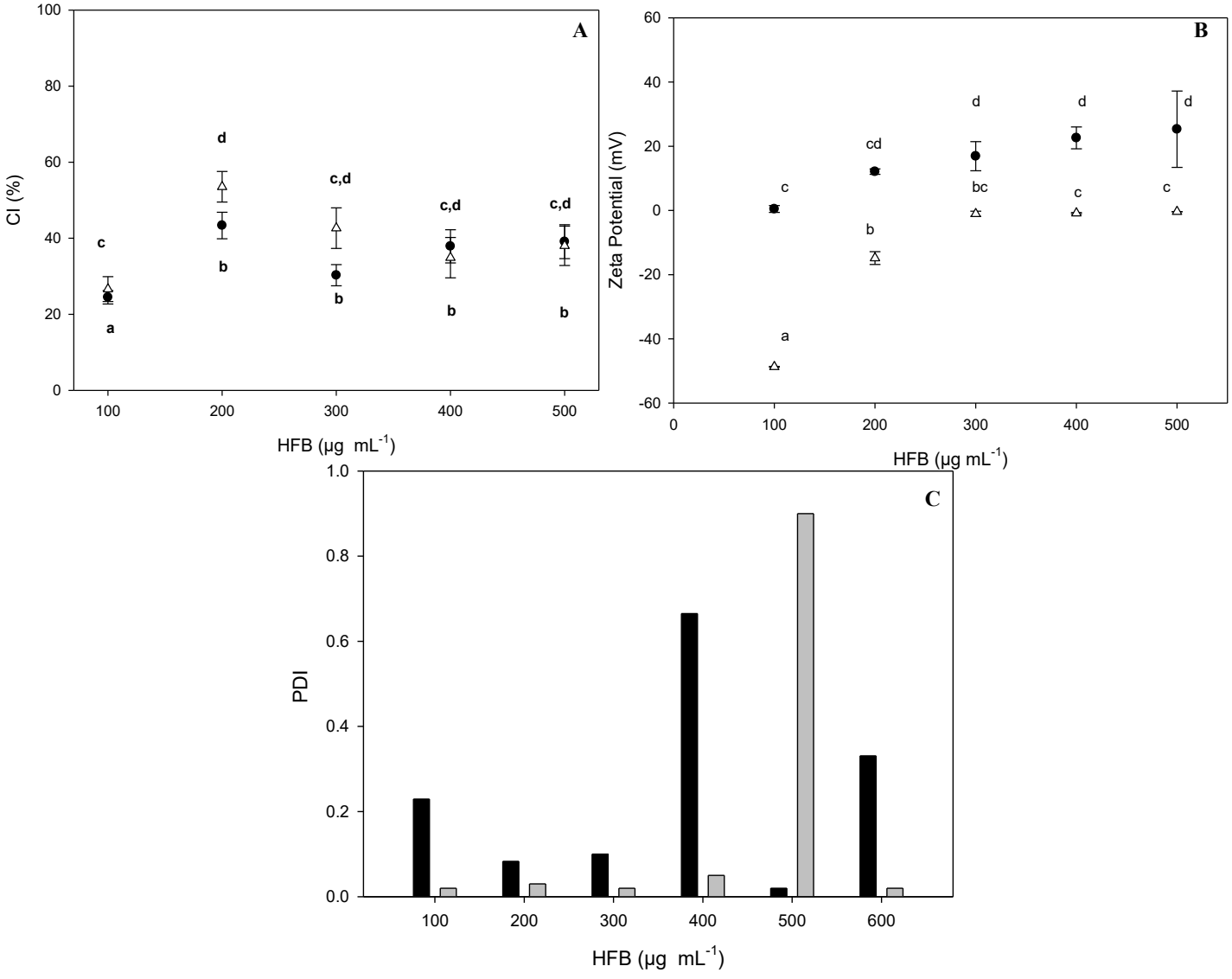

Figure 23. CI (A) and zeta potential (B) for HFBI (●) and II (△) emulsions at concentrations of 100, 200, 300, 400, and 500 μg mL^{-1} and JO in a 3:1 ratio, homogenized in an Ultraturrax in two phases at 9,500 rpm for 7 min and 13,500 rpm for 3 min with a 1-min rest interval at 25°C, and PDI of emulsions formulated with HFB-JO (C).

JO has a charge of -0.27 ± 0.22 with a pH of 6.37 ± 0.20. The zeta potential results showed that the incorporation of HFB significantly modified the surface charge. HFBI imparted increasing positive values with concentration, where a greater amount of HFBI causes greater coating of the interface by HFBI, providing electrostatic stability. The nature of hydrophobins, being amphiphilic, where the hydrophobic region could interact strongly with the fatty acid and triglyceride chains present in JO, forming a protein film around the oil droplets, preventing coalescence and stabilizing the emulsion. HFBII generated negative potentials, with a concentration-dependent trend, reaching values close to zero (≥300 μg mL^{-1}), suggesting areas of colloidal instability, which could be due to protein aggregation processes. These results are consistent with those reported for emulsions stabilized with amphiphilic proteins, where zeta potential values around (+/-) 30 mV indicate stability against flocculation and coalescence (McClements, 2007). In the case of biolubricants derived from vegetable oils, studies have shown that the adsorption of biopolymers or proteins at the interface can shift the zeta potential toward higher values, improving stability and tribological performance (Zadaka *et al*., 2010).

Polydispersity index (PDI) of the emulsion is a parameter that allows us to understand the uniformity of particle size in the emulsion, which is crucial for the stability and efficacy of the release of active ingredients in emulsified formulations. Formulations with a monomodal distribution were developed in which micrometer-scale particle sizes predominate, in the range of 1 to 10 μm (Figure 24), with particle sizes of 1-2.5 μm being favored, with an PDI of around 0.30. However, smaller size polydispersity was found for both classes in the 500 μg mL^{-1} formulation, with a value of around 0.2, in contrast to a CI of 39.10 ± 4.46% and 38.02 ± 5.18%, indicative of poor stability.

Although a high PID was obtained at 100 μg mL^{-1} of HFBI, the formulated emulsions showed greater stability, which is an essential parameter for their application as a biolubricant (Figure 23B). Similar behavior is observed in the case of emulsions with HFBII, the lowest CI occurs

at the minimum protein concentration, with PDI values indicating the presence of a single species size.

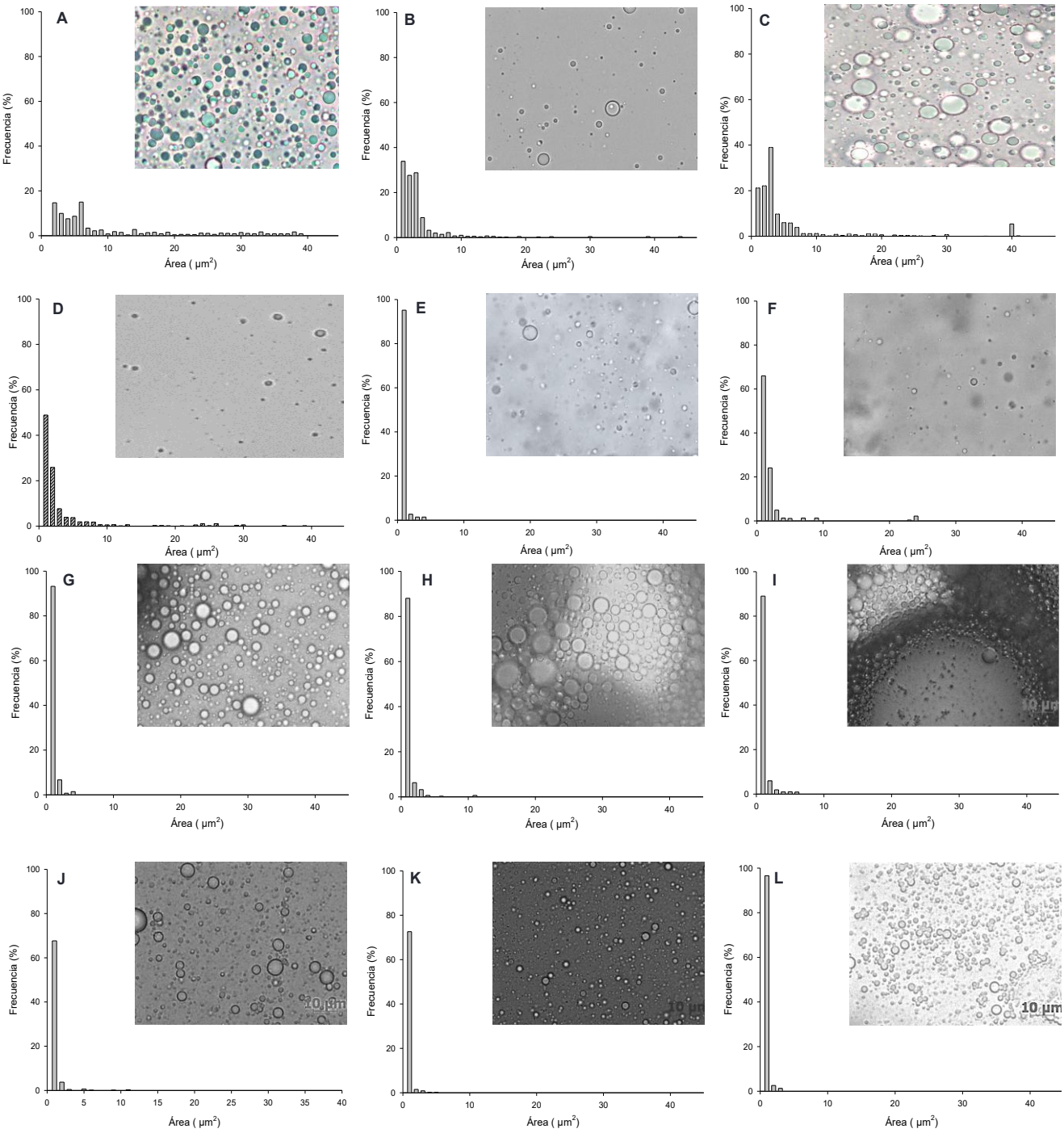

Figure 24. Distribution of droplet size in emulsions formulated with HFBI-JO (ratio 3:1) determined by microscopic observation (100x): A) 100 µg mL^{-1}, B) 200 µg mL^{-1}, C) 300 µg mL^{-1}, D) 400 µg mL^{-1}, E) 500 µg mL^{-1}, F) 600 µg mL^{-1} and observations of HFBII-JO

emulsions at concentrations of G) 100 µg mL^{-1}, H) 200 µg mL^{-1}, I) 300 µg mL^{-1}, J) 400 µg mL^{-1}, K) 500 µg mL^{-1}, and L) 600 µg mL^{-1}.

3.3.3. Four-ball test

Tribological tests were performed on HFBI and HFBII emulsions (100 µg mL^{-1}) mixed with JO (3:1) and compared with a commercial hydrocarbon-based chemical emulsion, CIMSTAR-60.

These tests were carried out under 23°C, speed of 1200 ± 60 rpm, with a load of 392 N (40 Kg) for 10 minutes, using a customized Arduino-based measurement system to evaluate the coefficient of friction. These parameters are crucial for determining the effectiveness of the emulsions developed as biolubricants in turning applications. Coefficient of friction is a measure that indicates the resistance generated by two surfaces due to movement; the lower this parameter, the less force is required to carry out the movement (Bird *et al*., 1993). Such is the case with HFBI, where a lower coefficient of friction was obtained, indicating less wear on materials, which could extend the life of the mechanical components used in turning processes (Figure 25).

During the process, the emulsion with HFB-I-JO has a lower coefficient of friction compared to the commercial lubricant CIMSTAR-60, indicating that the use of HFBI improves fluidity, reducing wear and heat generation in the fluid (Figure 25A). HFBI has been reported to have the ability to withstand high temperatures (100°C) due to the formation of rodlet structures during assembly, a characteristic that is important because cutting processes generate an increase in temperature (Aguilar Rosas *et al.,*2022).

Friction mark generated during testing using an optical microscope (Figures 25C, 25D, and 25E) provides information on wear and interaction between contacting surfaces, which is important for evaluating the effectiveness of emulsions as biolubricants.

Tribological properties, such as wear and coefficient of friction, are key to their application as lubricants. Lower friction could reduce the energy used in processes (Ahmad *et al*., 2022) and the frequency of replacement of the materials used.

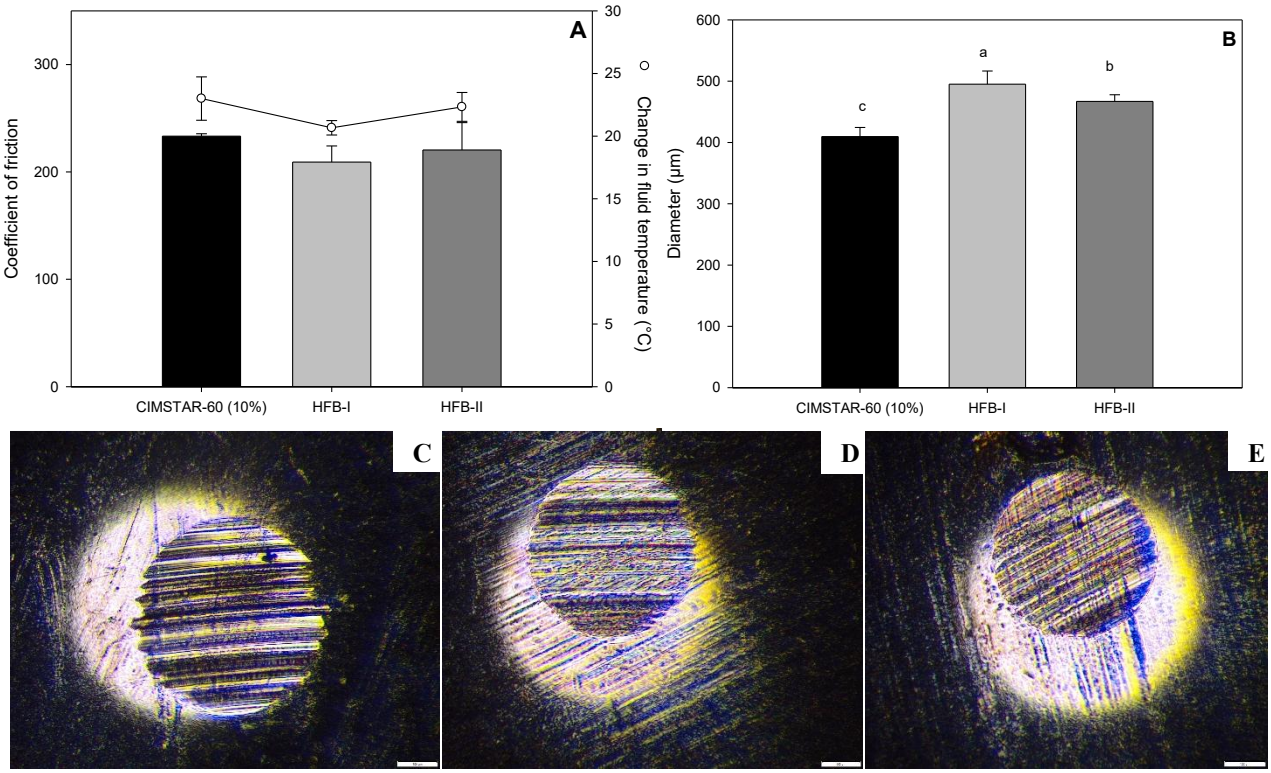

Figure 25. Friction coefficient generated, temperature change during the process (A), and diameter of the indentation generated by the friction of the materials using HFBI-JO (C), HFBII-JO (D), and CIMSTAR-60 (10%) (E), during the stress process using four-ball analysis at 25 °C, for 10 min at 1200 rpm with a force of 392 N.

In terms of cutting forces, the emulsion with HFBI showed lower values in all three force directions, indicating that it generated a protective layer between the cutting tip and the workpiece, reducing friction and corroborating the results obtained in the wear test. This may be due to the mechanism whereby the hydrophilic side of the HFB adheres to metal surfaces, while the hydrophobic end interacts with the cutting oil, thereby generating greater fluidity.

Roughness was higher in HFBII and I compared to the control (Figure 26D). Although this parameter is important because it can significantly affect the finish quality of machined parts, it could be used in the finishing of industrial parts where the finishing is not the primary characteristic.

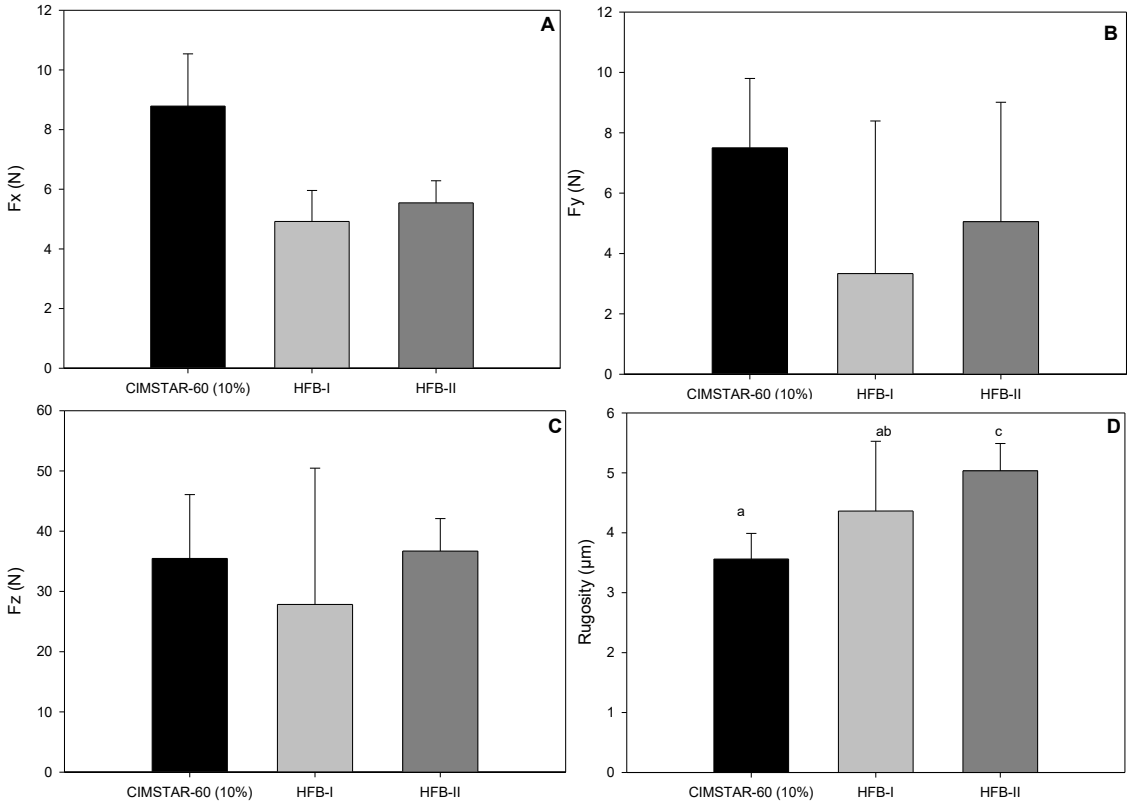

Figure 26. Cutting force (Fx) (A), radial force (Fy) (B), feed force (Fz) (C), and roughness in the finish of the machined part (D) in a cutting process at a speed of 860 rpm, with a cutting depth and speed of 0.5 mm and 70 m min^{-1}.

Mineral and chemical lubricants are toxic and harmful to human health (Ahmad *et al.,* 2022), while vegetable oils are more biodegradable than minerals (Narayana *et al*., 2022). Cutting fluids have been reported to become contaminated and develop microbial growth over time (Marchand *et al.,* 2010). These fluids are usually administered in spray form at different speeds, causing a fraction to be inhaled by workers and leading to respiratory and skin problems due to exposure (Thornéus *et al.,* 2021). Because of this, it is important to analyze the tendency of formulations to microbial growth. It has been observed that the use of HFBI and HFBII emulsions reduces the presence of airborne mesophiles (Figure 27) compared to CIMSTAR-60, as in the case of bacteria of the genus *Pseudomonas*, which have been reported to be present in cutting fluids throughout their use (Marchand *et al*., 2010). Similar behavior is observed in the contamination of fungi and yeasts, where HFB- shows the lowest presence of these types of microorganisms, important genera such as *Fusarium, Aspergillus*,

Cladosporium and *Cepalosporium*, which are associated with respiratory problems such as asthma and allergies, as well as hypersensitivity pneumonitis (Park, 2019).

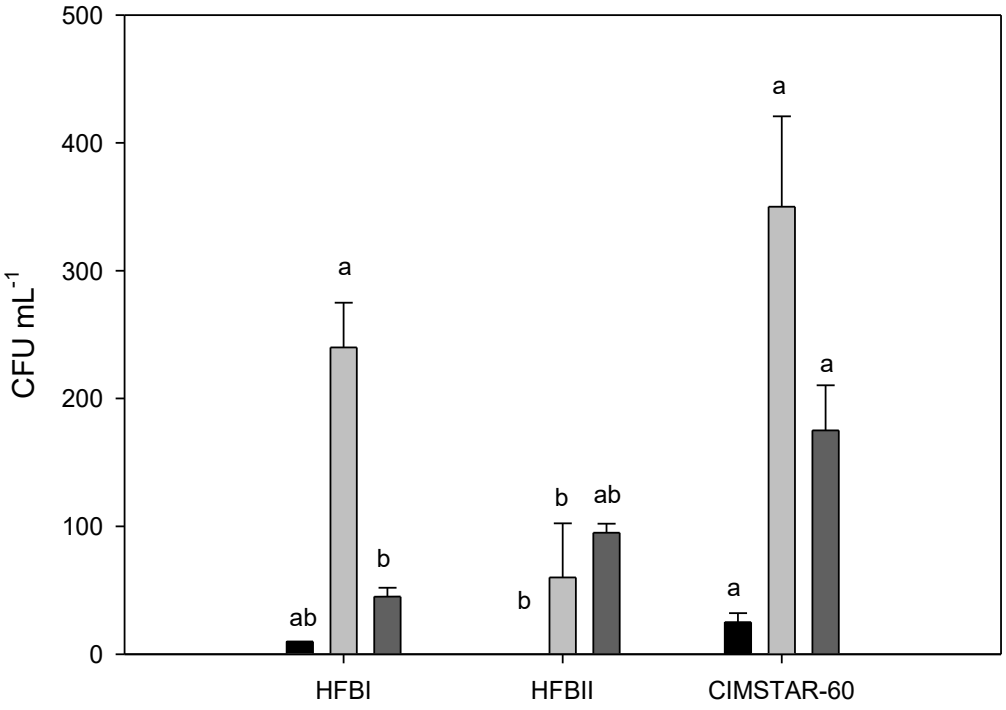

Figure 27. Microbiological analysis of emulsions formulated with HFBII and HFBII with JO, for total coliforms (black) on brilliant green agar at 35°C for 24 h, aerobic mesophiles (gray) on standard agar at 35°C for 48 h, and fungi and yeasts (dark gray) on potato dextrose agar at 25°C for 120 h. Different letters between treatments indicate significant differences using Tukey-Kramer multiple comparison test ($p<0.05$).

3.4. Conclusions

HFB I and II were produced in submerged cultures of *L. lecanii* using biological chitosan as the sole carbon source. At concentrations of 50 and 40 μg ml^{-1}, HFBI and II, respectively, successfully modified the contact angle of a water drop on a Teflon surface by 66% and 60% respectably. Tests were also carried out on hydrophilic surfaces (glass), where HFI successfully converted the surface into a hydrophobic one through its amphiphilic properties, resulting in contact angles of 89.7 ± 2.6°.

The purified HFBI and II had molecular masses of 8.7 and 5.8 kDa, as well as β-lamin and α/β structures, respectively.

Emulsions were made from purified HFBs with 24% (v/v) jatropha oil, which were stabilized with a minimum creaming index of between 24.48 and 26.63% for HFBI and II, respectively. Tribological tests provided evidence of their ability to reduce friction and wear forces, making them an attractive formulation for use as a biolubricant, replacing the commercial hydrocarbon-based products commonly used in industry. In this regard, the formulations tested in real lathe machining processes proved to be competitive with the commercial product CIMSTAR-60, as they match its lubrication properties, wear, and process conditions. However, they are competitive in terms of the microbiological growth of *Pseudomonas* and fungi, which cause significant health problems for workers. Therefore, emulsions of hydrophobins and jatropha oil are an attractive option to replace commercial lubricants used in the market, decreasing the negative environmental impact and approaching the potential of macromolecules.

3.5. References

Aguilar-Rosas, O., Blanco, S., Flores, M., Shirai, K., & Farfan-Cabrera, L. I. (2022). Partially deacetylated and fibrillated shrimp waste-derived chitin as biopolymer emulsifier for green cutting fluids—Towards a cleaner production. Polymers, 14(3), 525. https://doi.org/10.3390/polym14030525

Ahmad, U., Naqvi, S. R., Ali, I., Naqvi, M., Asif, S., Bokhari, A., ... & Klemeš, J. J. (2022). A review on properties, challenges and commercial aspects of eco-friendly biolubricants productions. *Chemosphere*, *309*, 136622. https://doi.org/10.1016/j.chemosphere.2022.136622

Alamprese, C., Rollini, M., Musatti, A., Ferranti, P., & Barbiroli, A. (2022). Emulsifying and foaming properties of a hydrophobin-based food ingredient from Trichoderma reesei: A phenomenological comparative study. LWT, 157, 113060. https://doi.org/10.1016/j.lwt.2021.113060

Barani, M., Mirzaei, M., Torkzadeh-Mahani, M., Lohrasbi-Nejad, A., & Nematollahi, M. H. (2020). A new formulation of hydrophobin-coated niosome as a drug carrier to cancer cells. Materials Science and Engineering: C, 113, 110975.https://doi.org/10.1016/j.msec.2020.110975.

Basheva, E. S., Kralchevsky, P. A., Christov, N. C., Danov, K. D., Stoyanov, S. D., Blijdenstein, T. B., ... & Lips, A. (2011). Unique properties of bubbles and foam films

stabilized by HFBII hydrophobin. Langmuir, 27(6), 2382-2392. https://doi.org/10.1021/la104726w

Bird, J. O., & Chivers, P. J. (1993). Friction. Newnes Engineering and Physical Science Pocket Book, 235–237. https://doi.org/10.1016/b978-0-7506-1683-6.50031-x

Kulkarni, S., Nene, S., & Joshi, K. (2017). Production of Hydrophobins from fungi. Process biochemistry, 61, 1-11. https://doi.org/10.1016/j.procbio.2017.06.012.

Manavalan, P., & Johnson Jr, W. C. (1983). Sensitivity of circular dichroism to protein tertiary structure class. Nature, 305(5937), 831-832.https://doi.org/10.1038/305831a0

Marchand, G., Lavoie, J., Racine, L., Lacombe, N., Cloutier, Y., Belanger, E., ... & Desroches, J. (2010). Evaluation of bacterial contamination and control methods in soluble metalworking fluids. Journal of occupational and environmental hygiene, 7(6), 358-366. https://doi.org/10.1080/15459621003741631

Mcclements, D. J. (2007). Critical review of techniques and methodologies for characterization of emulsion stability. *Critical reviews in food science and nutrition*, *47*(7), 611-649. https://doi.org/10.1080/10408390701289292

Mustalahti, E., Saloheimo, M., & Joensuu, J. J. (2013). Intracellular protein production in Trichoderma reesei (Hypocrea jecorina) with hydrophobin fusion technology. New biotechnology, 30(2), 262-268. https://doi.org/10.1016/j.nbt.2011.09.006

Narayana Sarma, R., & Vinu, R. (2022). Current status and future prospects of biolubricants: properties and applications. Lubricants, 10(4), 70. https://doi.org/10.3390/lubricants10040070

Park, R. M. (2019). Risk assessment for metalworking fluids and respiratory outcomes. Safety and health at work, 10(4), 428-436. https://doi.org/10.1016/j.shaw.2019.09.001

Ragesh, P., Ganesh, V. A., Nair, S. V., & Nair, A. S. (2014). A review on 'self-cleaning and multifunctional materials'. *Journal of Materials chemistry A*, *2*(36), 14773-14797. https://doi.org/10.1039/c4ta02542c

Ren, Q., Kwan, A. H., & Sunde, M. (2014). Solution structure and interface-driven self-assembly of NC2, a new member of the Class II hydrophobin proteins. *Proteins: Structure, Function, and Bioinformatics*, *82*(6), 990-1003. https://doi.org/10.1002/prot.24473

Rocha-Pino, Zaizy; Ramos-López, Jesús I.; Gimeno, Miquel; Barragán-Aroche, Fernando; Durán-Valencia, Cecilia; López-Ramírez, Simón; Shirai, Keiko (2018). Enhanced oil recovery by hydrophobins from Lecanicillium lecanii. Fuel, 224, 10–16. https://doi.org/10.1016/j.fuel.2018.03.058

Schor, Marieke; Reid, Jack L.; MacPhee, Cait E.; Stanley-Wall, Nicola R. (2016). The Diverse Structures and Functions of Surfactant Proteins. Trends in Biochemical Sciences, https://doi.org/10.1016/j.tibs.2016.04.009

Terauchi, Y., Nagayama, M., Tanaka, T., Tanabe, H., Yoshimi, A., Nanatani, K., ... & Abe, K. (2022). Adsorption kinetics and self-assembled structures of Aspergillus oryzae hydrophobin RolA on hydrophobic and charged solid surfaces. *Applied and environmental microbiology*, *88*(6).https://doi.org/10.1128/AEM.02087-21

Winandy, L., Hilpert, F., Schlebusch, O., & Fischer, R. (2018). Comparative analysis of surface coating properties of five hydrophobins from Aspergillus nidulans and Trichoderma reseei. Scientific reports, 8(1), 12033. https://doi.org/10.1038/s41598-018-29749-0

Wösten, H. A., & Willey, J. M. (2000). Surface-active proteins enable microbial aerial hyphae to grow into the air. Microbiology, 146(4), 767-773. https://doi.org/10.1099/00221287-146-4-767

Zadaka, D., Radian, A., & Mishael, Y. G. (2010). Applying zeta potential measurements to characterize the adsorption on montmorillonite of organic cations as monomers, micelles, or polymers. *Journal of Colloid and Interface Science*, *352*(1), 171-177. https://doi.org/10.1016/j.jcis.2010.08.010

General conclusions

This doctoral thesis demonstrates the biotechnological potential of *Lecanicillium lecanii* for the production of biomolecules with important industrial and biomedical applications. Using biological chitosan as an inducer and sole carbon source, a comprehensive strategy was developed for production in submerged cultures, its scaling up to pilot plant level, and the functional application of the biomolecules obtained. The chitosanase produced showed high catalytic efficiency in obtaining low molecular weight chitosan and chitooligosaccharides, positioning it as a promising method for the production of these compounds on a larger scale. At the same time, the HFBI and HFBII hydrophobins demonstrated remarkable amphiphilic and tribological properties, allowing the formulation of stable emulsions with jatropha oil that behaved as efficient and environmentally friendly biolubricants, capable of replacing conventional industrial products derived from hydrocarbons.

For their part, the nanoparticles developed from hydrophobins class II and glucosamine confirmed their potential in the medical field, showing adequate biocompatibility and significant antitumor activity both *in vitro* and *in vivo,* improving the pharmacological properties of the free drug. This biocompatibility is attributed to HFBII and GlcN, which not only exhibit anticancer properties but also significantly reduce the cytotoxicity of free THP. Taken together, the results obtained constitute the first reports on the production of chitinases from *L. lecanii*, as well as the application of hydrophobins as biolubricants under real machining conditions. Furthermore, this work represents the first study evaluating hydrophobins in animal models, marking a significant contribution.

Perspectives

This study provides solid evidence of the ability of *Lecanicillium lecanii* to produce chitinases and hydrophobins through submerged cultures using chitosan as the sole carbon source. However, several lines of research have been identified that will allow for further investigation and expansion of the scope of these findings.

First, it is suggested to move towards the in-depth molecular characterization of the chitosanase obtained, including its sequencing, structural identification, and classification within the reported enzyme families. Likewise, it would be relevant to evaluate the functional

properties and potential applications of chitosan oligomers (COS) and low molecular weight chitosans (LMWC) generated by this enzymatic process in fields such as agriculture, biomedicine, etc.

In relation to emulsions formulated as biolubricants, it is necessary to further the microbiological evaluation against specific strains of clinical relevance, particularly those associated with respiratory diseases linked to prolonged use of cutting lubricants. Additionally, it is proposed to conduct *in vitro* cytotoxicity studies using cell models such as human keratinocytes to determine the safety of the product for operators in industrial contexts. Complementarily, an economic analysis will allow the commercial viability of the biolubricant and its potential to replace conventional petroleum-based products to be estimated.

With regard to the system of nanoparticles formulated with hydrophobins, it is proposed to further quantify their distribution in plasma and organs of animal models in order to establish pharmacokinetic parameters and biodistribution profiles. It is also recommended to explore the development of nanoparticles based on class I hydrophobins, which would allow for a comparison of the structural and functional behaviors of both classes of proteins.

Appendix 1. Scientific congress participations

- XVIII National Congress of Biotechnology and Bioengineering, Mexican Society of Biotechnology and Bioengineering (June 2019) Poster: “Production and purification of hydrophobins in submerged cultures of Lecanicillium lecanii immobilized in polyurethane foam.” Guanajuato, Mexico.
- European Federation of Biotechnology (May 2021). Presentation: “Comparison of homo- and heterofermentative Lactobacilli as starters for the biological extraction of chitins from shrimp waste.” Virtual.
- XXX International Materials Research Congress and International Conference on Advanced Materials (August 2022).Presentation: “Biotechnological production of chitosan for use in tailored drug delivery systems.” Cancun, Mexico.
- XXX International Materials Research Congress and International Conference on Advanced Materials (August 2022. Conference: “Circular economy approach in the production of amphiphilic proteins for interface engineering.” Cancun, Mexico.

Appendix 2. Published articles

Hernández-Alcántara, J., Rojas-Osnaya, J., Anraku, M., Nakamura, H., & Shirai, K. (2026). Development of chitosanases of Lecanicillium lecanii in pilot-scale submerged cultures for production of low molecular weight chitosan and chitooligosaccharides. *Biocatalysis and Agricultural Biotechnology*, 103927. .https://doi.org/10.1016/j.bcab.2026.103927

Hernández-Alcántara, J., Nakamura, H., Tsukigawa, K., Yamasaki, K., Uchimura, R., Kuniyasu, A., ... & Shirai, K. (2026). Preparation and evaluation of hydrophobin-pirarubicin glucosamine-containing nanoparticles as an anticancer formulation. *International Journal of Biological Macromolecules*, 150460. https://doi.org/10.1016/j.ijbiomac.2026.150460.

Appendix 3. Calibration Curves

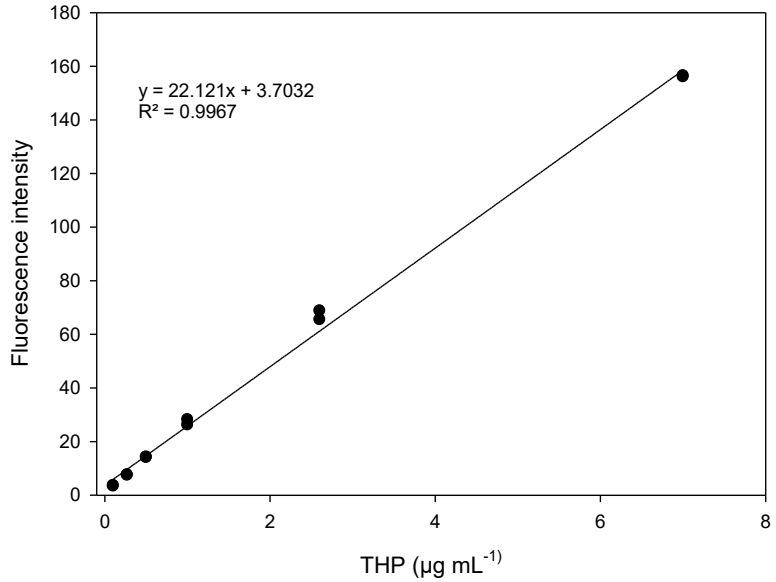

Figure A1. Calibration curve of THP at concentrations of 0 to 7 µg mL^{-1} by fluorescence spectroscopy with an excitation wavelength of 480 nm and an emission range between 450 and 600 nm

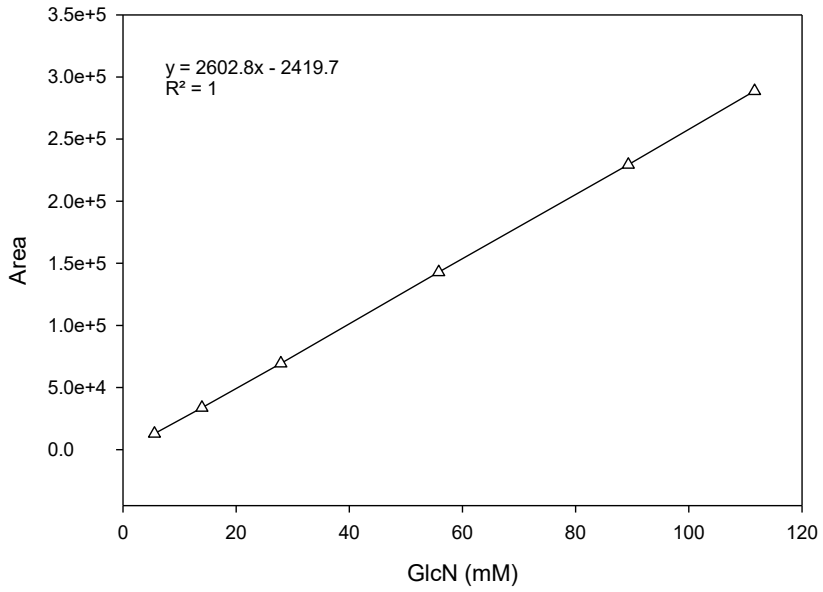

Figure A2. HPLC calibration curve for GlcN quantification using a column NH2P 50G 4A in a flow rate of 0.8 mL min^{-1} of acetonitrile: water (7:3) at 28°C for 30 min.

Casa abierta al tiempo
UNIVERSIDAD AUTÓNOMA METROPOLITANA

ACTA DE DISERTACIÓN PÚBLICA

No. 00302
Matrícula: 2192802272

Producción y purificación de quitosanasas e hidrofobinas de *Lecanicillium lecanii:* diseño de un nanoportador para la liberación controlada de fármacos.

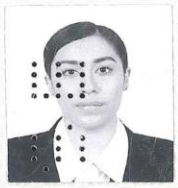

JENNYFER HERNANDEZ ALCANTARA
ALUMNA

En la Ciudad de México, se presentaron a las 16:00 horas del día 11 del mes de febrero del año 2026 en la Unidad Iztapalapa de la Universidad Autónoma Metropolitana, los suscritos miembros del jurado:

DRA. ZAIZY ROCHA PINO
DR. JESUS ROJAS OSNAYA
DR. HECTOR BERNARDO ESCALONA BUENDIA
DRA. CARMEN GUADALUPE HERNANDEZ VALENCIA

Bajo la Presidencia de la primera y con carácter de Secretaria la última, se reunieron a la presentación de la Disertación Pública cuya denominación aparece al margen, para la obtención del grado de:

DOCTORA EN BIOTECNOLOGÍA

DE: JENNYFER HERNANDEZ ALCANTARA

y de acuerdo con el artículo 78 fracción IV del Reglamento de Estudios Superiores de la Universidad Autónoma Metropolitana, los miembros del jurado resolvieron:

APROBAR

Acto continuo, la presidenta del jurado comunicó a la interesada el resultado de la evaluación y, en caso aprobatorio, le fue tomada la protesta.

REVISÓ

MTRA. ROSALIA SERRANO DE LA PAZ
DIRECTORA DE SISTEMAS ESCOLARES

DIRECTORA DE LA DIVISIÓN DE CBS

DRA. EDITH ARENAS RIOS

PRESIDENTA

DRA. ZAIZY ROCHA PINO

VOCAL

DR. JESUS ROJAS OSNAYA

VOCAL

DR. HECTOR BERNARDO ESCALONA BUENDIA

SECRETARIA

DRA. CARMEN GUADALUPE HERNANDEZ VALENCIA